Rochester Institute of Technology

RIT Digital Institutional Repository

11-2015

Water Based Inkjet Material Deposition Of Donor-Acceptor Nanoparticles For Usage In Organic Photovoltaics

Anirudh Raju Penmetcha
arp6270@rit.edu

Water Based Inkjet Material Deposition Of Donor-Acceptor Nanoparticles For Usage In Organic Photovoltaics

Anirudh Raju Penmetcha

B.E. Mechanical Engineering

Birla Institute of Technology and Science, Pilani - Dubai Campus

A thesis submitted in partial fulfillment of the

requirements for the degree of

Master of Science in Materials Science & Engineering in the

School of Chemistry & Materials Science,

College of Science

Rochester Institute of Technology

November 2015

Signature of the Author _____

Accepted by _____

Director, M.S. Degree Program   Date

SCHOOL OF CHEMISTRY AND MATERIALS SCIENCE
COLLEGE OF SCIENCE
ROCHESTER INSTITUTE OF TECHNOLOGY
ROCHESTER, NEW YORK

<u>CERTIFICATE OF APPROVAL</u>

M.S. DEGREE THESIS

The M.S. Degree Thesis of Anirudh Raju Penmetcha has
been examined and approved by the Thesis
Committee as satisfactory for the thesis required for
the M.S. degree in Materials Science and Engineering.

_____

Dr. Christopher Collison, *Thesis Advisor*

_____

Dr. Scott Williams, *Committee Member*

_____

Dr. Denis Cormier, *Committee Member*

_____

Dr. Michael Kotlarchyk, *Committee Member*

_____

Date

ABSTRACT

Significant efficiency increases are being made for bulk heterojunction organic photovoltaic prototype devices with world records at 11%. However the chlorinated solvents most frequently used in prototype manufacture would cause local health and safety concerns or large scale environmental pollution upon expansion of these techniques for commercialization. Moreover, research to bridge prototype and large-scale production of these solar cells is still in its infancy. Most prototype devices are made in inert glove box environments using spin-coating. There is a need to develop a non-toxic ink and incorporate it into a material deposition system that can be used in mass production.

In this thesis, P3HT:PCBM organic photovoltaic devices were fabricated with the help of inkjet printing. P3HT:PCBM blends were dissolved in organic solvent systems , and this solution was used as the ink for the printer. The "coffee-ring effect" as well as the effect of inkjet printing parameters on film formation were highlighted - thus the inkjet printing method was validated as a stepping stone between lab-scale production of OPVs and large-scale roll-to-roll manufacturing.

To address the need of a non-toxic ink, P3HT:PCBM blends were then dispersed in water, using the miniemulsion method. The nanoparticles were characterized for their size, as well as the blending between the P3HT and PCBM within the nanoparticle. These dispersions were then converted into inks. Finally, these nanoparticle inks were inkjet-printed to fabricate OPV devices.

Based on the results obtained here, tentative "next steps" have been outlined in order to improve upon this research work, in the future.

ACKNOWLEDGEMENTS

First and foremost, I would like to thank my parents and grandparents for their unyielding support of my research work and for pushing me to pursue a degree in Materials Science.

I would like to thank the Department of Chemistry and Materials Science at RIT (Autumn Madden, Brenda Mastrangelo) , for putting up with me for so long.

I want to thank all the professors who I have had many fruitful discussions (and from whom I "tactically borrowed" equipment from) mainly - Dr. Hans Schmitthenner, Dr. Shu Chang, Dr. George Thurston, Dr. Tom Smith, Dr. Lea Michel, Dr. Jeremy Cody, Dr. Kalathur Santhanam. I want to especially thank Prof. Richard Hailstone for his patience and generosity.

Next I want to thank Aaron Pulver, Scott Hambleton, Guy Wolfe II, Gaurav Tulsyan, Vineeth Patil and Devdatt Maganty - I am really blessed to have friends like this.

I wouldn't have gone very far if it was not for my research group: I want to thank Dr. Susan Spencer for spearheading the research group, during her time as a PhD student at RIT - I am constantly inspired by her work ethic and approach towards adversity. I want to thank Chenyu Zheng for being an amazing colleague and an ever more amazing friend.

I want to thank my thesis committee members: Dr. Scott WIlliams, Dr. Denis Cormier and Dr. Michael Kotlarchyk for their guidance during my thesis work - and for always having an open door when I have questions.

Last but not least, I want to express my immense gratitude towards my thesis advisor Dr. Chris Collison, for giving me a shot in his research group - this experience is invaluable to me.

TABLE OF CONTENTS

LIST OF FIGURES

Figure 2.1 : A cartoon of a typical organic photovoltaic device that is fabricated in research laboratories.

Figure 2.2 : Cartoon describing the step by step mechanism of generation of electricity from the OPV. The anode and cathode sandwich the active layer.

Figure 2.3: A cartoon describing the Working of the OPV in terms energy levels of the donor and acceptor

Figure 2.4: Energy Levels and Figure adapted from Conducting Polymer Materials for Flexible OPV Applications: Orgacon™ PEDOT : PSS by Luc Vanmaele, Ph.D.

Figure 2.5: Cartoon of the PEDOT:PSS coated ITO (blue) with Kapton tape affixed on top (red rectangle). The tape is removed when testing the devices to expose the ITO contact.

Figure 2.6: J-V Curve cartoon

LIST OF TABLES

CHAPTER 1 - Introduction to the thesis - Inkjet printing of organic photovoltaics using a water-based active layer ink

1.1 Introduction – The need for renewable energy

Fossil fuel consumption is at an all-time high due to the ever growing needs of ever growing populations. This is a concern because the world will eventually run out of fossil fuels such as coal and oil (a.k.a non-renewable sources of energy) and wanton consumption of these fuels causes increased air pollution as well as emission of greenhouse gases. These emissions manifest themselves in the form of Global Warming[1]; the melting of the Polar ice caps[2,3] is just one of the many alarming effects that threatens human life.

On the other end of the spectrum, it is very near impossible to stop consuming this energy! Developing countries like India and China are severely starved for electricity; large swathes of the populations do not have access to electricity. In poorly developed parts of the country, it leads to the women and children of the families having to travel large distances to scavenge for wood and biomass to use as fuel; fuel which becomes harder and harder to acquire as each day passes [4].

Thus, there must be an emphasis in developing infrastructure and improved technologies that use renewable sources of energy. Hydroelectric, wind and solar power can be harnessed to address the growing appetite for electricity by being able to supply off-grid power. This is an ideal situation as remote areas may be powered by using small scale wind turbines or solar

panels, without needing to invest large amounts of funds in connecting the said areas to the country's electricity grid.

1.2 Solar energy – Organic Photovoltaics (OPVs) / Organic Solar Cells

Solar power technology is advancing day by day. From conventional silicon based cells to thin-film CIGS solar cells all the way to Perovskites[5]; researchers are constantly working to improve device efficiencies and make solar power a competitive alternative to conventional fossil fuelled power generators.

In particular, the field of Organic Photovoltaics (OPVs) is garnering an immense amount of attention. Ching W Tang's [6] pioneering work with OPVs and OLEDs combined with Heeger, MacDiarmid and Shirakawa's [7] Nobel Prize winning work with conductive polymers has resulted in current interest in optimizing processes and materials for fabricating better OPVs.

OPVs are promising due to the following reasons:

- They are a thin film technology; the thicknesses of these devices are on the sub-micron range. This would mean that the quantity of material used to manufacture these cells would be low.
- They are "roll-to-roll" solution processable; these OPVs are generally made out of semiconducting polymers and organic small molecules. This means that the materials may be modified so as to make them soluble in different solvents. These solvents can then be deposited relatively easily using roll to roll methods such as Screen Printing, Gravure Printing, Inkjet Printing and so on.
- Flexibility; OPVs promise to be processed onto flexible substrates. This would mean that OPVs can be integrated into small scale devices efficiently.[8]

- They have a low cost of fabrication when compared with conventional silicon based photovoltaics.

- OPVs , once optimized thoroughly, may have an Energy Payback Time of 1 day. According to a study by Espinosa et al [9], in the future it would take only 1 day for manufactured OPVs to recoup their cost in terms of materials and energy used to make them.

  OPVs also have their share of disadvantages :

- The OPV technology is still in its infancy. Unlike silicon based solar cells which have reached the stage of commercialization, OPVs still have a way to go.

- There is still a lot left to study about OPVs - The sheer amount of possibilities in terms of new things to learn about OPVs (such as using different alternative Donor Acceptor materials, optimizing electrodes etc.) makes it challenging to narrow down on the "correct" parameter to focus on; hence the need for more study.

- Most of the results reported in literature regarding OPVs are done so by academia. These results are based on prototype devices which have been fabricated in the confines of an inert glove-box so as to get the best reportable result. This is well and good for prototyping but does not necessarily show that the process can be scaled up.

- OPV materials are generally solution processed using chlorinated and/or aromatic solvents. Similar to the prototyping point that was brought up before, there is only a small amount of research focus addressing the challenge of making the OPV materials soluble in less deadly solvents. This will inevitably result in scale-up issues when using chlorinated solvents on a large scale.[9]

- Everybody who is working on developing OPVs may not necessarily have the infrastructure in place to demonstrate high throughput fabrication of OPVs. This is an issue as prototype devices

that are (conventionally) made using spin coating on a small scale will require a different skill set than the skills required for dealing with devices made using a high throughput technique such as inkjet printing. As Frederik Krebs [10] succinctly puts it "…there is a huge difference between preparing and aligning a small multilayer structure typically on a solid substrate like glass, and the precise coating and/or printing of large areas with the same accuracy on flexible substrates …This requires a high degree of technical skill, and the combination of scientific knowhow on how to tune the chemical and physical properties of the ink that is to be processed, with the technical knowhow of different processing procedures and the conditions they apply to. This simple challenge may very well become a bottleneck in the further development as such combined skills are not necessarily present in a research group."

Thus there is a need to exert efforts in understanding how to make the OPV roll-to-roll processable while using an enviro-friendly solvent/ink system.

1.3 Focus of Thesis – Outline and summary of chapters

The primary objective of this thesis work was to develop a basic competency in inkjet printing of organic photovoltaics. The secondary objective was to inkjet print OPV devices using environmentally-friendly inks.

The thesis is outlined as follows:

Chapter 2 is the experimental and instrumentation section of the thesis. Here the fundamentals of OPV are discussed. The materials and methods that have been used in this study will also be outlined in brief. Techniques such as UV-Vis Absorbance and Photoluminescence spectroscopy, goniometry, light scattering techniques for particle sizing and inkjet printing are also discussed.

In **Chapter 3**, salient literature results on inkjet printed OPV are tabulated in the form of a literature survey; using this as a guideline, various inkjet printing parameters/concepts such as coffee-ring effect, marangoni-flow of inks, firing voltage, drop spacing, platen temperature are explained. By modifying the aforementioned parameters, and dissolving the active layer materials in an organic solvent ink system, proof-of-concept OPV devices were fabricated using inkjet printing, and characterized for their power conversion efficiencies. Thus, inkjet printing was validated as a roll-to-roll process for the fabrication of OPV.

Now, chlorinated solvents such as chloroform and chlorobenzene which are commonly used to process OPV materials (as seen in Chapter 3), may not be used on a large scale as they are highly flammable and carcinogenic; they pose serious threats to human health as well as towards the environment. To overcome this obstacle, the OPV active layer materials may be dispersed in the form of nanoparticles in relatively "non-toxic" solvents such as water. In **Chapter 4**, the miniemulsion method was used to disperse the active layer materials in the form of a nanoparticle dispersion, with the help of surfactants. The importance of the nanoparticle size, blending of the donor:acceptor materials within the nanoparticle, and wetting of nanoparticle inks in the context of printed OPVs, is highlighted. Finally, working OPV devices were fabricated through the use of spin-coating and inkjet printing of the aforementioned nanoparticle inks. Thus, water-based OPV nanoparticle inks were investigated as a possible stepping stone between lab-scale and large scale manufacturing.

To conclude ,**Chapter 5** explains the inter-dependence of the different steps taken in inkjet printing (inkjet printing settings, ink design, substrate modification etc.). To improve upon the results obtained in this thesis, each of these steps must be systematically addressed. Future experimental outlines and testable hypotheses have been written and explained here.

1.4 REFERENCES

[1] Spencer, Susan Demetra. "Charge Photogeneration Experiments and Theory in Aggregated Squaraine Donor Materials for Improved Organic Solar Cell Efficiencies." (2014).

[2]Mercer, John H. "West Antarctic ice sheet and CO 2 greenhouse effect- A threat of disaster." *Nature* 271, no. 5643 (1978): 321-325.

[3] Joughin, Ian, Benjamin E. Smith, and Brooke Medley. "Marine ice sheet collapse potentially under way for the Thwaites Glacier Basin, West Antarctica." *Science* 344, no. 6185 (2014): 735-738.

[4] Vaughan, Benjamin. "Towards large scale organic photovoltaics| NOVA. The University of Newcastle's Digital Repository." (2012).

[5] Lee, Michael M., Joël Teuscher, Tsutomu Miyasaka, Takurou N. Murakami, and Henry J. Snaith. "Efficient hybrid solar cells based on meso-superstructured organometal halide perovskites." *Science* 338, no. 6107 (2012): 643-647.

[6] Tang, Ching W. "Two-layer organic photovoltaic cell."*Applied Physics Letters* 48, no. 2 (1986): 183-185.

[7] Chiang, C. K_, C. R. Fincher Jr, Y. W. Park, A. J. Heeger, H. Shirakawa, E. J. Louis, S. C. Gau, and Alan G. MacDiarmid. "Electrical conductivity in doped polyacetylene." *Physical Review Letters* 39, no. 17 (1977): 1098.

[8] Hou, Jianhui, Hsiang-Yu Chen, Shaoqing Zhang, Ruby I. Chen, Yang Yang, Yue Wu, and Gang Li. "Synthesis of a low band gap polymer and its application in highly efficient polymer solar cells."*Journal of the American Chemical Society* 131, no. 43 (2009): 15586-15587.

[9] Espinosa, Nieves, Markus Hösel, Dechan Angmo, and Frederik C. Krebs. "Solar cells with one-day energy payback for the factories of the future."*Energy & Environmental Science* 5, no. 1 (2012): 5117-5132.

[10] Søndergaard, Roar R., Markus Hösel, and Frederik C. Krebs. "Roll-to-Roll fabrication of large area functional organic materials." *Journal of Polymer Science Part B: Polymer Physics* 51, no. 1 (2013): 16-34.

CHAPTER 2 - Experimental Methods

ABSTRACT/OBJECTIVE - The purpose of this chapter is to introduce some of the common experimental methods that are used in this thesis (such as inkjet printing, spin coating, spectroscopy measurements) as well as explore some basic fundamentals of the working of organic photovoltaics.

2.1 The structure of an OPV
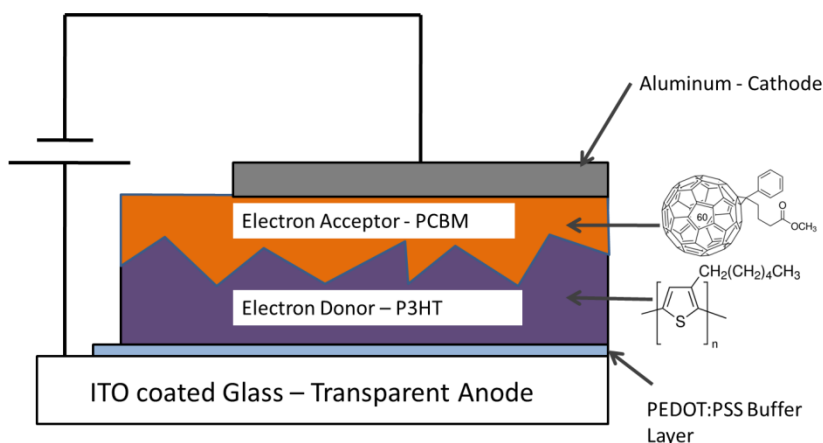
Figure 2.1 : A cartoon of a typical organic photovoltaic device that is fabricated in research laboratories.

The organic photovoltaic (OPV) devices fabricated for this study consist of the following functional layers (as shown in Figure 2.1)

The Anode –The most commonly used anodic material used in OPVs is Indium Tin Oxide (ITO). This is highly used due to it being a transparent conducting material [21]. The ITO is coated onto glass, enabling light to pass through it and get absorbed by the active layer materials.

The Buffer layer – An interfacial layer or buffer layer is used to (i) smoothen out the surface of the Anode/Cathode, (ii) tune the work function of the respective electrode. PEDOT:PSS (poly(3,4-ethylenedioxythiophene) polystyrene sulfonate) is a popular buffer layer [3] that is used as a hole transport layer between the active layer and the anode.

The Active Layer - The active layer forms the "bulk heterojunction" of the OPV. The active layer consists of an intimate mixture between an electron "Donor" (a semiconducting organic material In which, upon excitation, an electron is promoted to a higher lying state, leading to what may be described as a tightly bound electron-hole pair) and an electron "Acceptor" (a material which captures the electron from the Donor material). The most common active layer materials that are used as benchmark materials are P3HT or poly(3-hexylthiophene-2,5-diyl)which is a semiconducting polymer donor material and PCBM or (6,6)-phenyl-C61-butyric acid methyl ester, a fullerene derivative which acts as the electron Acceptor[22].

The Cathode – The cathode completes the OPV circuit, and thus the device. Aluminum is used as the cathode material in this study.

2.2 The working of an OPV
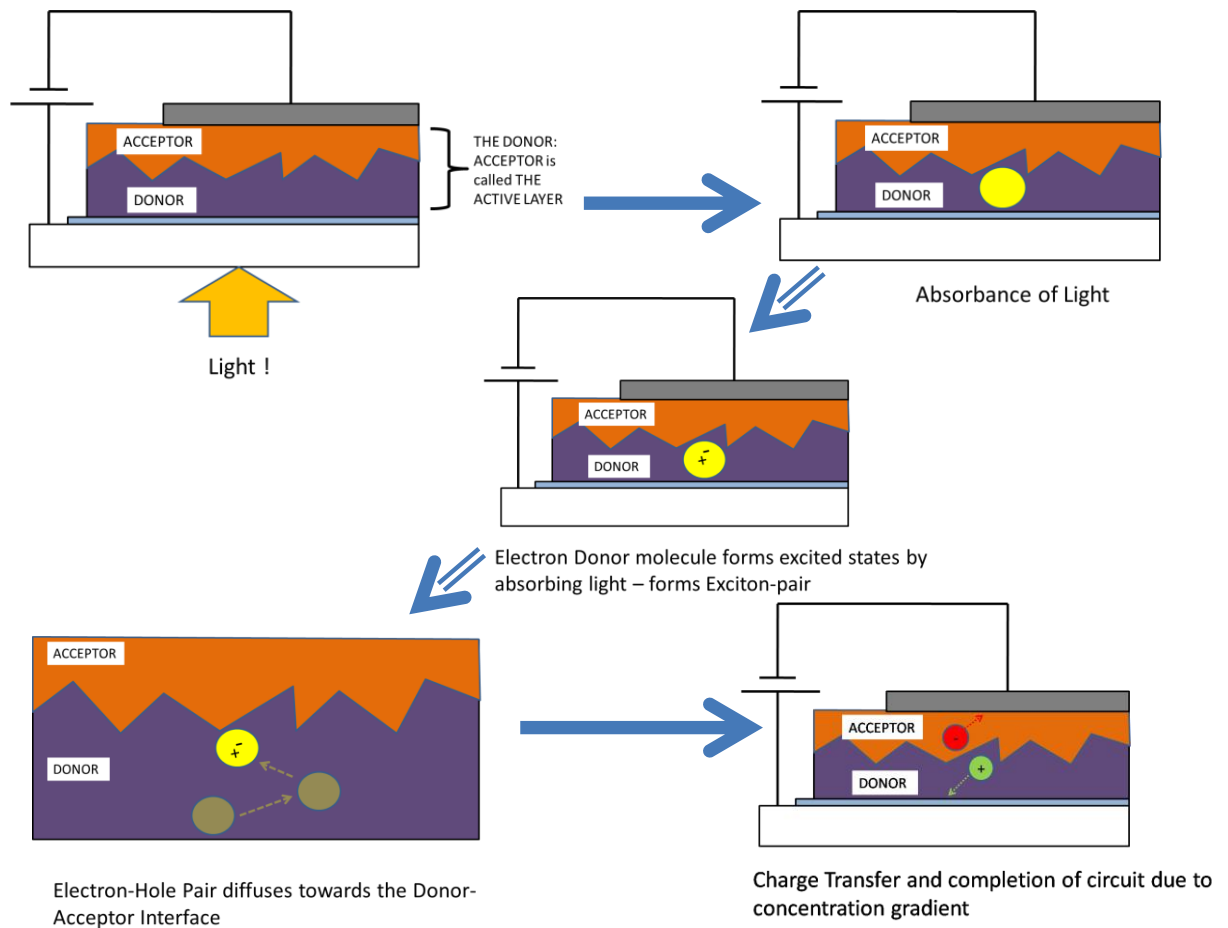
Figure 2.2 : Cartoon describing the step by step mechanism of generation of electricity from the OPV.

The anode and cathode sandwich the active layer.

The donor material within the active layer absorbs incoming light and generates a bound electron-hole pair or exciton. The exciton diffuses (through Förster resonance energy transfer - FRET [1]) towards the donor-acceptor (D-A) interface. At the D-A interface the electron from the exciton pair transfers over to the acceptor through Dexter electron/energy/charge transfer [2]. The electron then diffuses to the cathode; thus the hole left behind at the D-A interface diffuses towards the anode - the anode and cathode are presumably connected to the device of

interest (such as a phone or a battery) and the generated hole and electron travel through the device to recombine, thus completing the circuit.
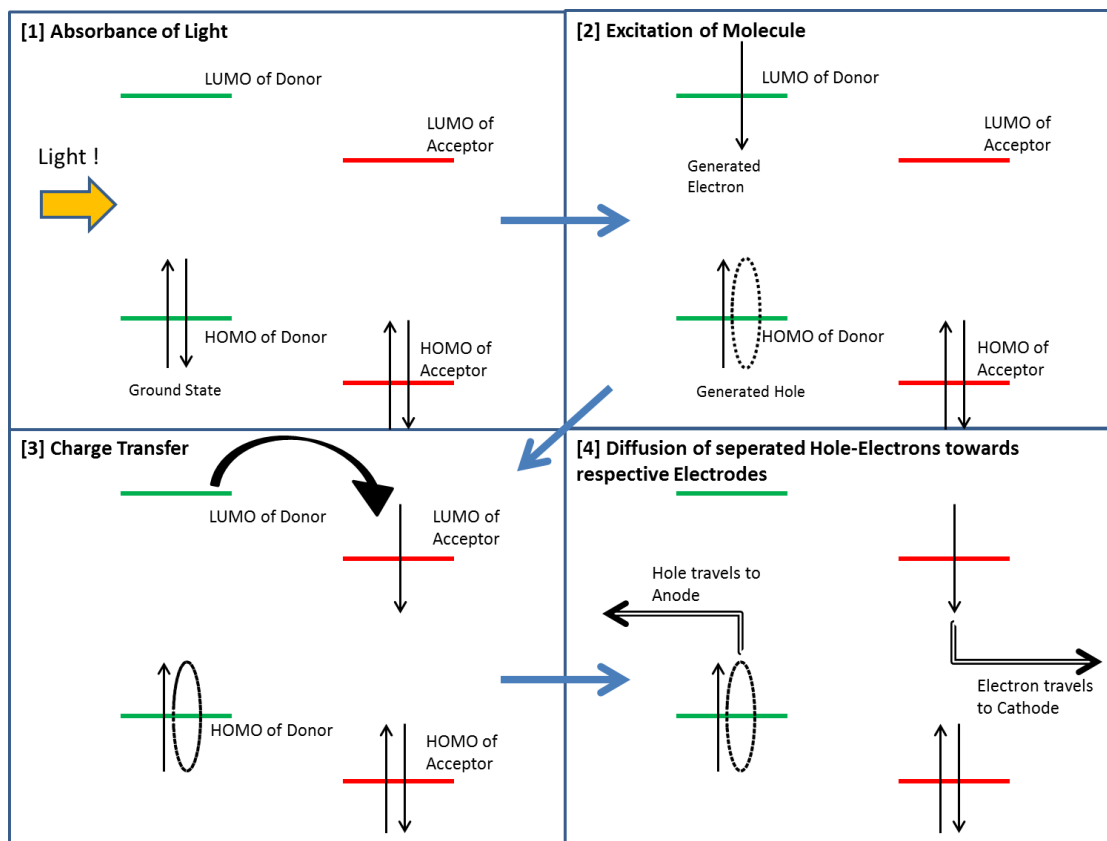
Figure 2.3: A cartoon describing the Working of the OPV in terms energy levels of the donor and acceptor.

The concept described in Figure 2.2 can be re-explained in Figure 2.3 in terms of the excited states and energy levels the of the donor and acceptor molecules. (From Figure 2.3) Light is absorbed by the donor molecule - this imparts energy to the electrons in the HOMO of the donor molecule. The molecule is now in its "excited" state. The excited electron can now relax back to the ground state (highest unoccupied molecular orbital - HOMO) either by releasing its energy through photoluminescence or undergo internal conversion and vibrational relaxations (see Absorbance and Fluorescence section). However, when the excited donor molecule is

sufficiently close to another molecule (acceptor) having a LUMO offset, the electron may transfer from the LUMO of the donor to the LUMO of the acceptor. Finally the electron from the LUMO of the of the acceptor diffuses to the cathode material (acts as an electron conductor)[7].

To prevent immediate recombination of charges as well as indeterminate flow of generated holes and electrons, the buffer layer (acting as the hole transport layer) allows only holes to travel towards the anode and blocks electrons due to the energy level mismatch between the buffer layer and the acceptor. This concept is shown in Figure 2.4 as a side-by-side comparison between the individual layers of the device and their energy (HOMO-LUMO) levels.
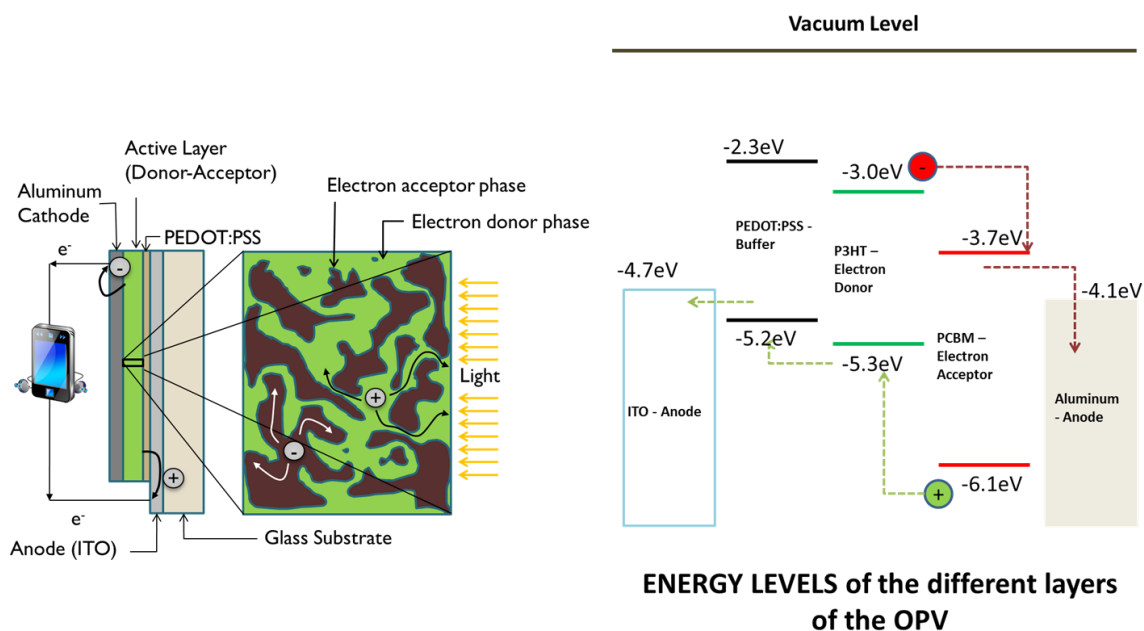
Figure 2.4: Energy Levels and Figure adapted from Conducting Polymer Materials for Flexible OPV Applications: Orgacon™ PEDOT : PSS by Luc Vanmaele, Ph.D.[8]

2.3 General steps involved in fabricating an OPV

Spincoating is used to fabricate prototype OPV devices. In this thesis, spin coated OPV devices are used as control devices i.e. spincoated devices are used to compare device performance

with inkjet printed devices (as seen in later chapters). The following is the Standard Operating Procedure [9] used in making spincoated OPV - this procedure is followed throughout the thesis.

Cleaning of ITO substrates- Isopropyl alcohol - IPA (purchased from Macron Fine Chemicals, ACS reagent grade quality) is used to clean ITO slides. ITO slides are immersed in IPA and sonicated in a VWR Model 75D bath sonicator for 30 minutes. The slides are then gently wiped with kim-wipes and immersed in acetone (purchased from Fischer Scientific Chemicals, ACS histological grade quality) and sonicated for 30 minutes. After this, the ITO slides are again wiped with kim-wipes and quickly blow-dried with clean-room air. Once the substrates have been cleaned, a small piece of Kapton tape is used to mask off the ITO (anode) contact for the completed device (Figure 2.5)

Figure 2.5: Cartoon of the PEDOT:PSS coated ITO (blue) with Kapton tape affixed on top (red rectangle). The tape is removed when testing the devices to expose the ITO contact.

Preparation and coating of PEDOT:PSS solution- 2.5ml of PEDOT:PSS (purchased from Sigma Aldrich, high-conductivity grade)is diluted with 2.5ml of deionized (DI) Water. This mixture is then filtered through a 0.45um-PTFE syringe filter. The cleaned ITO substrates are then spincoated with the prepared PEDOT:PSS solution using a Chemat Technology spin coater (model KW-4A)for 30 seconds and at a speed of 5000 rpm. The PEDOT:PSS coated ITO slides are then placed onto a hot plate at 160°C inside fume hood (or a vacuum oven at elevated temperature) to get rid of any residual solvent in the PEDOT:PSS film, for 30 minutes.

Preparing and coating the Active Layer solution- The active layer materials (P3HT:PCBM) are dissolved in the chosen ratio using the requisite solvent system (chloroform for spin coating, 1,2 dichlorobenzene for inkjet printing). Specific active layer formulations are outlined in pertinent chapters of this thesis.

The active layer solution is then either spincoated/printed onto the prepared PEDOT:PSS coated ITO slides. The active layer is spincoated using the spincoater inside a glove box to ensure no external contamination occurs within the film. The films are coated using a speed of 800 rpm and a time period of 18 seconds. Once this is done, the films are left to dry for about 2-3 minutes.

Deposition of aluminum top contact (cathode)- Prepared active layer films are transferred to the evaporation chamber where the cathode material is vapor deposited on top of the active layer. The evaporator is an Angstrom vacuum deposition system, Model numberS6458, powered by an Inficon SQC-310 Deposition Controller, and vacuum controlled with a Varian Turbo-V 81-AG turbomolecular pump. The rotation of the device holder is mediated by an Oriental Motor Company Gearhead, model 2GN36KA, whose functionality is controlled by the deposition controller. Tungsten evaporation boats

(purchased from R.D. Mathis) are used as holders for 2 aluminum pellets (Alfa Aesar Puratronic, alumina shot, 4-8mm, 99.999% purity). The evaporation boat is placed inside the evaporator. Once the active layer films and aluminum has been attached and secured within the evaporator, the chamber is closed and is evacuated using a vacuum pump. Deposition of aluminum cathode may start when the pressure inside the evaporator has reached ~10^{-6}-10^{-7}torr.Depending on the device requirement, 100-200nm of aluminum is deposited onto the active layer. Once this is

done, the evaporation process is stopped and the evaporation chamber is depressurized so as to remove the finished films.

2.4 Characterizing the Power Conversion Efficiency of an OPV

The Power Conversion Efficiency of an OPV device is extrapolated from the J/V characteristics of the device. Figure 2.6 shows the typical JV characteristics of a photovoltaic device. The J/V curves are measured using the 4-point probe method [9,23].
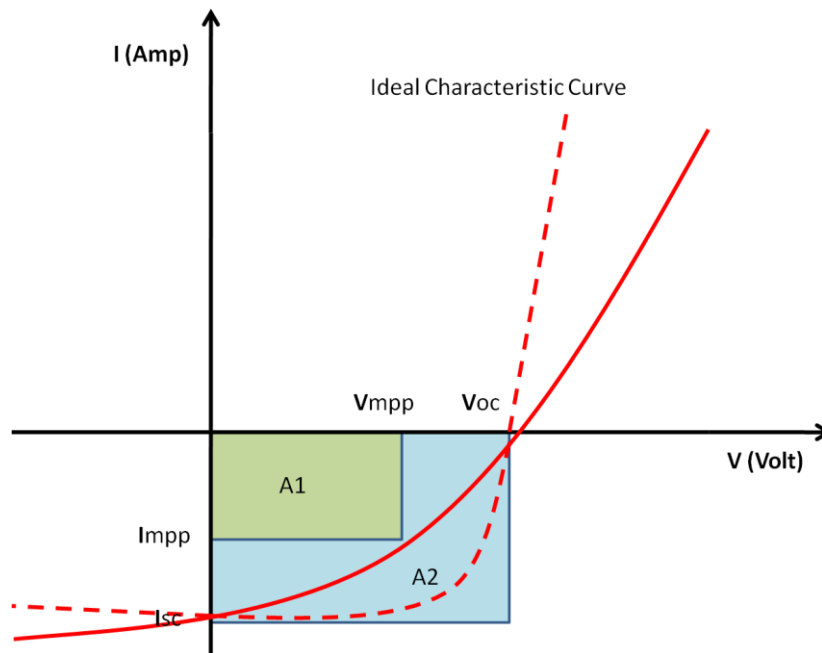
Figure 2.6: J-V Curve cartoon adapted from[10].

The Power Conversion Efficiency (PCE%) is determined by:

$$PCE = \frac{(Voc * Isc * FF)}{Pin}$$

Where Voc is the Open Circuit Voltage i.e the Voltage across the device when no current is flowing through it. This is essentially a parameter that is determined by the materials in use.

Different Donor materials will have different HOMO levels thereby determining the Voc of the material.[11,12,13,14]

The Isc is the Open Circuit Current i.e the Current flowing through the device when there is no voltage applied across the device. Here, Isc = $ne\mu E$

Where n is the density of charge carriers, e is the elementary charge, µ is the mobility and E is the electric field.

The FF is the Fill Factor. Fill Factor is a parameter that quantifies the process involved in fabricating the solar cell.

$$FF = {A1}/{A2} = {Vmmp * Immp}/{Voc * Isc}$$

Where Vmmp and Immp are the Voltage and Current at the maximum power point.

Current density-Voltage (J-V) characteristics of the devices were obtained in the dark and under simulated 1 sun, 100 mW cm^{-2} power density, provided by a Newport 91159Full Spectrum solar simulator with xenon lamp that had been calibrated with a round-robin InGaAs photovoltaic cell fabricated at NASA. The NASA calibration photovoltaic was independently calibrated at NASA before shipment. The devices are tested as soon as possible after evaporation of the aluminum contacts. The devices are measured in 2014 using a Keithley 2400 Sourcemeter (4-point probe measurement). The data is tabulated and collected using an internally-developed LabView program. A dark current measurement is made, and then the shutter is opened and the active device is measured. The film is placed in the same location on the testing surface every time in an effort to minimize errors.

2.5 The DIMATIX 2831 Inkjet Printer
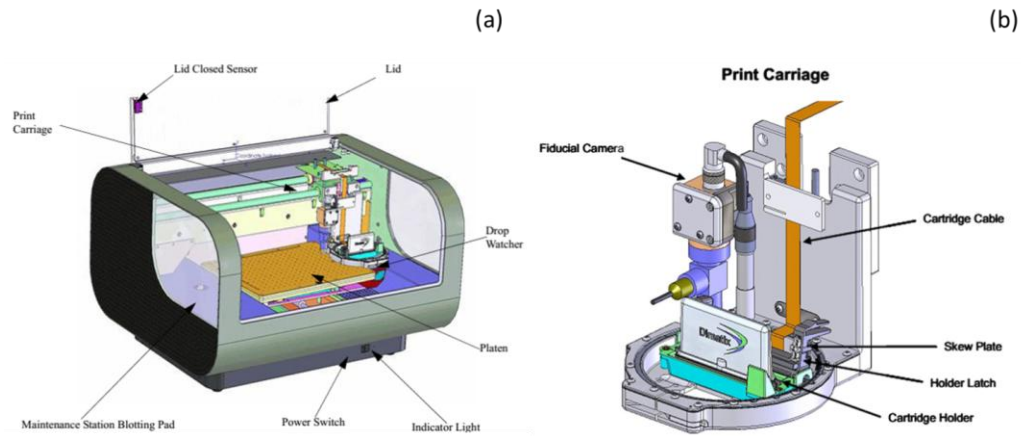
Figure 2.7: The Fujifilm Dimatix 2831 Deposition Printer - (a) cartoon showing the external features of the Dimatix - (b) print carrriage housing the ink cartridge.

The DIMATIX 2831 Materials Printer (see Figure 2.7) was used to inkjet print the OPV devices as reported in Chapters 3 and 4.

Inkjet printing is a versatile materials deposition technique that offers (i) low material wastage (ii) large amount of control over patterning , (iii) excellent printed resolution depepnding on the inkjet printer specifications [18].

Inkjet printing has been used to coat and print a large variety of functional materials to be used in functionally printed devices [19]. Some of them include - thin-film transistors,light-emitting devices, memory and magnetic applications ,contacts and conductive structures , sensors [20] and of course organic solar cells
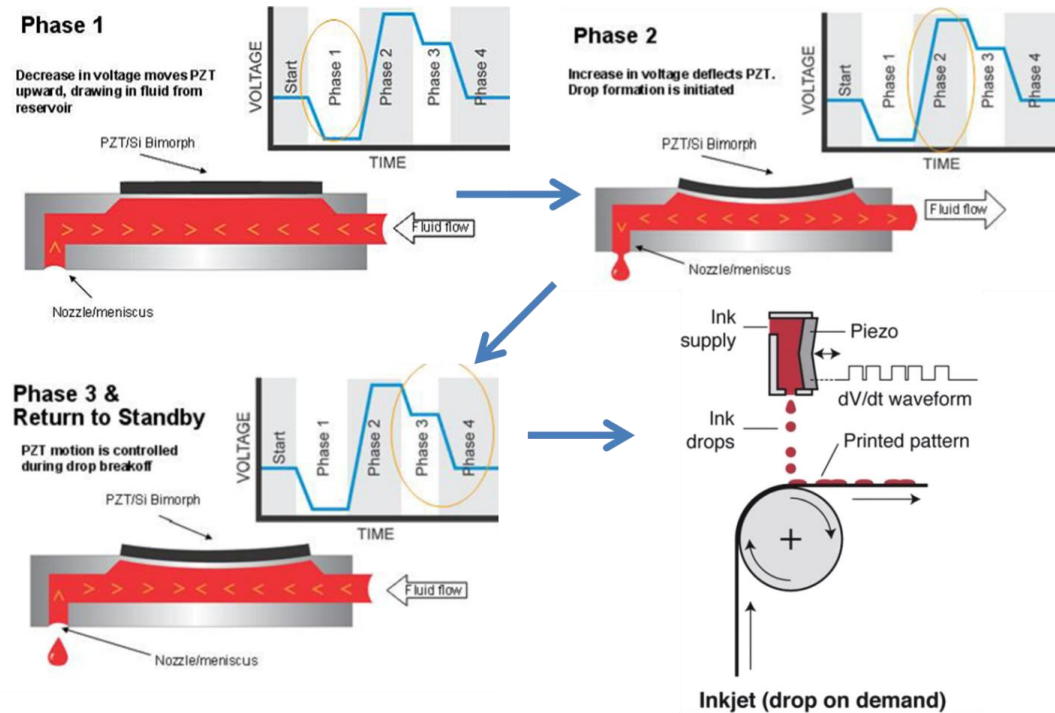
Figure 2.8 : Cartoon schematic showing the working of the inkjet process.

In the Dimatix, The jetting is carried out using a piezo-electric diaphragm that is located inside the inkjet nozzles. This basically takes place in 3 phases (Figure 2.8)

PHASE 1 – Here the ink fluid is drawn towards the nozzle when the piezo-electric diaphragm relaxes.

PHASE 2 – Here, the voltage is increased in the piezo-electric element causing it to deform. This deformation pushes the ink out of the nozzle in the form of a jetted droplet.

PHASE 3 – Finally, the voltage inside the piezo-electric is decreased again causing the ink to flow back inwards due to capillary action.

Thus, it is a Drop-on-Demand system ;the pattern to be printed may be designed using the proprietary Dimatix CAD software. Parameters such as firing voltage, drop spacing etc. will be discussed in Chapter 3 of this thesis.

2.6 UV-Vis Absorbance and Fluorescence measurements
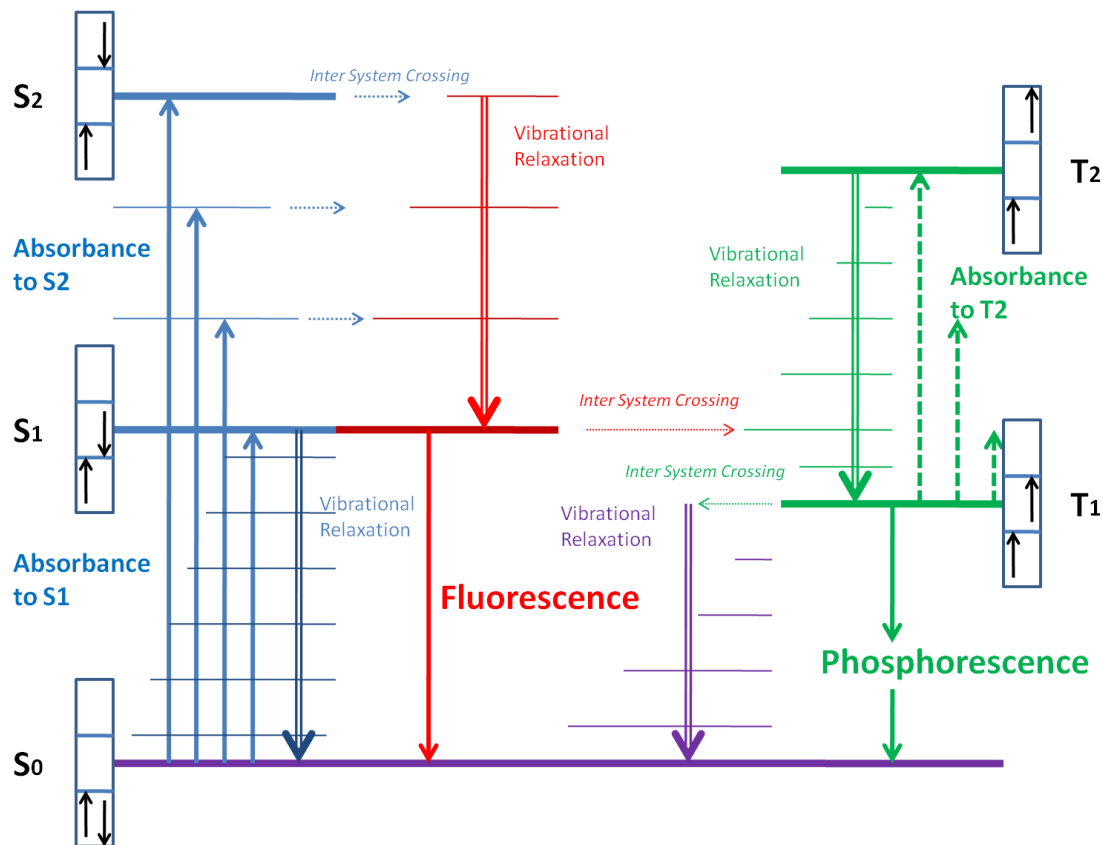
Figure 2.9 : Jablonski Diagram describing the various photophysical mechanisms taking place in excited states of semiconducting materials[15]. Absorbance and Fluorescence spectroscopy were used in characterizing blend ratios of the P3HT:PCBM when making solutions/inks for active layers.

UV-Vis absorbance spectroscopy (Figure 2.9) is a powerful and versatile tool that is used in characterizing the photophysical properties of the donor and acceptor materials used in this

thesis. UV-Vis spectroscopy was used to study the blending of the P3HT:PCBM nanoparticles, as seen in Chapter 4.

The absorption measurements of all solutions/dispersions were taken using a Shimadzu UV-2100PC spectrophotometer. The instrument was set to scan from 900nm to 300nm. A fast scan speed, 0.5 nm wavelength increments and 2 nm slit width were applied when taking the measurements. A "control" solution (which contains pure solvent)was always used to baseline the spectrum and remove excess noise from the signal and to account for the light scattering of the solvent and the cuvette.

Similarly, fluorescence spectroscopy is another versatile measurement for materials characterization, that was used to examine the relaxation mechanisms of the excited states for each material as a function of molecular structure as well as study the blending of P3HT:PCBM nanoparticles (as explained in Chapter 4).

The fluorescence emission measurements of all solutions/dispersions were taken using a HORIBA Jobin-Yvon Fluoro Max fluorometer. Quartz cuvette (type 23/Q/10) with a patch length of 10 mm was used for determining absorbance and fluorescence spectra of all solutions/dispersions. The cuvette was cleaned using the THF/IPA/Acetone/Water when finishing each reading.

2.7 Goniometry

A Rame-hart Goniometer was used for characterizing the surface tension of inks used for inkjet printing (Chapter 4). Goniometry was also used for characterizing the wetting of inks on different substrates. Surface tension measurements were made using the pendant drop method [17].

Contact Angle measurements were made using the sessile drop method [16].

2.8 Quasi-elastic Light Scattering

[4] Correlator

[5] Computer – Data Analysis and Display

[3] Light Detector

Scattered Light

[1] LASER – Light Source

Focusing the Light Source

Beam Stop

[2] Sample Holder
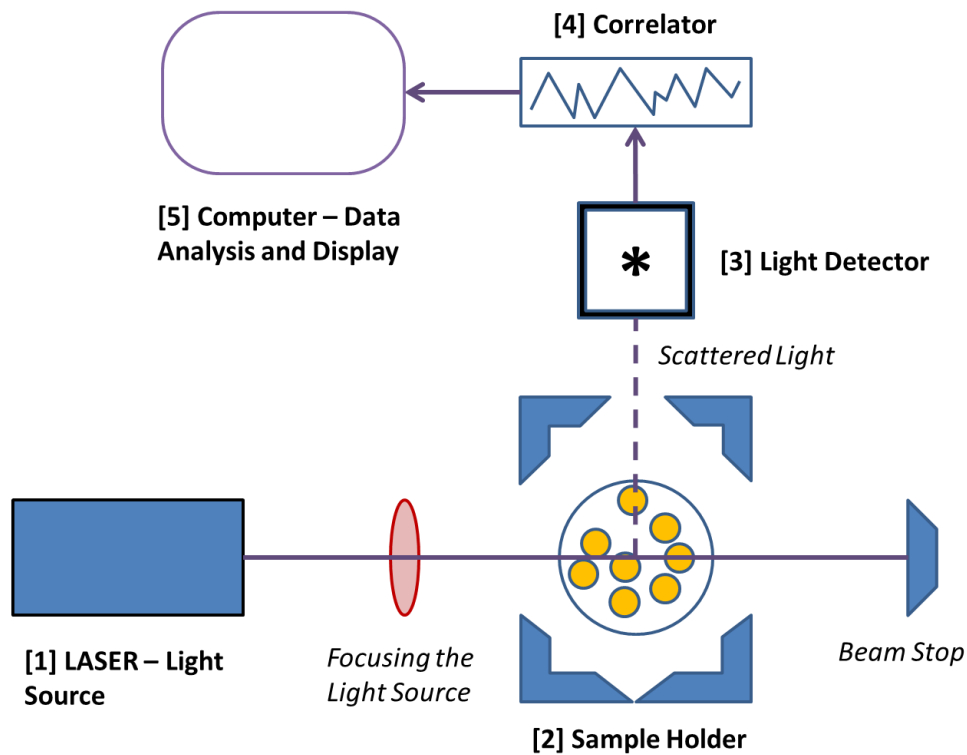
Figure 2.10 : Cartoon schematic of Quasi-elastic light scattering setup.

Quasi-elastic light scattering (or in some cases Dynamic Light Scattering)[4,5,6] is a versatile technique that can be used to measure and study the size, shape and size distributions of nanoparticles suspended in liquids – this is a particularly useful alternative to conventional imaging techniques like Scanning Electron Microscopy or Transmission Electron Microscopy which may prove to be more time and energy consuming.

As shown in Figure 10, the QLS system may consist of 5 main components –

1)The Light Source (typically a LASER of particular wavelength), which provides light of a specific wavelength and intensity of the incident beam as well as the geometry of the illuminated volume.

2) The Sample/ Sample Holder, which contains the sample cuvette, influences the scatter of the light at the entrance and exit points of the incident beam. The scatter is determined by some factors which include –the nature of the particles in the sample, sample concentration and cuvette size (volume).

3) Light/Photo Detector, which collects and registers the intensity of the scattered light coming out of the exit point of the sample.

4) The Correlator is continually fed data from the photodetector ; the correlator then computes the correlation function of the intensity fluctuations from the photodetector.

5) Finally, the Computer analyses the correlation function and determines the size and size distribution of the particles.

The specifications of the QLS setup used in this thesis work are as follows –

- Quasi-elastic light scattering was performed on a Brookhaven Instruments Light Scattering Goniometer. Samples were illuminated by a 35 mW He-Ne Laser (Spectraphysics) and hydrodynamic radii were obtained from 2nd order Cumulance Analysis of the resulting correlation function. The equipment was operated by Dr. George Thurston.

- Care was taken to ensure that samples were devoid of external contaminants like dust particles by preparing the samples in the confines of a well-ventilated fume hood; random contaminants floating around in the sample will cause excess scattering of light which will result in erroneous measurements.

2.9 REFERENCES

[1] Förster, Th. "Zwischenmolekulare energiewanderung und fluoreszenz." *Annalen der physik* 437, no. 1-2 (1948): 55-75.

[2] Dexter, David L. "A theory of sensitized luminescence in solids." *The Journal of Chemical Physics* 21, no. 5 (1953): 836-850.

[3] Groenendaal, L., Friedrich Jonas, Dieter Freitag, Harald Pielartzik, and John R. Reynolds. "Poly (3, 4-ethylenedioxythiophene) and its derivatives: past, present, and future." *Advanced Materials* 12, no. 7 (2000): 481-494.

[4] Lomakin, Aleksey, David B. Teplow, and George B. Benedek. "Quasielastic light scattering for protein assembly studies." In *Amyloid Proteins*, pp. 153-174. Humana Press, 2005.

[5] Lomakin, Aleksey, George B. Benedek, and David B. Teplow. "[27] Monitoring protein assembly using quasielastic light scattering spectroscopy." *Methods in enzymology* 309 (1999): 429-459.

[6] Pecora, R. "Dynamic light scattering measurement of nanometer particles in liquids." *Journal of nanoparticle research* 2, no. 2 (2000): 123-131.

[7] Pope, Martin, and Charles E. Swenberg. *Electronic processes in organic crystals and polymers*. Oxford University Press on Demand, 1999.

[8] http://www.sigmaaldrich.com/materials-science/organic-electronics/agfa opv.html#sthash.GaRYBeUA.dpuf

[9] Spencer, Susan Demetra. "Charge Photogeneration Experiments and Theory in Aggregated Squaraine Donor Materials for Improved Organic Solar Cell Efficiencies." (2014).

[10] Ulum, M. Syahrul. "Improving nanoparticle organic photovoltaic device performance| NOVA. The University of Newcastle's Digital Repository." (2013).

[11] Scharber, M. C., N. A. Schultz, N. S. Sariciftci, and C. J. Brabec. "Optical-and photocurrent-detected magnetic resonance studies on conjugated polymer/fullerene composites." *Physical Review B* 67, no. 8 (2003): 085202.

[12] Liu, Jie, Yijian Shi, and Yang Yang. "Solvation-induced morphology effects on the performance of polymer-based photovoltaic devices." *Advanced functional materials* 11, no. 6 (2001): 420.

[13] Ramsdale, C. M., J. A. Barker, A. C. Arias, J. D. MacKenzie, R. H. Friend, and N. C. Greenham. "The origin of the open-circuit voltage in polyfluorene-based photovoltaic devices." *Journal of applied physics* 92, no. 8 (2002): 4266-4270.

[14] Günes, Serap, Helmut Neugebauer, and Niyazi Serdar Sariciftci. "Conjugated polymer-based organic solar cells." *Chemical reviews* 107, no. 4 (2007): 1324-1338.

[15] Lakowicz, Joseph R., ed. *Principles of fluorescence spectroscopy*. Springer Science & Business Media, 2013.

[16] Shang, Jianying, Markus Flury, James B. Harsh, and Richard L. Zollars. "Comparison of different methods to measure contact angles of soil colloids."*Journal of colloid and interface science* 328, no. 2 (2008): 299-307.

[17] Woodward, Roger P. "Surface tension measurements using the drop shape method." *Technical Guide, http://www. firsttenangstroms. com/papers/papers. html* (1948).

[18] Derby, Brian. "Inkjet printing of functional and structural materials: fluid property requirements, feature stability, and resolution." *Annual Review of Materials Research* 40 (2010): 395-414.

[19] Singh, Madhusudan, Hanna M. Haverinen, Parul Dhagat, and Ghassan E. Jabbour. "Inkjet printing-process and its applications." *Advanced materials* 22, no. 6 (2010): 673.

[20] Dua, Vineet, Sumedh P. Surwade, Srikanth Ammu, Srikanth Rao Agnihotra, Sujit Jain, Kyle E. Roberts, Sungjin Park, Rodney S. Ruoff, and Sanjeev K. Manohar. "All-organic vapor sensor using inkjet-printed reduced graphene oxide." *Angewandte Chemie International Edition* 49, no. 12 (2010): 2154-2157.

[21] Espinosa, Nieves, Rafael Garcia-Valverde, Antonio Urbina, and Frederik C. Krebs. "A life cycle analysis of polymer solar cell modules prepared using roll-to-roll methods under ambient conditions." *Solar Energy Materials and Solar Cells* 95, no. 5 (2011): 1293-1302.

[22] Dang, Minh Trung, Lionel Hirsch, and Guillaume Wantz. "P3HT: PCBM, best seller in polymer photovoltaic research." *Advanced Materials* 23, no. 31 (2011): 3597-3602.

[23] Sinton, R. A., and A. Cuevas. "A quasi-steady-state open-circuit voltage method for solar cell characterization." In *Proceedings of the 16th European Photovoltaic Solar Energy Conference*, vol. 1152. 2000.

CHAPTER 3 - Validating the Inkjet Printing Method by printing functional organic photovoltaic devices

ABSTRACT/OBJECTIVE - The objective of this chapter was to validate the inkjet printing method by printing a working OPV device. A malfunctioning Dimatix 2831 inkjet printer was repaired and brought up to working condition. P3HT:PCBMwas dissolved in 1,2 dichlorobenzene and toluene to form an ink. This ink was then inkjet printed onto PEDOT:PSS-coated ITO substrates to form P3HT:PCBM thin films. Various printing parameters (including solvent choice, drop spacing, firing voltage) were varied in an attempt to understand and optimize the uniformity of the film. Finally, aluminum cathodes were evaporated onto the films to form functional OPV devices. These devices were characterized for their power conversion efficiencies. The inkjet printing method was thusly validated by this result.

3.1 Introduction

One of the main promises of OPV materials is that they can be solution processable i.e. the materials can be dissolved in appropriate solvents; these solutions can then be cast, coated or printed using a wide variety of roll-to-roll / reel-to-reel material deposition techniques such as screen printing, gravure printing [2] and so on.

Krebs, in his excellent reviews of printing and coating techniques used for making OPVs [3,4] , states that it is imperative that efforts be put into making roll-to-roll processing more efficient. Indeed, the majority of OPV literature [13,14] cites the advantages of roll-to-roll processing of OPV materials, yet very few journal papers actually deal with the processing of the OPV materials, and herein lies the challenge. A vast majority of prototype OPV devices are fabricated by spin-coating the active layer onto a small, rigid conductive substrate (usually a glass/ITO substrate); this spin coating is usually done in the confines of a clean room and/or a glove box containing an inert atmosphere inside. While this method is extremely effective in screening and characterizing OPV materials for their performance, it is a far cry from large scale coating techniques. In spin-coating, the thin film is formed by dynamically shearing off excess material from the wet film, a process which is not seen in conventional coating and printing methods, where the film is formed without any forces of shear acting on it. Not only does spin-coating lead to a wastage of material (due to shear), this process does not translate well when coating large-area rolls of flexible substrates, which is required to lead to a low dollar-per-watt market entry point. Ultimately, if the prototype device obtained from spin coating gives a high efficiency, but researchers are unable to translate this system into a mass-production setting, it will become a waste of effort. By focusing on the end-goal i.e. large area roll-to-roll coating of OPV, *and starting to prototype devices using these roll-to-roll methods*, researchers may then

focus their attention on improving the final product; failure modes of OPV materials in the presence of the outside atmosphere will be significantly more different when comparing large scale vs. small. Also, heretofore largely overlooked factors such as the adhesion [49] between the various layers of a fully printed flexible OPV module, encapsulation and the logistical design challenges that will eventually arise [48]all need to be solved.

The purpose of this thesis chapter is to start to bridge the gap between spin-coating and roll-to-roll coating. An attractive alternative to spin-coating that also offers roll-to-roll scalability, is inkjet printing. In this chapter, the inkjet printing method was successfully adapted to fabricate proof-of-concept OPV devices; the challenges accompanying inkjet printing (such as appropriate solvent choice, complexity of formulations and printing parameters) are highlighted.

3.2 Advantages of using Inkjet Printing

The advantages to inkjet printing are manifold. Primarily, inkjet printing has very low materials usage; it can be used to deposit ink only where it's needed and proof of concept prototypes can be made on a small scale using small quantities of inks. Other coating methods such as slot-die coating and screen printing require much larger quantities of materials to operate [15].Indeed, large materials usage is not typically conducive to research and development purposes due to the high cost of the active layer materials. Inkjet printing thus also fares better than spin-coating when it comes to materials usage, again as most of the materials are sheared off of the substrate in spin-coating.

Inkjet printing is also a mask-less and non-contact method of coating, unlike gravure printing and doctor-blading. This reduces the chance for the deposited films to get contaminated by impurities that may be present on the gravure-web /knife-blade. [16]

Another innovative idea proposed by Teichler et al.,[15] is to use inkjet printing as a tool to rapidly and reproducibly fabricate and populate a thin-film library with maximum materials efficiency[15,17,18]. Changing the donor or acceptor, concentration of inks, thicknesses of printed films may be automated by inkjet printing; this may be a very appealing method for study. The structure-property characteristics of these films may be rapidly elucidated by using UV-vis absorbance and fluorescence quenching to quickly determine effective blending of materials. This concept can be taken a step further by changing the substrates that the inks are printed on, or by, for example, modifying the hole/electron transport layers. Ink vehicle formulations may also be rapidly validated for their effect on uniform film formation (the importance of ink formulation is elaborated later on in the chapter).

3.3 Experimental details

3.3.1 Repairing the printer

A prerequisite for conducting this thesis works was to, in fact, get access to a working inkjet printer that was capable of printing novel functional materials. The Dimatix Materials Printer DMP-2831 is one such tool that fit the bill; a malfunctioning Dimatix printer was obtained and repaired by the author. Once it was repaired, standard tests and calibrations were run using Dimatix test fluids; the jetting of model fluids was observed to be uniform and it was thus determined that the machine was successfully repaired.

3.3.2 Literature Guidelines

Inkjet-printed organic photovoltaics have been fabricated by other research groups using widely different conditions such as different active layer materials, solvent formulations, PEDOT:PSS

thicknesses and different ink concentrations. A brief literature survey has been tabulated as follows, with respect to these different conditions.

References	Ref	Factors influencing the Power Conversion Efficiencies of Inkjet Printed OPV										
		1	2	3	4	5	6	7	8	9	10	11
		PEDOT:PSS Thickness	D:A Materials	Ratio of D:A	Conc. of ink	Drop Spacing	Platen Temperature	Post-Print Drying	Post-Print Annealing	Solvent System used	PCE%	Thickness of Active Layer(nm.)
	7	50nm	P3HT:PC61BM	[1.5:1]	2.5mg/ml or (4.5mg/ml)	12 um	28C	Vacuum drying	140C, 10 minutes	ButylBenzene:Toluene (8:2)	1.4 / 2.2	77 / 101
	5	60nm	P3HT:PC61BM	[1:1]	1wt% + 1wt% = 20mg/ml	35 um	40C		140C, 10 minutes	100% Tetralin 68% oDCB + 32% Mesitylene	1.29 / 3.47	200 / 230
	8	-	PFDTBTP:PC61BM /PC71BM	[1:2]	0.6wt% = 6mg/ml	-	-	Vacuum Drying for Tetralin, 50-100C for others	80C, 5 minutes	[pc61bm]Chlorobenzene/Trichlorobenzene (90%-10%) [pc61bm]Anisole/Tetralin (90%-10%) [pc61bm]p-Xylene/Tetralin (90%-10%) [pc61bm]p-Xylene/Mesitylene/Tetralin (80%-10%-10%) [pc61bm]Tetralin [pc71bm]Chlorobenzene/Trichlorobenzene (90%-10%) [pc71bm]Anisole/Tetralin (90%-10%)	3.5 2.7 2.7 2.8 1.7 3.1 2.8	86 95 68 66 85 68 69
	9	30nm	P3HT:PC61BM	[1:1]	0.3wt% +0.3wt% = 6mg/ml	-	-	100,130 or 160 till dried	100 or 140 for 30 minutes	Chlorobenzene/Trichlorobenzene (55%-45%)	2.4	180
	10	-	P3HT:PC61BM	[1:1]	1wt% = 10mg/ml	-	-	-	-	Chlorobenzene/Tetralin (50%-50%)	1.40	160
	11	-	PFDTBTP:PCB61BM	[1:2]	0.64wt% = 6.4mg/ml	-	-	-	-	Chlorobenzene/Trichlorobenzene	3.50 / 3.70	86 / 221
	12	60nm	RR-P3HT:PCBM	[1:1]	1wt% +1wt% = 20mg/ml	-	-	-	-	Tetralin, 93% rr P3HT Tetralin, 96% rr P3HT Tetralin, 98% rr P3HT oDCB-Mesitylene (68% -32%), 93% rr P3HT oDCB-Mesitylene (68% -32%), 96% rr P3HT oDCB-Mesitylene (68% -32%), 98% rr P3HT	1.3 2.1 0.7 2.9 3.5 0.1	200 200 300 200 230 300

Table 3.1 : Factors that impact the Power Conversion Efficiency of OPV devices, tabulated from salient literature references.

The power conversion efficiencies obtained from inkjet printed OPVs ,depend on multiple factors (as mentioned in Table 3.1).

Factor 1 - (PEDOT:PSS Thickness)- PEDOT:PSS layers of different thicknesses have been reported in literature, as tabulated above (see Chapter 2 and Appendix A for more on PEDOT:PSS) . Different thickness layers may affect the morphology of the printed active layer, thereby impacting device efficiency.

Factors 2 and 3 - Donor: Acceptor Materials and Ratios. Power conversion efficiencies are highly dependent on the materials used and the ratio that they are combined in.

Factor 4 - Concentration of the ink. The solid loading fraction/concentration of the ink has an impact on the thickness of the final film (Factor 11) , and thus impacting the power conversion efficiency of the OPV device[20].

Factor 5 - Drop Spacing - This is the distance between consecutively printed ink droplets. The larger the drop spacing, the larger the distance between the deposited ink droplets. Different concentrations of inks require optimized drop spacings for the deposition of uniform films.

Factors 6,7,8 - Evaporation of solvent - The method by which the printed wet film is dried impacts the morphology of the dried film.

Factor 9 - Solvent system - Different solvent systems have different rates of drying, which influence Factors 6,7 and 8. The "coffee-ring" drying of films is also affected by the solvent system, as will be discussed in the later sections if this chapter.

Table 3.1 highlights another non-obvious parameter: The effect of the regioregularity of the polymer on the inkjet printing, and subsequently the devices is not obvious but its importance is explained by Hoth et al. [12] . That study showed that having a highly regioregular polymer donor results in very rapid gelation of the polymer within the solvent, and causes the printed devices to fail in efficiency. This causes the internal viscosity of the ink to increase until it is not printable anymore as the polymer forms an extremely viscous gel. This highlights a major discrepancy as normally, a highly regioregular P3HT tends to yield high efficiencies when spin-coated; when the same is tried for printing, the material fails as it loses its solubility over time, hindering its processability.

From Table 3.1, it can be inferred that there is no one "correct" method to fabricate an OPV through inkjet printing. It can even be said that there is only an empirical relation between the

processing method, choice of materials, solvents and the operator[21]; indeed, since this is a nascent field of research, it behooves the researcher to first understand a few core parameters of inkjet printing, before delving into a full-factorial design of experiments that studies and optimizes all the parameters step by step. Thus, the objective of this thesis chapter was to develop a baseline understanding about inkjet printing, and validate inkjet printing as a viable method of fabricating OPV. Keeping this in mind, the parameters used in the inkjet printing studies conducted in this thesis chapter were chosen and discussed below.

3.3.3 The coffee ring effect

Solids, whether dissolved or dispersed over the entire ink drop, will become concentrated into a ring-like deposit as long as (i) the ink droplet meets the surface of the substrate at a non-zero angle, (ii) the contact line of the ink drop is pinned to its initial position (good wetting of the solvent) and (iii) the solvent evaporates[22]. As described by Deegan et al., this phenomenon is due to the geometrical constraints of the droplet; the free surface of the ink droplet "squeezes" the fluid outward to compensate for evaporative losses. This phenomenon is commonly seen in spilled coffee drops, where the coffee solids dispersed in the water form this ring-like pattern, hence the moniker "the coffee-ring" effect. This phenomenon is ubiquitous in many practical applications such as uniform coatings, complex self-assembly of nanomaterials/molecules, painting and washing[23].

The coffee-ring is generally overlooked in spin-coated OPV devices as the thin film is formed by dynamically shearing off excess solvent, leaving behind a uniform thin film. However, in the case of inkjet printing of OPV, the thin film is formed under static shear i.e. the excess solvent is removed only through evaporation, giving rise to the coffee-ring [10]. This is not ideal when considering the fact that the desired film should be uniformly thick across large areas.

The coffee-ring can be alleviated, however, by modifying the surface tension gradient within the ink droplet. This induced surface tension gradient is called the "Marangoni Eddy" attributed to the "Marangoni Effect"[24]. Since the coffee-ring is caused due to the outward flow of liquid caused by capillary forces - solvent lost at the edges of the droplet through evaporation is replenished by liquid from the center of the droplet, the flow can be turned inward by adding "contaminants" to the droplet - these contaminants may be surfactants [25,26] or even co-solvents [27] in the case of the Marangoni effect. This inward flow is induced from regions of low surface tension (surfactant/contaminant/co-solvent) and high surface tension (primary solvent).

3.3.4 Solvent selection and ink formulation

Keeping the above discussion in mind, the solvent selection and ink formulation was chosen based on the extensive inkjet printing work conducted by Hoth et al[1,5,12]. Here, Hoth et al. demonstrated the importance of utilizing a binary solvent formulation of ortho-dichlorobenzene (oDCB) and 1,3,5-trimethylbenzene (mesitylene) in fabricating inkjet-printed OPV devices. They first showed that using a "pristine" ink formulation such as 100% oDCB resulted in highly irregular film formation, de-wetting between the ink and underlying PEDOT:PSS and micrometer scale thickness variations in the printed areas. This ultimately combined to give poor device performance. Next, they used a pristine 100% tetralene formulation and found that resulting films also suffered from poor morphology and rough surfaces. The thought is that this is attributed to the high boiling point of the solvent (260°C) allowing coffee-ring formation of the ink droplets. Finally, they demonstrated that using a binary solvent system - 68% v/v oDCB and 32% v/v mesitylene mixture (oDCB having a higher surface tension of 37 dynes cm^{-1}, mesitylene with a lower surface tension of 28.2dynes cm^{-1}) resulted in the best results. By

combining solvents with different surface tensions, Marangoni eddies could be induced within the wet film and reduce the effect of the coffee-ring as seen in pristine ink formulations [8]. This ink formulation ideology has been further referenced by other research groups as seen in Table 3.1, where different donor:acceptor material combinations were inkjet printed in a variety of solvent formulations such as [7,9,10,11]. Therefore, in this thesis, the procedure used by Hoth et al. was used as a foundational approach.

3.3.5 Donor:Acceptor materials choice

P3HT:PCBMblends have been widely used as benchmarking materials in OPV[19], and will continue to be studied in the years to come due to the enormous knowledge gleaned from them for the past 20 years and their commercial availability. Indeed, the majority of printed/coated organic photovoltaics, regardless of processing techniques, have used P3HT:PCBMblends as benchmarks. Thus, it was a logical choice to choose these materials as results obtained from devices made from them may be easily compared to results obtained in literature, thereby educating the author in future iterations of studies.

P3HT (highly regioregular poly (3-hexylthiophene-2,5-diyl)) was obtained from Reike Materials . PCBM (Phenyl-C61-butyric acid methyl ester, 99% pure) was obtained from American Dye Source. 42mg of P3HT and 33mg of PCBM were dissolved in 5ml of solvent formulation.

The P3HT:PCBM ratio was chosen to be around ~1:0.8 - this ratio was chosen based on the work by Muller et al.[6] Here, Muller showed that the donor:acceptor ratio that yields the best device efficiency for P3HT:PCBM was at 1:0.8, where the P3HT:PCBM blend is described as slightly hypoeutectic i.e. the blend contained a combination of a P3HT:PCBM mixed phase, and a pure PCBM phase. Muller demonstrated that the best device efficiencies were obtained by exploiting this particular interpenetrating microstructure.

This was a deviation from Hoth's approach[5], where a ratio of 1:1 was used. The reasoning behind this was not explicitly stated in the paper; one may hypothesize that the film formation and thus the phase separation between the P3HT:PCBM in the case of [6] (where spin-coating was used) will be different from the case of [5] (inkjet printing) and thus yield to different optimal conditions for different processing techniques.

3.3.6 Drop spacing and Firing Voltage of the Inkjet Printer

In conventional spin-coated films[50], the thickness of the film is dependent on properties such as the concentration of the polymer i.e. the solid loading of the ink, the initial viscosity of the liquid, spin time, liquid density and finally the spin speed. As mentioned before, the film is formed due to dynamic shearing off of the excess liquid.

However, when using the Dimatix inkjet printer, the final thickness of the film is affected by the concentration of the ink, inkjet nozzle diameters, drop spacing (Figure 3.1) between individual ink-jetted droplets and the firing voltage (Figure 3.2) with which the ink is jetted out of the nozzle. This is in addition to the wetting caused by the ink itself; typically the inks have a surface tension ranging between 27 dynes cm-1 and 40 dynes cm-1; a low surface tension ink would spread across the substrate well, requiring less overall ink to cover the substrate and vice versa. (See Table 3.2 and 3.3)
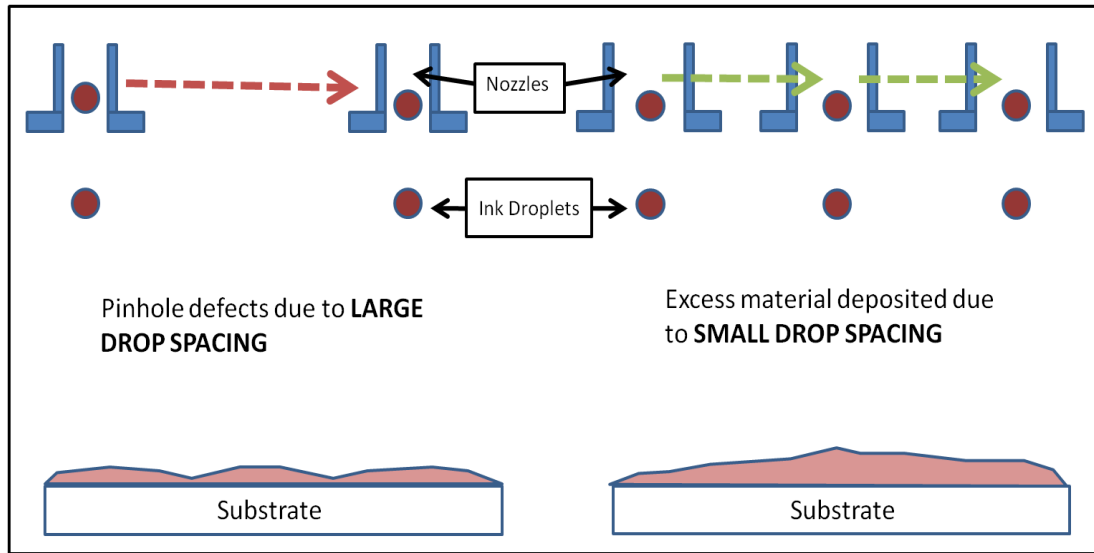
Figure 3.1: Cartoon describing the effect of inkjet drop spacing on film formation

The drop spacing determines the distance between successive inkjet drops as they fall towards the substrate. The printed drop will hit the substrate and spread out, and individual drops should connect with each other. If the drop spacing is too large, the final dried film that is formed may not be fully interconnected. Such a film may have large gaps and pinhole defects. On the other hand, if the drop spacing is too small, the material will be deposited excessively over very small areas causing the film to be too thick. Optimal drop spacing also depends on the solid loading fraction of the ink.
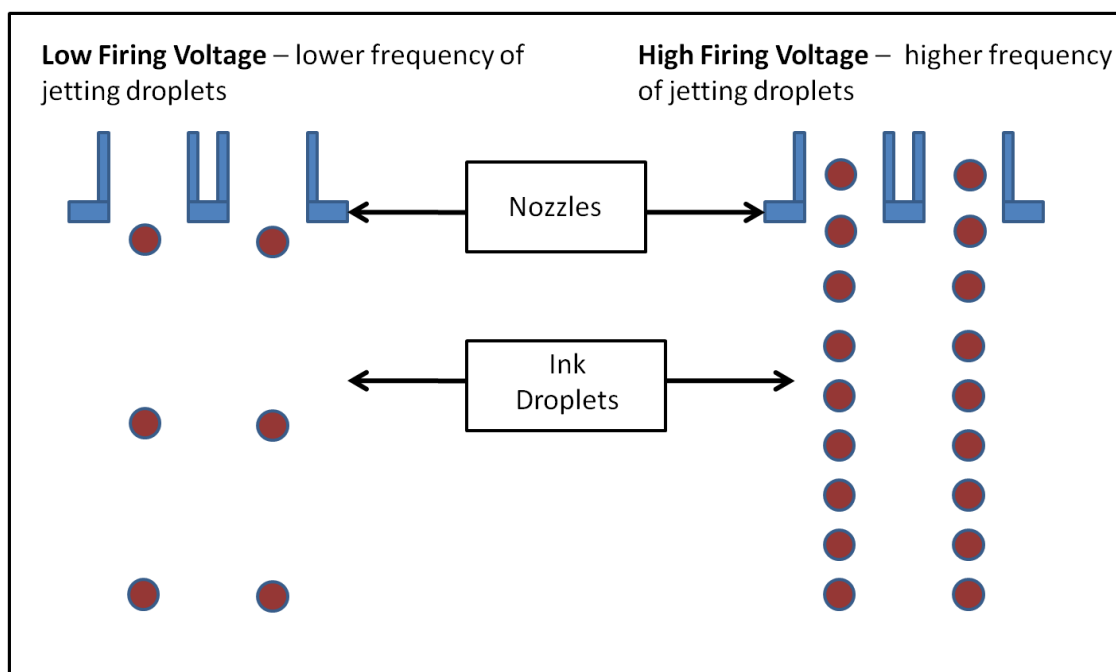
Figure 3.2: Cartoon describing the effect of inkjet cartridge firing voltage on the jetting of materials

A piezo-electric diaphragm controls the frequency and velocity with which ink is jetted out of the nozzles [51]. A voltage is passed through the piezo-electric material, causing it to change shape. This shape change causes material to be ejected out of the nozzle. The higher the firing voltage, the more material is shot out of the nozzle per drop. Higher firing voltages may be used to inkjet inks of higher viscosities[5].

Thus for each different concentration of ink used, and each different solvent mixture that has its own wetting characteristics, there is a different range of drop spacing and firing voltages that can be used to yield uniform, pinhole free-free films. Here, for an ink concentration of 15mg/ml and a solvent system of 68% oDCB and 32% mesitylene, the drop spacing and firing voltage were selected by conducting a screening experiment for the different settings. The results are outlined in the "Results and Discussion" section, in Tables 3.2 and 3.3.

3.4 Results and Discussion

3.4.1 Screening experiment results for the Drop Spacing and Firing Voltage

To narrow down the different possible drop spacing and firing voltage ranges that may yield uniform films, the film quality with respect to different drop spacings and firing voltages were recorded using optical microscopy (Table 3.2 and Table 3.3).

Plain glass microscope slides were cleaned by sonication in acetone followed by sonication in IPA. These glass slides were used as the substrates in the screening experiment. The printer platen temperature was set at $40^{o}C$.

$5mm^2$ squares were printed onto the substrates by varying the drop spacing and firing voltage. The concentration of the ink was 15mg/ml P3HT:PCBM dissolved in a 1:0.8 w/w ratio. Solvent was 68% oDCB and 32% mesitylene. (See following sections on "Device making process" and "Effect of platen temperature...")

For the first iteration, the Drop Spacing was set to 20µm and the Firing Voltage was varied between 8 Volts and 20 Volts. Empirically, it was determined that for "high" firing voltages of 15V and 20V, excess materials were deposited resulting in concentrated material build up at the center of the dried film. This is not ideal for 2 reasons: (i) the final film is non-uniform and (ii) excess material is used. Thus, in the second iteration, "lower" firing voltages (8V and 10V) were now kept constant, and the drop spacing was varied between 10µm and 30µm. The results are tabulated as follows:

Table 3.2 : Effect of changing drop spacing and firing voltage on final dried inkjet-printed P3HT:PCBM films.

		Firing Voltage			
		8	10	15	20
Drop Spacing	10	🟨	🟨		
	15	🟩	🟨		
	18	🟥	🟩		
	20	🟥	🟥	🟨	🟨
	25		🟥		
	30	🟥	🟥		

	Untested
🟨	Film is too thick / excess material in centre
🟩	Film is uniform - may be used for printing
🟥	Film has pinholes- may not be used for printing

Table 3.3 : Firing Voltage and Drop Spacing screening experiment results.

Thus, through screening the parameters (as seen in Tables 2 and 3), it was determined that a firing voltage of 10V and a drop spacing of 18μm was appropriate for reproducibly yielding uniform printed films.

3.4.2 Device making process

ITO glass substrates, $(24mm)^2$ in area were cleaned by sonicating for 30 minutes in acetone followed by a 30 minute sonication in IPA. PEDOT:PSS solution (Baytron PH, σ = 10–100Scm^{-1}, diluted 1:1 with deionized water) was spin-coated onto the cleaned ITO substrates at 4000 rpm for 30 seconds, in air. These films were then left to dry on a hotplate at 160°C for 20 minutes.

Inkjet Printing of the P3HT:PCBM inks was done using a Dimatix 2831 Materials Printer in the open air. The ink was printed onto the PEDOT: PSS-coated ITO substrates using a Drop Spacing of 18μm. The firing voltage was set at 10 Volts and the platen temperature at 40°C. Finally, the dried films were then transferred to an inert atmosphere followed by deposition of a 150nm thick aluminum top electrode. Aluminum (pellets, used as purchased from Alfa Aesar Puratronic,

alumina shot, 4-8mm, 99.999% purity) was evaporated under a low pressure (<10−6 Torr) to form the top electrode. The evaporator used was an Angstrom vacuum deposition system, Model numberS6458, powered by an Inficon SQC-310 Deposition Controller, and vacuum controlled with a Varian Turbo-V 81-AG turbomolecular pump.

3.4.3 Film Thickness

The Dimatix 2831 has a line-by-line rastering pattern of material deposition. To print a square P3HT:PCBM active layer square of 20mm^2, it can take up to 100 passes to complete the print, wherein a single line is printed in each pass. Thus, the thin film thickness gets affected by how quickly each individual line dries, and by the re-dissolution of material when the next successive line is printed. It is assumed that the inkjet droplet has a volume of 10 picoliters = 10^{13}nm^3. For the purpose of rough calculation, if the drop is considered to be a cube, it will have a height (thickness) of ~21544nm. The droplet, once deposited onto the substrate, spreads out due to wetting; thus the wet film thickness decreases. If it is assumed that the height/thickness is decreased by 50%, the wet film thickness will be ~10772nm or 10.7μm. The dry film thickness can then be calculated using the following formula

$$Dry\ Film\ Thickness = (Wet\ Film\ Thickness) * (Volume\%\ Solid\ Loading\ Fraction\ of\ ink)$$

Thus, if the ink has a solid loading of 1.5%, and a wet film thickness of 10.7μm, the final dry film thickness comes out to ~161.6nm.

3.4.4 Effect of Platen Temperature on the drying of wet films

Another printing parameter that was briefly investigated was the platen temperature of the inkjet printer. The platen's (substrate holder) temperature can be regulated. Once the substrate temperature has been set, the printer will not print until the substrate has reached the set temperature. Substrate temperature is very crucial to printing, as film formation is dependent on both solvent components as well as substrate temperature. Unoptimized substrate temperatures lead to films that dry either too fast, where the solvent dries much too quickly leaving behind gaps or too slow where the materials are given time to crystallize out of the solvent without forming a uniform film. The platen temperature for the Dimatix 2831 has an upper limit of 60°C.

For the first iteration, the devices were printed onto a platen temperature set arbitrarily at 50°C.Visually, it was observed that the film solution rapidly accumulated at the center of the substrate. This caused the material to be highly concentrated in the middle of the film and much more thin at the edges of the film - an oversight on the author's part, as this phenomenon had already been outlined by Hoth et al. [5,12] . For the given solvent system of 68% oDCB and 32% mesitylene, they empirically found that the optimum temperature setting was at 40°C. At 40°C, the film formation was much more uniform as the materials were deposited evenly across the surface of the substrate.

Thus for the second iteration, the films were printed onto the platen set at a temperature of 40°C, and the films were visually observed to be much more smooth and uniform. This confirms the applicability of Hoth's approach for our system.

Outlined below are the device results obtained from different platen temperatures; the more uniform devices obtained at 40°C yielded higher efficiencies due to the more uniform contact

between the aluminum electrodes and the printed film. it was found that the power conversion efficiencies of the devices increased from 0.32% (for the films printed at 50°C) to 0.67%(for the films printed at 40°C).This is also attributed to the increase in the open circuit voltage shown in Figure 3.4 and Table 3.4.
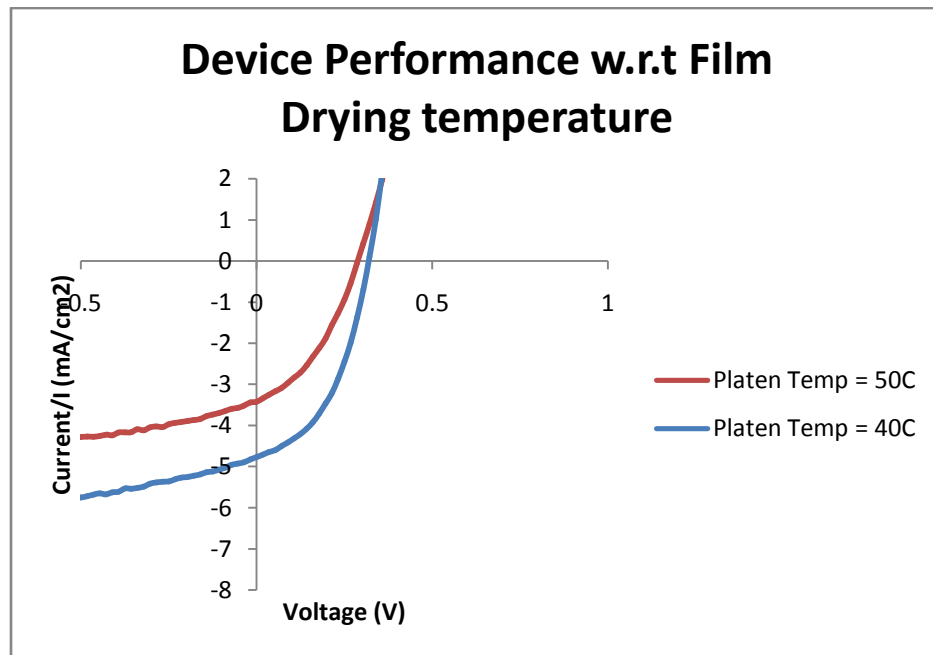
Figure 3.3: J/V Curves of devices measured with respect to the platen heating temperature.

PCE w.r.t Drying Temperature of wet film

Voc w.r.t Drying Temperature of wet film
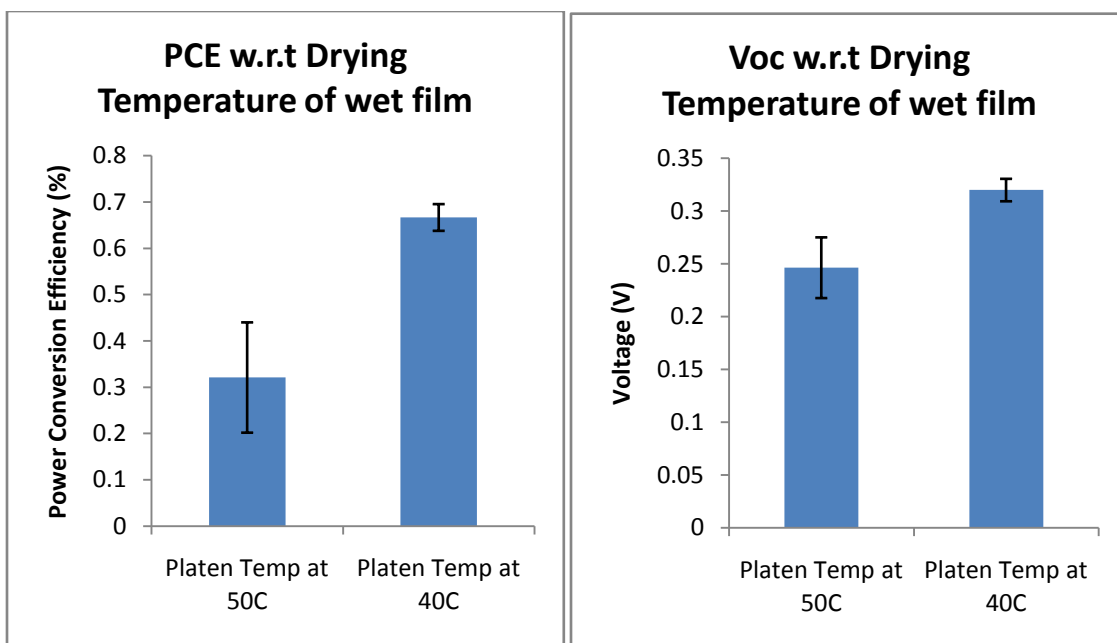
Platen Temperature	PCE%	Voc (V)
50°C	0.321 +/- (0.119)	0.246 +/- (0.028)
40°C	0.667 +/- (0.028)	0.320 +/- (0.010)

Table 3.4 : PCE and Voc tabulated with respect to the platen heating temperature

3.4.5 Inkjet-Printed device performance with respect to further annealing of printed films

In bulk heterojunction organic photovoltaics, the physical [40],optical [39] and electrical properties of the active layer films[41] exhibit a strong structure-property relation with the morphology of the active layer. Thus miniscule changes within the morphology/arrangement of molecules within the active layer result in changes in the aforementioned properties, and finally the device performance. For P3HT:PCBM based systems, it is common for device performance to be improved by modifying and reordering the nanoscale morphology of the bulk heterojunction. This restructuring of the morphology can be accomplished through processes such as (i) thermal Annealing [6,31,32], (ii) solvent Annealing [33,34] and through the addition of (iii) processing additives [35,36,37,38].

In freshly processed films, it is found that the PCBM negatively impacts the hole mobility of the P3HT due to the disruption of the P3HT crystallinity. By annealing and reordering the nanoscale morphology of the active layer, the P3HT and PCBM phases may be optimally arranged [6] such that the hole mobility of the P3HT increases and gives rise to a higher device efficiency. On the other hand, the diffusivity of the PCBM, the functional groups present on the fullerene, and the molecular weight of the P3HT all influence how well the PCBM "mixes" with the P3HT and thus determines the ease or difficulty with which the PCBM is able to disrupt the crystallinity of the P3HT on the nanoscale. Through annealing, the PCBM can be induced to diffuse out of the P3HT chains and allow the P3HT to reorganize in a device-favorable morphology [42]. A note must be made here about "optimal" phase separation through annealing - if the annealing process is carried out for an extensive period of time, the favorable nanoscale phase separation will convert to unfavorable micrometer-scale phase seperation [43] resulting in poor device efficiencies.

Similarly, Jenny Nelson outlined the relation between the nanoscale morphology and the charge mobility through the P3HT [44]; according to Lilliu et al.[45], the hole mobility within the P3HT is highly anisotropic and is greatest along the backbone of the polymer chain. By rearranging the morphology of the P3HT:PCBM and improving the conjugation between individual P3HT chains, highly efficient devices were fabricated[46].

This rearrangement of the molecules is also reflected in the open circuit voltage of the OPV. A "higher" short-circuit current Voc indicates a higher driving force for charge separation between the P3HT and PCBM. The Voc is directly related to the energy band gap between the LUMO of the P3HT and the LUMO of the PCBM [47]. This is shown in Figure 3.5.
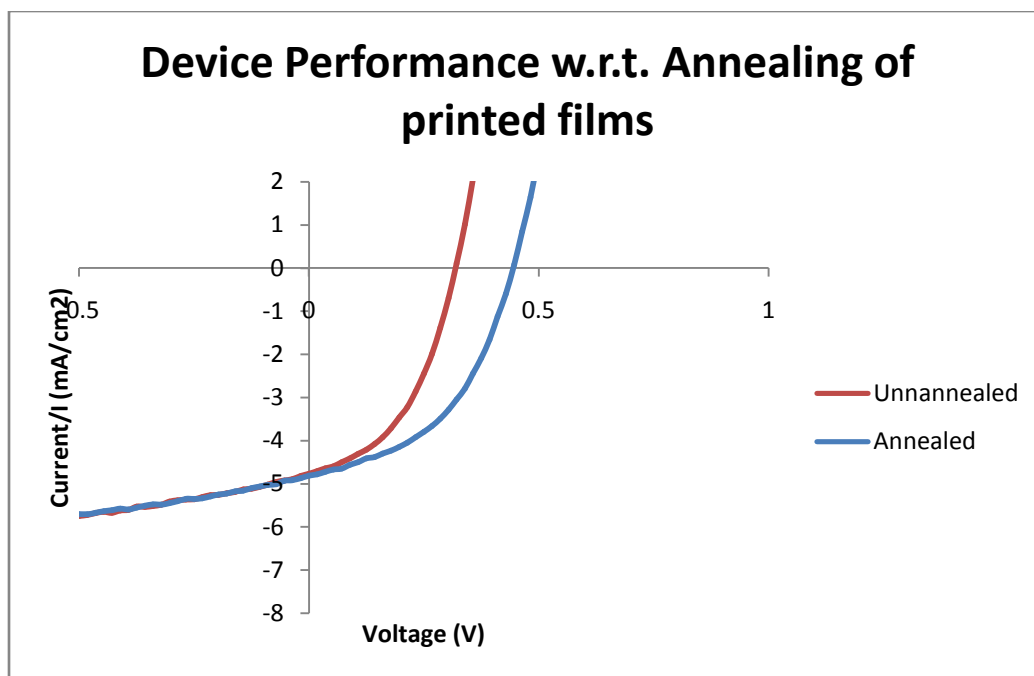
Figure 3.4 : J/V Curves of devices measured with respect to post-annealing of completed devices
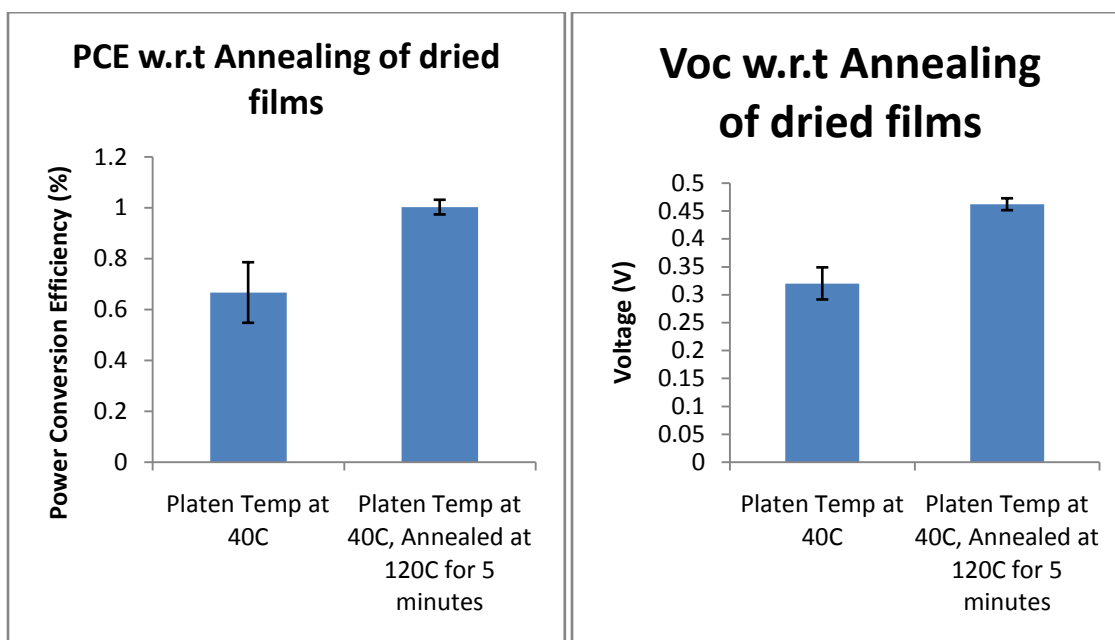
	PCE%	Voc (V)
Unannealed	0.667 +/- (0.028)	0.320 +/- (0.010)
Annealed at 120°C	1.002 +/- (0.018)	0.462 +/- (0.023)

Table 3.5 : PCE and Voc tabulated with respect to the post-annealing of completed devices

For the thesis, the inkjet-printed devices were subjected to thermal annealing to investigate the change in device performance. The completed OPV devices were placed on a hotplate set at $120^{\circ}C$ for 5 minutes, with references [5,12] used as a guideline for the annealing parameters. The annealed devices were then measured for their power conversion efficiency, open circuit voltage and short circuit current. The PCE% improves from 0.67% to 1.00%. There is also an increase in the open circuit voltage from 0.32V to 0.46V.

These trends show good correlation with the phase separation studies referenced; thus, the potential for further improving inkjet-printed device efficiency through thermal annealing was investigated and validated.

3.5 Conclusion and future work with solvent based Inkjet printing

A malfunctioning DIMATIX 2831 inkjet printer was repaired and used to successfully fabricate functioning P3HT:PCBM-based organic photovoltaic devices. The solvent system for the ink was chosen based on the methodology put forward by Hoth et al. Inkjet Printing parameters such as drop spacing and firing voltage were investigated. The settings for yielding a uniform film visually devoid of pinholes and film forming defects were obtained. The film thickness was estimated to be around ~160nm in thickness. After optimizing the platen temperature and annealing the printed films, the best power conversion efficiency of the devices was seen to peak at around 1.03%. Thus the inkjet printing method is validated for the first time in this research group.

The results obtained from this thesis chapter can be used as a baseline or "jumping off point" for further studies. By identifying the new variables (i.e. ones that are not obvious in spin-coating) that arise from inkjet–printing,i.e film formation influenced by drop spacing and firing voltage, film thickness variation due to changing concentrations of inks,a more in depth iteration of

study can be conducted in the future. By iteratively and systematically tweaking the printing parameters, more promising OPV materials may be investigated using this method. P3HT being a semi-crystalline donor material may "print" much differently than some of the new OPV materials currently being studied such as poly (2, 5-bis (3-hexadecylthiophen-2-yl) thieno [3, 2-b] thiophene (pBTTT), and squarylium dye based donor materials [28,29,30]. Very little study has been conducted on the much more crystalline [29] and small-molecule[30] materials, in terms of printing.This will pose new challenges when considering the final goal of roll-to-roll processability of materials. By validating new and novel materials using a roll-to-roll processing technique such as inkjet printing, decisions can be taken in improving molecule design to be more suited for large scale processing methods. (See Chapter 5)

3.6 REFERENCES

[1] Hoth, Claudia N., Stelios A. Choulis, Pavel Schilinsky, and Christoph J. Brabec. "High photovoltaic performance of inkjet printed polymer: fullerene blends." *Advanced Materials* 19, no. 22 (2007): 3973-3978.

[2] Yang, Junliang, DoojinVak, Noel Clark, Jegadesan Subbiah, Wallace WH Wong, David J. Jones, Scott E. Watkins, and Gerry Wilson. "Organic photovoltaic modules fabricated by an industrial gravure printing proofer." *Solar Energy Materials and Solar Cells* 109 (2013): 47-55.

[3] Krebs, Frederik C. "Fabrication and processing of polymer solar cells: a review of printing and coating techniques." *Solar Energy Materials and Solar Cells* 93, no. 4 (2009): 394-412.

[4]Søndergaard, Roar R., Markus Hösel, and Frederik C. Krebs. "Roll-to-Roll fabrication of large area functional organic materials." *Journal of Polymer Science Part B: Polymer Physics* 51, no. 1 (2013): 16-34.

[5]Hoth, Claudia N., Pavel Schilinsky, Stelios A. Choulis, and Christoph J. Brabec. "Printing highly efficient organic solar cells." *Nano letters* 8, no. 9 (2008): 2806-2813.

[6]Müller, Christian, Toby AM Ferenczi, Mariano Campoy-Quiles, Jarvist M. Frost, Donal DC Bradley, Paul Smith, Natalie Stingelin-Stutzmann, and Jenny Nelson. "Binary organic photovoltaic blends: a simple rationale for optimum compositions." *Advanced Materials* 20, no. 18 (2008): 3510-3515.

[7]Lim, Guan-Hui, Jing-Mei Zhuo, Loke-Yuen Wong, Soo-Jin Chua, Lay-Lay Chua, and Peter KH Ho. "A transition solvent strategy to print polymer: fullerene films using halogen-free solvents for solar cell applications." *Organic electronics* 15, no. 2 (2014): 449-460.

[8] Lange, Alexander, Wolfram Schindler, Michael Wegener, Konstantinos Fostiropoulos, and Silvia Janietz. "Inkjet printed solar cell active layers prepared from chlorine-free solvent systems." *Solar Energy Materials and Solar Cells* 109 (2013): 104-110.

[9]Lange, Alexander, Michael Wegener, Christine Boeffel, Bert Fischer, Armin Wedel, and Dieter Neher. "A new approach to the solvent system for inkjet-printed P3HT: PCBM solar cells and its use in devices with printed passive and active layers." *Solar energy materials and solar cells* 94, no. 10 (2010): 1816-1821.

[10]Aernouts, Tom, Tsvetan Aleksandrov, Claudio Girotto, Jan Genoe, and Jozef Poortmans. "Polymer based organic solar cells using ink-jet printed active layers." *Applied Physics Letters* 92, no. 3 (2008): 033306.

[11] Lange, Alexander, Wolfram Schindler, Michael Wegener, Konstantinos Fostiropoulos, and Silvia Janietz. "Inkjet printed solar cell active layers based on a novel, amorphous polymer." *Journal of nanoscience and nanotechnology*13, no. 7 (2013): 5209-5214.

[12]Hoth, Claudia N., Stelios A. Choulis, Pavel Schilinsky, and Christoph J. Brabec. "On the effect of poly (3-hexylthiophene) regioregularity on inkjet printed organic solar cells." *Journal of Materials Chemistry* 19, no. 30 (2009): 5398-5404.

[13]You, Jingbi, Letian Dou, Ziruo Hong, Gang Li, and Yang Yang. "Recent trends in polymer tandem solar cells research." Progress in polymer science 38, no. 12 (2013): 1909-1928.

[14]You, Jingbi, Letian Dou, Ken Yoshimura, Takehito Kato, Kenichiro Ohya, Tom Moriarty, Keith Emery et al. "A polymer tandem solar cell with 10.6% power conversion efficiency." *Nature communications* 4 (2013): 1446.

[15] Teichler, Anke, Rebecca Eckardt, Stephanie Hoeppener, Christian Friebe, JolkePerelaer, AlessiaSenes, Mauro Morana, Christoph J. Brabec, and Ulrich S. Schubert. "Combinatorial screening of polymer: fullerene blends for organic solar cells by inkjet printing." *Advanced Energy Materials* 1, no. 1 (2011): 105-114.

[16] Yang, Junliang, Doojin Vak, Noel Clark, Jegadesan Subbiah, Wallace WH Wong, David J. Jones, Scott E. Watkins, and Gerry Wilson. "Organic photovoltaic modules fabricated by an industrial gravure printing proofer." *Solar Energy Materials and Solar Cells* 109 (2013): 47-55.

[17]Bundgaard, Eva, Francesco Livi, Ole Hagemann, Jon E. Carlé, Martin Helgesen, Ilona M. Heckler, Natalia K. Zawacka et al. "Matrix Organization and Merit Factor Evaluation as a Method to Address the Challenge of Finding a Polymer Material for Roll Coated Polymer Solar Cells." *Advanced Energy Materials* 5, no. 10 (2015).

[18]Choi, Hyung Woo, Tianlei Zhou, Madhusudan Singh, and Ghassan E. Jabbour. "Recent developments and directions in printed nanomaterials." *Nanoscale* 7, no. 8 (2015): 3338-3355.

[19]Dang, Minh Trung, Lionel Hirsch, and Guillaume Wantz. "P3HT: PCBM, best seller in polymer photovoltaic research." *Advanced Materials* 23, no. 31 (2011): 3597-3602.

[20] Teichler, Anke, Rebecca Eckardt, Christian Friebe, Jolke Perelaer, and Ulrich S. Schubert. "Film formation properties of inkjet printed poly (phenylene-ethynylene)-poly (phenylene-vinylene) s." *Thin Solid Films* 519, no. 11 (2011): 3695-3702.

[21] Søndergaard, Roar, Markus Hösel, Dechan Angmo, Thue T. Larsen-Olsen, and Frederik C. Krebs. "Roll-to-roll fabrication of polymer solar cells." *Materials today* 15, no. 1 (2012): 36-49.

[22] Deegan, Robert D., Olgica Bakajin, Todd F. Dupont, Greb Huber, Sidney R. Nagel, and Thomas A. Witten. "Capillary flow as the cause of ring stains from dried liquid drops." *Nature* 389, no. 6653 (1997): 827-829.

[23]Yunker, Peter J., Tim Still, Matthew A. Lohr, and A. G. Yodh. "Suppression of the coffee-ring effect by shape-dependent capillary interactions." *Nature* 476, no. 7360 (2011): 308-311.

[24]Hu, Hua, and Ronald G. Larson. "Marangoni effect reverses coffee-ring depositions." *The Journal of Physical Chemistry B* 110, no. 14 (2006): 7090-7094.

[25]Still, Tim, Peter J. Yunker, and Arjun G. Yodh. "Surfactant-induced Marangoni eddies alter the coffee-rings of evaporating colloidal drops." *Langmuir* 28, no. 11 (2012): 4984-4988.

[26] Li, Yueh-Feng, Yu-Jane Sheng, and Heng-KwongTsao. "Evaporation stains: suppressing the coffee-ring effect by contact angle hysteresis." *Langmuir* 29, no. 25 (2013): 7802-7811.

[27]Tekin, Emine, Patrick J. Smith, and Ulrich S. Schubert. "Inkjet printing as a deposition and patterning tool for polymers and inorganic particles." *Soft Matter*4, no. 4 (2008): 703-713.

[28]Cates, Nichole C., Roman Gysel, Zach Beiley, Chad E. Miller, Michael F. Toney, Martin Heeney, Iain McCulloch, and Michael D. McGehee. "Tuning the properties of polymer bulk heterojunction solar cells by adjusting fullerene size to control intercalation." *Nano letters* 9, no. 12 (2009): 4153-4157.

[29]Chen, Guo, Hisahiro Sasabe, Zhongqiang Wang, Xiaofeng Wang, Ziruo Hong, Junji Kido, and Yang Yang. "Solution-processed organic photovoltaic cells based on a squaraine dye." *Physical Chemistry Chemical Physics* 14, no. 42 (2012): 14661-14666.

[30]Zheng, Chenyu, Anirudh Raju Penmetcha, Brandon Cona, Susan D. Spencer, Bi Zhu, Patrick Heaphy, Jeremy A. Cody, and Christopher J. Collison. "Contribution of Aggregate States and Energetic Disorder to a Squaraine System Targeted for Organic Photovoltaic Devices." *Langmuir* 31, no. 28 (2015): 7717-7726.

[31] Keivanidis, Panagiotis E., Tracey M. Clarke, SamueleLilliu, TizianoAgostinelli, J. Emyr Macdonald, James R. Durrant, Donal DC Bradley, and Jenny Nelson. "Dependence of charge separation efficiency on film microstructure in poly (3-hexylthiophene-2, 5-diyl):[6, 6]-phenyl-C61 butyric acid methyl ester blend films." *The Journal of Physical Chemistry Letters* 1, no. 4 (2010): 734-738.

[32] Clarke, Tracey M., Amy M. Ballantyne, Jenny Nelson, Donal DC Bradley, and James R. Durrant. "Free energy control of charge photogeneration in polythiophene/fullerene solar cells: the influence of thermal annealing on P3HT/PCBM blends." *Advanced Functional Materials* 18, no. 24 (2008): 4029-4035.

[33] Li, Gang, Yan Yao, Hoichang Yang, Vishal Shrotriya, Guanwen Yang, and Yang Yang. "" Solvent annealing" effect in polymer solar cells based on poly (3-hexylthiophene) and methanofullerenes." *Advanced Functional Materials* 17, no. 10 (2007): 1636.

[34] Nam, Sooji, Jaeyoung Jang, Hyojung Cha, Jihun Hwang, Tae KyuAn, Seonuk Park, and Chan Eon Park. "Effects of direct solvent exposure on the nanoscale morphologies and electrical characteristics of PCBM-based transistors and photovoltaics." *Journal of Materials Chemistry* 22, no. 12 (2012): 5543-5549.

[35] Peet, Jeffery, Jin Young Kim, Nelson E. Coates, Wang Li Ma, Daniel Moses, Alan J. Heeger, and Guillermo C. Bazan. "Efficiency enhancement in low-bandgap polymer solar cells by processing with alkane dithiols." *Nature materials* 6, no. 7 (2007): 497-500.

[36] Hermerschmidt, Felix, Andreas S. Kalogirou, Jie Min, Georgia A. Zissimou, Sachetan M. Tuladhar, TayebehAmeri, Hendrik Faber et al. "4 H-1, 2, 6-Thiadiazin-4-one-containing small molecule donors and additive effects on their performance in solution-processed organic solar cells." *Journal of Materials Chemistry C* 3, no. 10 (2015): 2358-2365.

[37] Chen, Hsiang-Yu, Hoichang Yang, Guanwen Yang, Srinivas Sista, Ruben Zadoyan, Gang Li, and Yang Yang. "Fast-grown interpenetrating network in poly (3-hexylthiophene): methanofullerenes solar cells processed with additive." *The Journal of Physical Chemistry C* 113, no. 18 (2009): 7946-7953.

[38] Guo, Xia, Chaohua Cui, Maojie Zhang, LijunHuo, Ye Huang, JianhuiHou, and Yongfang Li. "High efficiency polymer solar cells based on poly (3-hexylthiophene)/indene-C 70 bisadduct with solvent additive." *Energy & Environmental Science* 5, no. 7 (2012): 7943-7949.

[39] Niles, Edwards T., John D. Roehling, Hajime Yamagata, Adam J. Wise, Frank C. Spano, Adam J. Moulé, and John K. Grey. "J-aggregate behavior in poly-3-hexylthiophene nanofibers." *The Journal of Physical Chemistry Letters* 3, no. 2 (2012): 259-263.

[40] Scharsich, Christina, Ruth H. Lohwasser, Michael Sommer, UdomAsawapirom, Ullrich Scherf, MukundanThelakkat, Dieter Neher, and Anna Köhler. "Control of aggregate formation in poly (3-hexylthiophene) by solvent, molecular weight, and synthetic method." *Journal of Polymer Science Part B: Polymer Physics* 50, no. 6 (2012): 442-453.

[41] Sirringhaus, Henning, P. J. Brown, R. H. Friend, Martin Meedom Nielsen, KlaasBechgaard, B. M. W. Langeveld-Voss, A. J. H. Spiering et al. "Two-dimensional charge transport in self-organized, high-mobility conjugated polymers." *Nature* 401, no. 6754 (1999): 685-688.

[42] Watts, Benjamin, Warwick J. Belcher, Lars Thomsen, Harald Ade, and Paul C. Dastoor. "A quantitative study of PCBM diffusion during annealing of P3HT: PCBM blend films." *Macromolecules* 42, no. 21 (2009): 8392-8397.

[43] Huang, Yu-Ching, Yu-Chia Liao, Shao-Sian Li, Ming-Chung Wu, Chun-Wei Chen, and Wei-Fang Su. "Study of the effect of annealing process on the performance of P3HT/PCBM photovoltaic devices using scanning-probe microscopy." *Solar Energy Materials and Solar Cells* 93, no. 6 (2009): 888-892.

[44] Nelson, Jenny. "Organic photovoltaic films." *Current Opinion in Solid State and Materials Science* 6, no. 1 (2002): 87-95.

[45] Lilliu, Samuele, Tiziano Agostinelli, Ellis Pires, Mark Hampton, Jenny Nelson, and J. Emyr Macdonald. "Dynamics of crystallization and disorder during annealing of P3HT/PCBM bulk heterojunctions." *Macromolecules* 44, no. 8 (2011): 2725-2734.

[46] Campoy-Quiles, Mariano, Toby Ferenczi, TizianoAgostinelli, Pablo G. Etchegoin, Youngkyoo Kim, Thomas D. Anthopoulos, Paul N. Stavrinou, Donal DC Bradley, and Jenny Nelson. "Morphology evolution via self-organization and lateral and vertical diffusion in polymer: fullerene solar cell blends." *Nature materials* 7, no. 2 (2008): 158-164.

[47] Peumans, Peter, Aharon Yakimov, and Stephen R. Forrest. "Small molecular weight organic thin-film photodetectors and solar cells." *Journal of Applied Physics* 93, no. 7 (2003): 3693-3723.

[48] Espinosa, Nieves, Frank O. Lenzmann, Stephen Ryley, DechanAngmo, Markus Hösel, Roar R. Søndergaard, Dennis Huss et al. "OPV for mobile applications: an evaluation of roll-to-roll processed indium and silver free polymer solar cells through analysis of life cycle, cost and layer quality using inline optical and functional inspection tools." *Journal of Materials Chemistry A*1, no. 24 (2013): 7037-7049.

[49]Zhu, Rui, Chang-Yun Jiang, Xi-Zhe Liu, Bin Liu, Abhishek Kumar, and Seeram Ramakrishna. "Improved adhesion of interconnected TiO2 nanofiber network on conductive substrate and its application in polymer photovoltaic devices."*Applied physics letters* 93, no. 1 (2008): 013102.

[50] Hall, David B., Patrick Underhill, and John M. Torkelson. "Spin coating of thin and ultrathin polymer films." *Polymer Engineering and Science* 38, no. 12 (1998): 2039-2045.

[51] https://www.fujifilmusa.com/shared/bin/PDS00085-DMP2831.pdf

CHAPTER 4 - Inkjet Printing of Organic Photovoltaics using water based inks

ABSTRACT/OBJECTIVE - P3HT: PCBM nanoparticle based inks were fabricated using the miniemulsion technique. The nanoparticles were characterized for their size using a quasi-elastic light scattering technique. The average diameter of P3HT:PCBM nanoparticles was found to be 52nm. The blending of the P3HT and the PCBM was tested using UV-Vis absorbance and fluorescence spectroscopy – it was found that the blend ratio of the nanoparticle can be controlled by varying the individual concentrations of the P3HT and PCBM in chloroform ("the oil phase") of the miniemulsions. Finally the P3HT:PCBM nanoparticle inks were spin coated/inkjet printed onto PEDOT:PSS coated ITO substrates to form the active layer of the organic photovoltaic cell. Aluminum cathodes were evaporated onto the printed nanoparticle active layer film to form functioning OPVs.

4.1 Introduction

Life cycle analyses for polymer solar cells conducted by Espinosa et al. [1,2] revealed some interesting results. According to the study, the projected increase in the energy demand between the years 2011 and 2050 is on the order of 1 GW a day - equivalent to building a new nuclear power plant every day for the span of 40 years. The study hypothesized that if the current challenges plaguing organic photovoltaics (stability, performance, processability)[4] were addressed, then OPVs could potentially have an energy payback time anywhere between 7 to 1 days i.e. the energy it would take to manufacture 1 GW worth of OPV modules can be reclaimed within 7 to 1 days. One of the issues mentioned was processability: most OPV materials are currently being processed by dissolving them in aromatic and/or chlorinated [3] solvents. This poses major long term issues when it comes to manufacturing OPV on a large scale. The most apparent issue is that the solvents are not friendly towards the environment; aromatic solvents such as toluene, benzene etc. are inflammable whereas chlorinated solvents such as chloroform, chlorobenzene and dichlorobenzene are carcinogenic, posing severe threats to human health. Secondly, to come close to a target OPV production of "1 GW a day", 16 million gallons of chlorinated solvents would be needed to produce 1 GW worth of OPV. A logical solution to this would be to design materials which are soluble in relatively "non-toxic" solvents such as water, ethanol and isopropanol. By solubilizing the materials through addition of (i) ionic side chains (such as sulfonic acids, carboxylic acids) or (ii) by the addition of nonionic alcohol and/or glycol side chains, the materials may conceivably be processed using water[3]. However, this would result in a complete paradigm shift in terms of OPV materials design, where the solvent-material interaction, film formation and device performance would have to be completely rethought. There would also be a significant effort and time cost associated with the synthesis of the necessary new materials. To overcome this challenge, an intermediate

solution is proposed: the *currently-used* active layer materials may be *dispersed* in water, thereby bypassing the usage of harmful organic solvents.

This chapter's study describes two goals. Firstly, to formulate and characterize a water-based nanoparticle ink consisting of poly(3-hexylthiophene-2,5-diyl) as the donor (P3HT) and phenyl-C61-butyric acid methyl ester as the acceptor (PCBM). Blending of the PCBM within the P3HT nanoparticle was confirmed by UV-Vis absorbance and fluorescence spectroscopy – it is crucial that the PCBM is sufficiently blended within the P3HT so that the P3HT:PCBM domains within the nanoparticle may be further optimized by annealing and phase separation of the PCBM within the P3HT [5].

The second goal is to fabricate working devices out of the P3HT:PCBM nanoparticle inks. These inks are spin coated as well as inkjet printed onto poly(3,4-ethylenedioxythiophene) polystyrene sulfonate (PEDOT:PSS) coated indium tin oxide (ITO) substrates. Here, inkjet printing is used as the "roll-to-roll analogue" instead of conventional coating techniques such as slot-die coating and screen printing [7]. Inkjet printing is a non-contact method of printing; less material is wasted in inkjet printing because the printer is designed to "drop-on-demand" and requires only 2-3ml of formulated ink to print devices - this makes it very convenient to pattern the substrate. Aluminum cathodes are evaporated onto these active layer films to form OPV devices. These devices are characterized for their power conversion efficiencies.

4.2 Dispersing active layer materials in water using the miniemulsion method

The miniemulsion method is a versatile approach for fabricating organic (polymer/small molecule) nanoparticles dispersed in aqueous solvents. These emulsions are made as follows: the target material (which needs to be dispersed) is first dissolved in the appropriate solvent. This is called the "oil-phase". The oil-phase is highly immiscible with the water due to the

interfacial tension between the two phases. (the continuous phase). This interfacial tension is reduced by adding emulsifying agents (or surfactants); finally, by applying high shear, the oil-water-surfactant mixture can be homogenized to form a stable suspension of oil-phase droplets within the water.

According to Landfester [6], the homogenization step is critical for obtaining a highly monodisperse, small-size droplets within the miniemulsion. By applying a high shear (either through ultrasonication or high-pressure homogenization) the polydispersity of the suspended droplets is gradually reduced (by constant fusion and fission of the droplets) until a steady state is reached, where the final size distribution will not change much even with extended application of shear[8]. Another factor that influences the final droplet/particle size is the surfactants/emulsifying agents that are used - by varying the type of the surfactant i.e. anionic/cationic/nonionic and the *concentration* of the materials, the particle sizes can be influenced (see Chapter 5).

4.3 Literature Review

The miniemulsion approach is quickly becoming a popular method of fabricating OPV; some of the pertinent academic findings are listed below and were used by the author to develop a basic understanding of nanoparticle-based OPV.

Kietzke et al. in collaboration with Landfester et al. [12,13] were the first researchers to report on nanoparticle-based OPV. They pioneered the miniemulsion method; working OPV devices were fabricated using M3EH-PPV (poly[2,5-dimethoxy-1,4-phenylene-1,2-ethenylene-2-methoxy-5-(2-ethylhexyloxy)–(1,4-phenylene-1,2-ethenylene)]) as the hole-accepting material (donor) and   CN-Ether-PPV(poly[oxa-1,4-phenylene-1,2-(1-cyano)ethenylene-2,5-dioctyloxy-1,4-phenylene-1,2-(2-cyano)ethenylene-1,4-phenylene]) as the electron-accepting

material (acceptor). The highest external quantum efficiency obtained using this method was 14%.

In the next iteration of study [14,15], Kietzke et al. showed that the device performance varied heavily depending on the *blending* of the nanoparticles, using PFB [poly(9,9-dioctylfluorene-2,7-diyl-co-bis-N,N'-(4-butylphenyl)-bis-N,N'-phenyl-1,4-phenylenediamine)] as the donor and F8BT [poly-(9,9 dioctylfluorene-2,7-diyl-co-benzothiadiazole)] as the acceptor. In a study comparing devices made from separate donor and acceptor particles with devices made from particles containing both the donor:acceptor blended within the same particle, it was shown that the blended particles performed much more efficiently. They concluded that the length scales of charge dissociation between the donor and acceptor are much smaller in the case of blending due to the larger donor:acceptor interface surface area. This larger interfacial area was more favorable for efficient extraction of charge from the OPV device. The power conversion efficiencies for these devices peaked at ~0.004%.[16]

Since the seminal work of Kietzke, Paul Dastoor and colleagues began to champion the concept of "solar paints" - they were able to adapt the miniemulsion method to yield highly efficient OPVs, as compared to the preliminary attempts by Kietzke et al. From the year 2010 to present day, the Dastoor group has managed to improve spincoated device efficiency from 0.39% to 2.50% [16]. Some of the salient findings of their work are that the power conversion efficiencies depended on the molecular weights of the donor materials (P3HT) as well as the side-chains present on the acceptor (PCBM) molecules [17]. This heavily influenced the miscibility of the PCBM within the P3HT thereby giving rise to different bulk heterojunction morphologies, and thus different power conversion efficiencies(see Chapter 5). They also determined that the structure of the blended nanoparticle depended on the surface energies of the donor and the

acceptor[18]. PCBM was experimentally shown to form the "core" of the P3HT:PCBM nanoparticle due to it having a higher surface energy than the P3HT.

Excess Surfactant molecules at the Active Layer/ Electrode interface may block generated charge carriers from reaching the electrode

Removal excess surfactant leads to better connected active layer + reduction of trap layer at Active Layer/Electrode interface

Presence of excess surfactant reported to affect packing of nanoparticles in deposited thin film – leads to improperly interconnected active layer

Figure 4.1 - Excess surfactant molecules act as charge traps at the electrode interface [11] and impact the morphology and connectivity of the dried nanoparticle film [9]

Feron et al. [11] showed that the presence of impurities and defects/improper connection at the cathode/bulk-heterojunction active layer interface gave rise to an "s-shaped" J/V curve, indicative of charge traps, as shown in Figure 4.1. These charge traps caused loss in fill factor as well as deterioration of power conversion efficiency in OPV devices. This is relevant to nanoparticulate devices as well; the morphology of nanoparticulate films may not provide an optimum interface with the cathode materials deposited on top of the active layer, thus giving rise to suboptimal device performance. By adding more interfacial layers between the active layer and the cathode (such as an extra layer of PCBM, Bathocuproine) the interfacial connection can be improved, giving rise to improved device performance.

The aggregation/arrangement of P3HT molecules within the bulk heterojunction of the device is intimately related to the optoelectronic as well as charge transport properties of the device (as

explained in Chapter 3). Nagarjuna et al. [19] showed that this aggregation could be manipulated within the miniemulsion nanoparticles, by manipulating the "oil-phase" solvent. By using an oil-phase solvent mixture consisting of a good solvent and a marginal solvent, highly ordered and monodisperse P3HT aggregates could be obtained (see Chapter 5).

Bag et al. [9] , using TOF (time-of-flight) measurements and photocurrent measurements, showed that the presence of excess surfactant/emulsifying agent within the dispersions heavily impact the device performance. They showed that "good" dispersions were those which had very little excess surfactants present in the final deposited film. It was shown that excess surfactant disrupted the packing of the deposited nanoparticles, thereby impacting the charge transport within particle-to-particle, as shown in Figure 4.1. They also showed that the surfactant present on the surface of the nanoparticles was responsible for disrupting some generated photocurrent by blocking the electrons' path between the active layer and the electrode.

Recently Bag et al. also published a journal article outlining some of the procedures that the Venkataraman group [10] used to fabricate nanoparticle based OPVs. They reported that the methods used by Dastoor et al. were not very reproducible, and that the success of the procedure was highly dependent on the person conducting the experiment itself.

4.4 Importance of Blending between the Donor and Acceptor

There is a large body of published work that alludes to the importance of the blending and domain sizes of the donor and acceptor within the bulk heterojunction of the OPV. In conventional inorganic semiconductors, the binding energy for the generation of free carriers is very small; free charges are generated freely under ambient conditions,upon excitation of the material across the band gap. Organic semiconducting materials on the other hand, possess an

exciton binding energy that needs to be overcome before the free charges are generated (hole-electron dissociation)[21]. A successful pathway of splitting this exciton and generating free charges is at the donor/acceptor interface (see Chapter 2). Other factors that determine the generation of free charge sare the free carrier mobility and lifetime. Diffusion lengths and lifetimes of excited states in organic semiconducting materials are extremely low; typical diffusion lengths of exciton pairs are in the range of 10-20nm [24]. By intimately mixing the donor with the acceptor material, a large surface area of the donor/acceptor interface is obtained[22,23], as well as reducing the average distance that the generated exciton has to travel to reach that interface. This concept of blending is explored in more detail in the later parts of this chapter: it was seen that the miniemulsion method can be used to fabricate blended P3HT:PCBM particles, thereby effectively creating intermixed domains of P3HT and PCBM within a single nanoparticle itself.

4.5 Experimental details

4.5.1 Preparation of P3HT: PCBM nanoparticles using the miniemulsion method
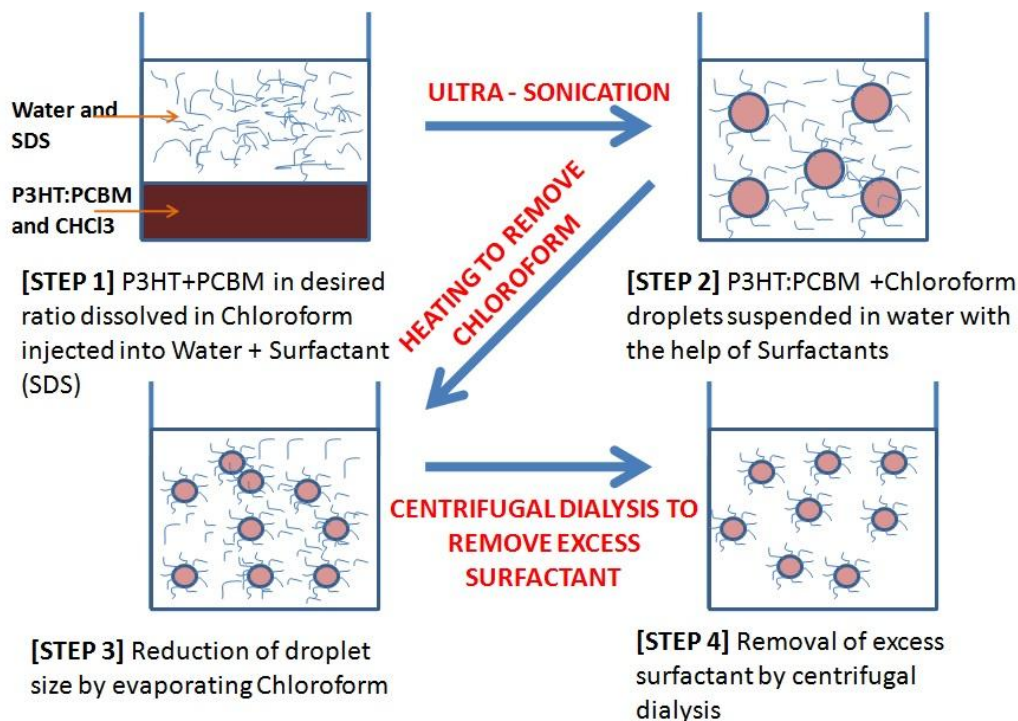
Figure 4.2: Cartoon schematic describing the minimemulsion method of fabricating P3HT:PCBM nanoparticles; adapted from reference [8].

From Figure 4.2, the step wise method for fabricating P3HT:PCBM miniemulsion nanoparticles is

as follows:

[STEP1] - P3HT (highly regioregular poly (3-hexylthiophene-2,5-diyl)) was obtained from Reike

Materials. PCBM (Phenyl-C61-butyric acid methyl ester, 99% pure) was obtained from American

Dye Source. Reagent grade chloroform was obtained from Sigma-Aldrich. SDS (sodium dodecyl

sulfate) was obtained from MP Biomedicals, Inc (Ultra-Pure, M.W = 288.38).

SDS was dissolved in DI water to yield a 40mM concentration solution [17,18].The critical micelle

concentration of SDS in water is 8mM. Thus, to ensure that the P3HT:PCBM is completely

suspended within the micelles, excess SDS is added [17]. P3HTand PCBM can be dissolved using

~ 59 ~

chloroform, in the desired ratio and concentration. The P3HT:PCBM chloroform solution is then injected into the surfactant solution.

BLEND RATIO	Volume of P3HT stock added (mL)	Volume of PCBM stock added (mL)	Extra volume of Chloroform added (mL)
[1:0]	1.00	0	1.00
[1:0.25]	1.00	0.25	0.75
[1:0.50]	1.00	0.50	0.50
[1:0.75]	1.00	0.75	0.25
[1:1]	1.00	1.00	0
[0:1]	0	1.00	1.00

Table 4.1 : A description of the precursor blend solutions used in the formation of nanoparticles of P3HT:PCBM (for blend study). Each precursor blend solution had a final volume of 2mL.

*Stock solutions of P3HT and PCBM dissolved in chloroform with a concentration of 2mg/ml were prepared as shown in Table 4.1. They were then added in the requisite amounts to make a total volume of 2ml. 0.1ml of each of these solutions was injected into 2.78ml of aqueous SDS solution (40mM).*Nanoparticles made using these solutions were used to **investigate the blending and formation of nano-domains within the P3HT:PCBM nanoparticles** , as detailed in the prior section of this thesis chapter*

*P3HT and PCBM in the ratio of 1:0.8 (27mg total) were dissolved in 0.6ml of chloroform; this solution was then injected into 2.78ml of aqueous SDS solution (40mM).*Nanoparticles made using this solution were used in fabricating OPV devices**, as explained in a later section of this chapter.*

[STEP 2] - These mixtures were then subjected to high shear –i.e. they were sonicated using a Misonix Qsonica XL2000 horn sonicator for 50 seconds at a power setting of 3, with a horn tip of 3mm diameter to form miniemulsions.

[STEP 3] - The freshly made miniemulsion samples were heated at 66°C for 90 minutes whilst stirring at 300 rpm to evaporate off the chloroform. The remaining solutions were stable dispersions of P3HT:PCBM nanoparticles. A Ramé-hart Contact Angle Goniometer Model 200, using the sessile pendant drop method (Chapter 2), was used to measure the surface tension of this dispersion. It was found to have a surface tension of 30-33 dynes cm^{-1}, indicating that excess SDS surfactant is still present within the dispersion, as shown in Figure 4.3. (In Step 1, excess surfactant was used to ensure that all the P3HT:PCBM would be efficiently dispersed within the water - Once the materials have been dispersed, the excess surfactant needs to be removed from the water as it deteriorates device performance[9].)

No Dialysis

Excess Surfactants : YES
Surface Tension: ~33 dynes/cm
Wetting of ink? YES
Good for Devices? **NO**

Presence of Excess surfactants act as impurities in OPV devices hindering device performance

4 Dialysis cycles with DI Water

Excess Surfactants : NO
Surface Tension: ~66 dynes/cm
Wetting of ink? **NO**
Good for Devices? **YES**
Excess surfactants have been removed, however surface tension increases again due to this removal. High surface tension of ink makes it difficult for the ink to wet the substrate

5th Dialysis cycle with 20% vol/vol Ethanol soln.

Excess Surfactants : NO
Surface Tension: ~37 dynes/cm
Wetting of ink? **YES**
Good for Devices? **YES**

By dialyzing with an ethanol solution, surface tension is reduced again, without having to resort to excess surfactant molecules

Figure 4.3 : Effect of dialysis steps on the surface tension of the ink

[STEP 4] - Reducing surface tension for better wetting of ink - Excess surfactant was removed by dialyzing the dispersion with DI water. Dialysis of these dispersions was carried out using Amicon Ultra-4 (10 kDa MWCO) centrifugal dialysis tubes, purchased from Millipore. The dispersions were added to the tubes and centrifuged at 4000 rpm for 30 minutes. The filtrate was discarded and the retentate was re-diluted with 2ml of DI water again. The tubes were centrifuged at 4000 rpm again for 30 minutes. This process was carried out 4 times. Then, the surface tension of this dispersion was measured to be 66 dynes/cm – this increase in surface tension indicated that the majority of the SDS was successfully removed after dialyzing. For the 5th time, the retentate was diluted with 2mL of 20 vol. % ethanol in water[10], and centrifuged until the final retentate volume was 0.5mL yielding the final ink. The surface tension of the resulting dispersion was again measured to be 37dynes/cm. Thus, the final ink is devoid of excess SDS surfactant which may hinder charge transport in the active layer [9] by inducing charge traps (for reference see Figure 4.1 & 4.3), and has a low surface tension which facilitates better wetting of the substrate as seen below, in Figure 4.4.
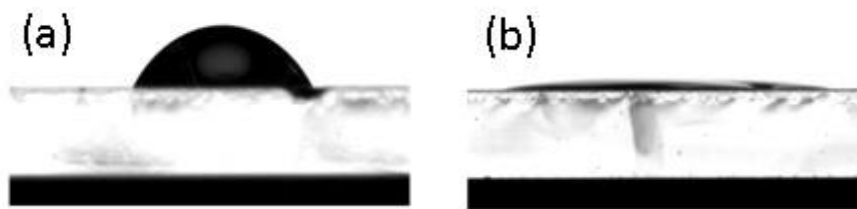
Figure 4.4 : [Step 4] Wetting of ink on PEDOT:PSS coated ITO (a) after dialyzing 4 times with DI water (contact angle of 46.74°) and (b) dialyzing with 20 vol.% ethanol solution for a 5th time (contact angle of <10°)

4.5.2 Determining average nanoparticle diameter using Quasi-Elastic Light Scattering

Quasi-elastic light scattering was performed on a Brookhaven Instruments Light Scattering Goniometer. Samples were illuminated by a 35mW He-Ne Laser (Spectraphysics) and hydrodynamic radii were obtained from 2nd order Cumulance analysis of the resulting correlation function. Refer to Chapter 2 for experimental setup details.

4.5.3 Spectroscopic Analysis

UV-Vis absorbance spectra of the dispersions were characterized using a Shimadzu UV-2100PC spectrophotometer. Fluorescence of the dispersions was characterized using a HORIBA Jobin-Yvon Fluoro Max fluorimeter – an excitation wavelength of 485nm (a characteristic wavelength for P3HT) was used; slit widths of 5nm were selected for the fluorimeter.

4.5.4 Device Fabrication by Spin Coating

ITO glass substrates $(24mm)^2$ in area were cleaned by sonicating for 30 minutes in acetone followed by a 30 minute sonication in IPA. Then the substrates were subjected to oxygen plasma treatment for 2-3 minutes, using the experimental setup found in [20] .PEDOT:PSS solution (Baytron PH, σ = 10–100Scm^{-1}, diluted 1:1 with deionized water) was spin coated onto cleaned ITO substrates at 4000 rpm for 30 seconds. These films were then left to cure on a hotplate at 160°C for 20 minutes. After drying the films, the substrates were subjected to ozone treatment again for another 2-3 minutes.

P3HT:PCBM nanoparticle inks were spin coated onto these substrates at 1000RPM for 30 seconds. These films were then transferred to an inert atmosphere, within 5 minutes of spincoating. This was followed by deposition of a 150nm thick aluminum top electrode. Aluminum (pellets, used as purchased from Alfa Aesar Puratronic, alumina shot, 4-8mm,

99.999% purity) was evaporated under a low pressure (<10^{-6} Torr) as the top electrode. The evaporator used was an Angstrom vacuum deposition system, Model number S6458, powered by an Inficon SQC-310 Deposition Controller, and vacuum controlled with a Varian Turbo-V 81-AG turbomolecular pump.

4.5.5 Device Fabrication by Inkjet Printing

ITO glass substrates (24mm)^2 in area were cleaned by sonicating for 30 minutes in acetone followed by a 30 minute sonication in IPA. PEDOT:PSS solution (Baytron PH, σ = 10–100Scm^{-1}, diluted 1:1 with deionized water) was spin-cast onto cleaned ITO substrates at 4000 rpm for 30 seconds. These films were then left to cure on a hotplate at 160°C for 20 minutes.

Inkjet Printing of the P3HT:PCBM nanoparticle inks were done using a Dimatix 2831 Materials Printer. The ink was printed onto the PEDOT: PSS coated ITO substrates. Each OPV active layer film consisted of 2 printed layers printed using a drop spacing of 20μm and a firing voltage of 20V. The platen temperature was set to 35°C; this ensured that the printed films would dry within 2 minutes of printing. As soon as a film was printed, it was immediately (within 30 seconds) transferred to an inert atmosphere followed by deposition of a 150nm thick aluminum top electrode (same as the method followed for the spin coated devices)

4.5.6 Device Performance Characterization

The OPV devices were tested immediately after fabrication, using a four-point probe method. Current density–voltage (J–V) characteristics of the devices were obtained under simulated 1 sun - 100mW cm^{-2} power density, provided by a Newport 91159 Full Spectrum solar simulator with xenon lamp (see Chapter 2 for full method).

4.6 Results and Discussion

<u>**4.6.1 Diameter of Nanoparticles**</u>

Nanoparticle samples for size distribution analysis were prepared by removing an aliquot (~50μl) of dialyzed ink and diluting it with 10ml of DI water. Then 1ml of this diluted dispersion was decanted into the glass tubes used by Dr. George Thurston's QLS setup. The particle size distributions were calculated by obtaining the hydrodynamic radii of the nanoparticles. Samples from inks (made the same way, 8 different times) were tested. The following is the raw data obtained:

Sample Number	Effective Diameter [nm]	RMS Error [10^-3]
1	50.3	3
	52.2	3.8
	50.5	4
	49.3	4.6
	49.3	14.4
	51.7	2.29
	50.1	2.7
2	46.9	4.72
	48.1	840
	41.7	5.7
	48.8	6.6
3	49.3	7.1
	50.3	7.1
	47.4	6.39
	44.9	8.8
4	36.6	16
	55.9	14.6
	47	1.8
	46	2.4
	45.9	8.1
5	56.6	5
	57.1	2.46
	55.4	3.7
	57.2	2.59
	55	3.72
6	59.4	2.455
	58.9	2.5
	57.7	2.3
	57.6	2.06
	59.7	2.1
7	59.1	11.8
	62	0.4
	57.2	9.8
	53.8	2.3
	62.4	5.93
	56.5	5.9
8	50.5	6.9
	50.1	8.4
	49.3	5.1
	53.4	5.5
	55	10.8
	47.9	8.3

Table 4.2 : The effective diameter of the nanoparticles as measured by quasi-elastic light scattering.

Using quasi-elastic light scattering, the effective average diameter of the nanoparticles (made for devices) was found to be 52.2nm +/- (5.5nm). This is useful in two ways - 1) the Dimatix inkjet printer manufacturer suggests that the maximum particle diameter must be less than 200nm so as to not clog the inkjet nozzles and 2) the nanoparticle size must be small (see literature guidelines) for efficient exciton diffusion between the P3HT: PCBM interface. If the P3HT: PCBM domains inside the nanoparticles are too large then it becomes difficult to extract charge due to the poor exciton diffusion lengths of the generated electrons. [24]

4.6.2 Blending of Nanoparticles

In conventional bulk heterojunction OPV [9], the active layer film is spincoated onto the substrate. Usually this leaves an amorphous mixture of the donor and acceptor[19]; a subsequent annealing step is applied to the film so as to phase separate the donor and the acceptor into domains which benefit device performance [25]. As mentioned earlier in this chapter, it is extremely important for the P3HT and the PCBM to be well blended with each other and in close proximity with each other. This blending results in effective charge dissociation at the donor/acceptor interface. Moreover by blending the donor and acceptor together, the surface area of the donor/acceptor interface can be maximized thereby increasing possibility of charge transfer at this interface [26].

The first blending experiment was to determine if the results obtained by Dastoor et al. [17] could be reproduced; it was shown that the P3HT:PCBM nanoparticle formed a core-shell nanoparticle, where the PCBM formed the core of the nanoparticle.

To determine if blending of P3HT and PCBM is taking place, absorbance and fluorescence of (i) P3HT nanoparticles by themselves,(ii) P3HT and PCBM nanoparticles that have dispersed separately and (iii)P3HT: PCBM nanoparticles that have been supposedly blended together are measured.
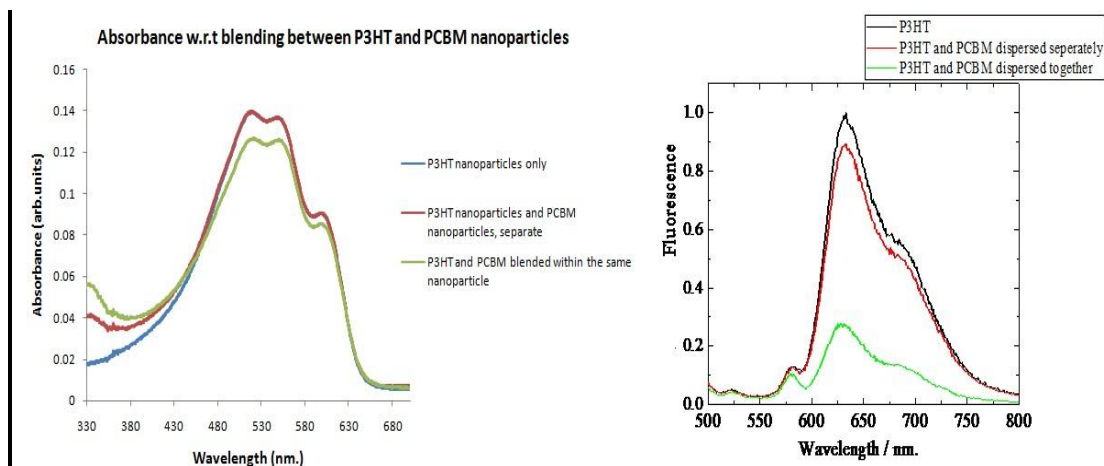
Figure 4.5 : Absorbance and Fluorescence of Just P3HT nanoparticles ,P3HT and PCBM nanoparticles that have been formed from separate solutions of pure P3HT and PCBM and then added together in nanoparticle form in the ratio of [1:0.25] and P3HT:PCBM nanoparticles formed from a single P3HT:PCBM blend solution in the ratio of [1:0.25]. All the solutions are of the same optical density at the excitation wavelength.

From Figure 4.5, it is observed that the fluorescence for the P3HT nanoparticles by themselves is relatively high, whereas in the nanoparticles made from a single mixed P3HT and PCBM precursor solution the fluorescence is heavily quenched. When the P3HT and PCBM nanoparticles are made separately but are present in the same sample, only a small reduction in fluorescence is observed which is attributed to the collisional quenching between the P3HT and the PCBM nanoparticles. From this result, it was concluded that the PCBM does indeed blend with the P3HT nanoparticles when both of them are present in the oil phase before the emulsification process. This is somewhat consistent with results obtained by Dastoorand co-workers [17].This blending occurs at all concentrations of P3HT and PCBM(as will be shown in

the upcoming section of the chapter). Blending also takes place *without the presence of surfactant*(see Appendix B); in this thesis, no work has been conducted on the effect of sonication power on the blending - this will be addressed in future work (see Chapter 5).

After confirming that the PCBM can be blended within the P3HT component of the nanoparticle, the absorbance and fluorescence of nanoparticles with different ratios of P3HT:PCBM are measured.
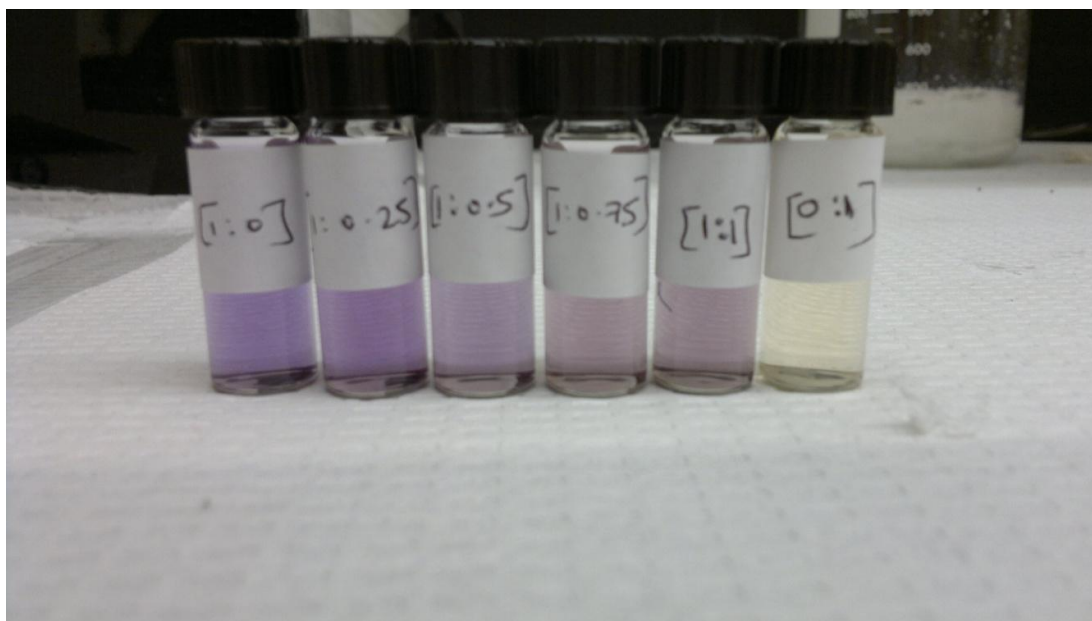
Figure 4.6 : Miniemulsions of P3HT:PCBM made with different ratios of P3HT and PCBM

Using the details specified in Table 4.1, miniemulsion nanoparticles with varying P3HT:PCBM ratios were fabricated. The resulting nanoparticle dispersions can be seen in Figure 4.6, above.
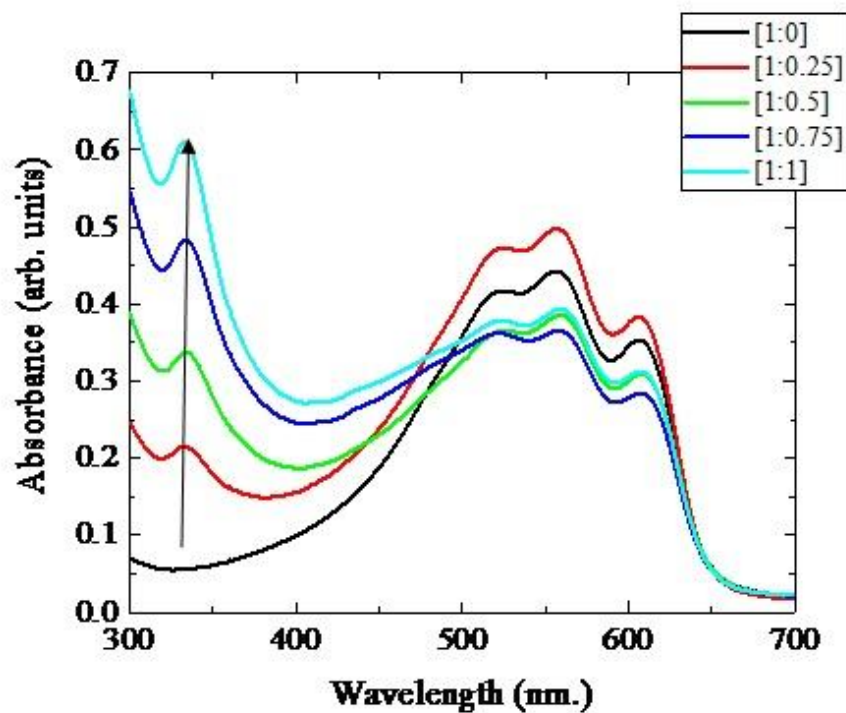
Figure 4.7 : Absorbance spectra of P3HT nanoparticles with increasing amounts of PCBM blended within. As the concentration of PCBM increases, the absorbance signal at 330nm increases.

By comparing Figures 4.7 and 4.8 it can be seen that the P3HT absorbance spectrum changes with respect to the PCBM concentration. As the PCBM concentration is increased, the respective absorbance signal is also increased at ~330nm. The P3HT concentration is always kept constant (see Table 1).
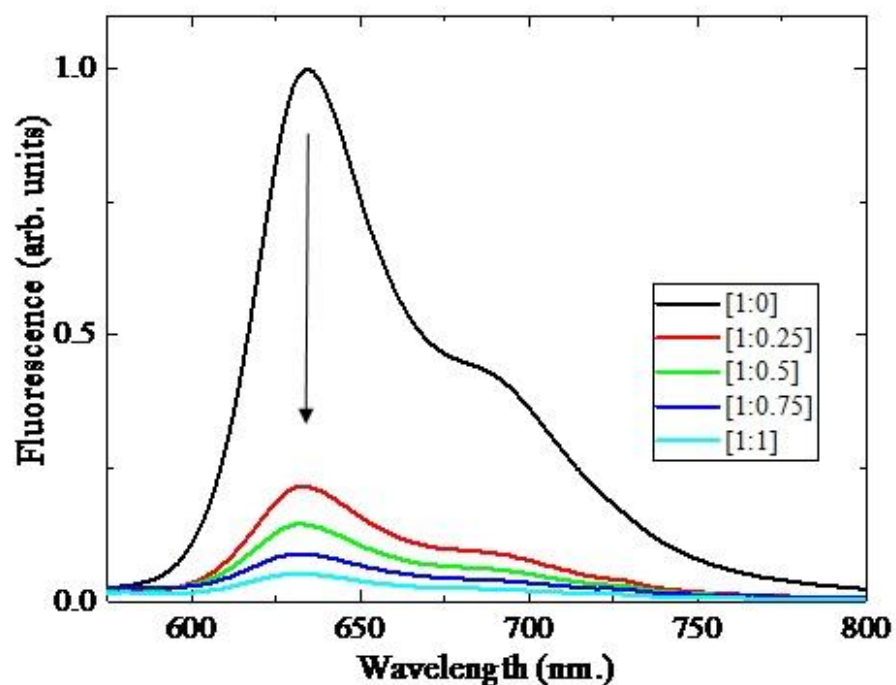
Figure 4.8 : Fluorescence quenching of nanoparticles with different P3HT: PCBM ratios. As PCBM concentration increases, the fluorescence signal decreases indicating efficient quenching of emission as well as blending of PCBM with the P3HT

From Figure 4.7, it can be seen that the PCBM signal at 330nm increases with an increase in P3HT:PCBM ratio (from [1:0] to [1:1] P3HT:PCBM)The increase in PCBM concentration is also reflected in Figure 4.8 where the fluorescence signal continues to decrease with the increase in PCBM ratio. This indicates that the PCBM is in close proximity with the P3HT, hence the P3HT and PCBM are successfully blended. The concentrations of the P3HT is kept constant.

Io/I (Total Fluorescence)
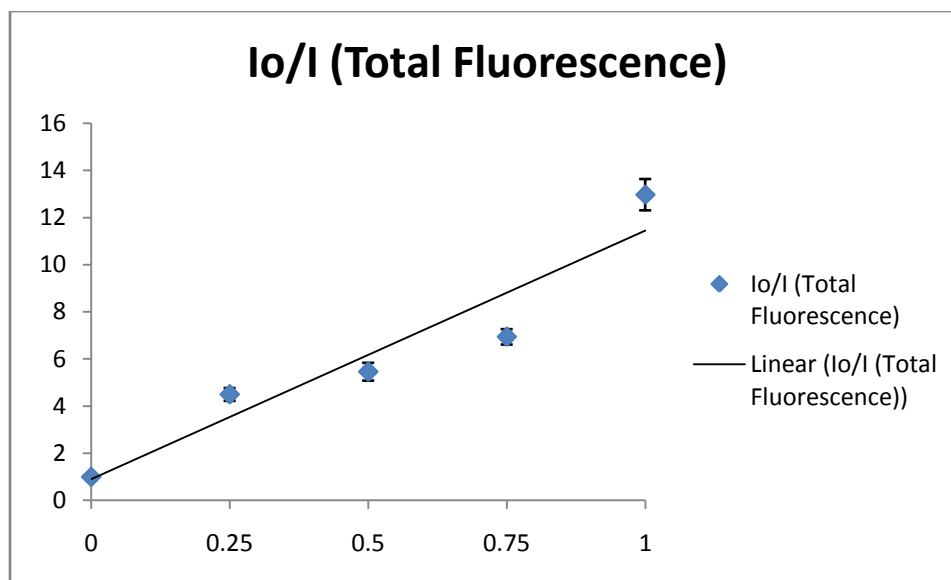
Amt of Quencher	Io/I (Lambda max)	Standard Deviation
0	1	0
0.25	4.49303227	0.271649039
0.5	5.457512424	0.376990873
0.75	6.937478783	0.32643348
1	12.96807554	0.663700357

Figure 4.9 : A Stern-Volmer plot of the quenching of P3HT fluorescence in blended nanoparticles. Fluorescence intensity was summed over the range 500-800nm and was divided by the absorbance of the solution at the excitation wavelength of 485nm.

From Figures 4.7,4.8 and 4.9 it can be concluded that the concentration of PCBM within the P3HT can be effectively controlled. The stern-volmer plot indicates that the relation between fluorescence quenching and concentration of quencher is not completely linear. There is a substantial increase in quenching between [1:0.75] and [1:1] nanoparticles; this indicates that the PCBM domains inside the P3HT are well mixed; a possible explanation for this is that for P3HT:PCBM at a ratio of [1:1], the blend forms a hypoeutectic blend where the PCBM is well mixed with the P3HT, as reported by Müller et al.[27]

This is also an indication that the makeup of the nanoparticle can be effectively controlled by modifying the concentrations and ratios of the P3HT and PCBM inside the chloroform prior to

the miniemulsion process, and that this methodology may be translated to other donor/acceptor materials as well. [14]

4.6.3 P3HT:PCBM nanoparticle based OPV film formation : Spin Coating Vs. Inkjet Printing

The film morphology of inkjet printed films were characterized for uniformity using optical micrographs.
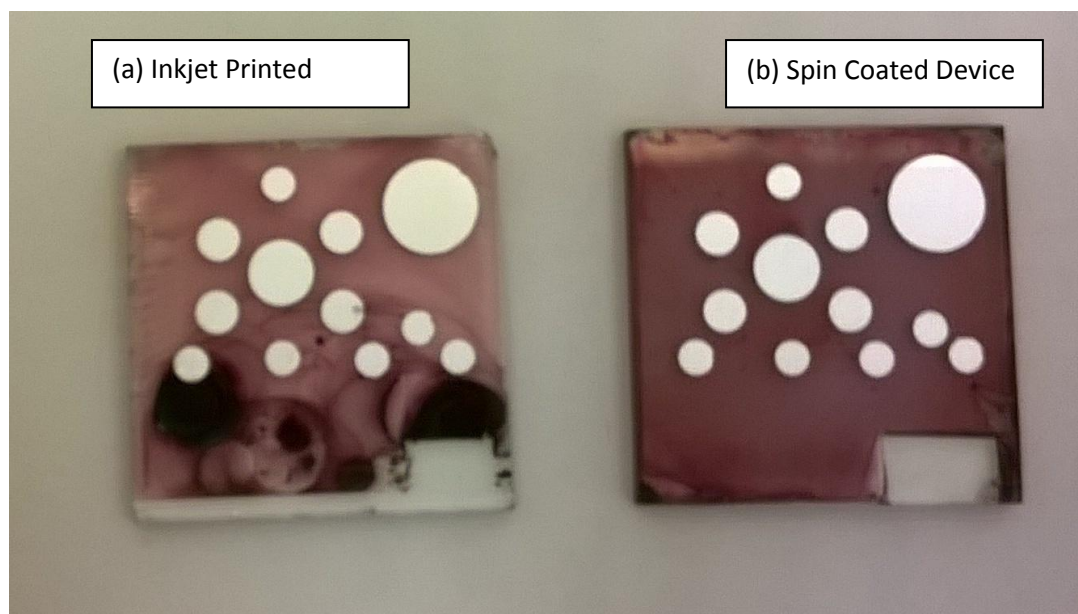
Figure 4.10 :(a) Inkjet Printed and (b) Spin Coated P3HT:PCBM nanoparticle based OPVs
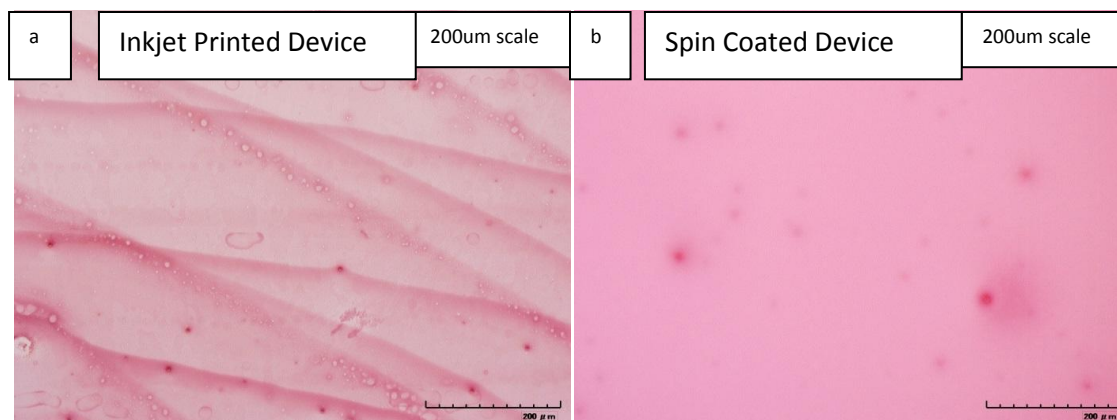
Figure 4.11 : Zoomed in optical micrographs of the (a) inkjet printed film and (b) spin coated film of nanoparticulate films

From Figures 4.10 and 4.11, it can be seen that the inkjet printed film is highly irregular as compared to the spin coated film. Unlike in chapter 3 (printing of organic solvents), the printing parameters were not fully optimized for the water-based ink in chapter 4, resulting in non-uniform inkjet printed nanoparticulate films.
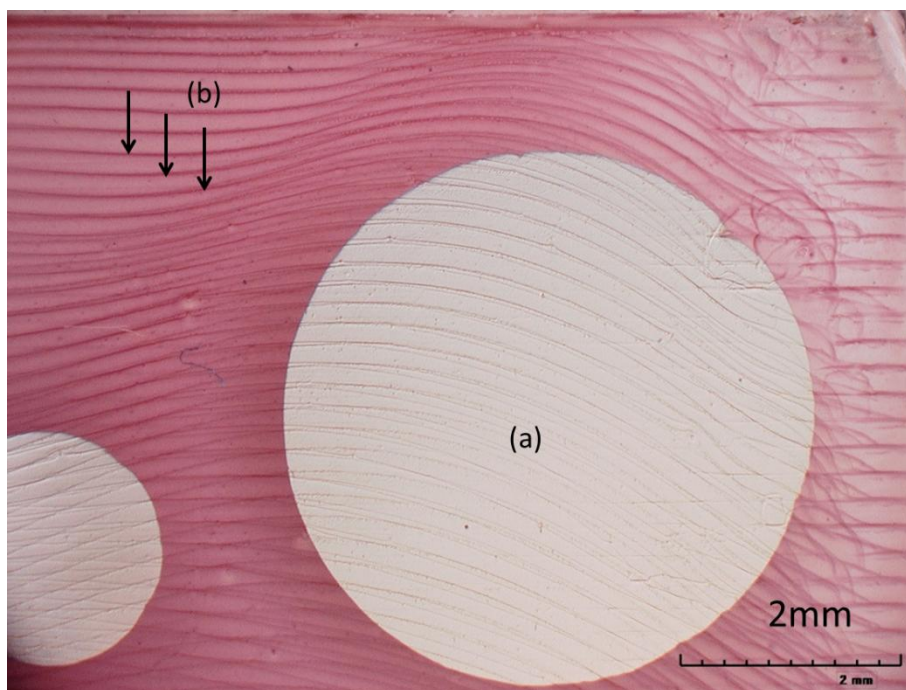
Figure 4.12 : Top-down optical micrograph of an inkjet printed P3HT:PCBM nanoparticle film showing the (a) aluminum cathode evaporated onto the P3HT:PCBM layer to form an OPV and (b) dried patterns of printed P3HT:PCBM ink. (Scale bar of 2mm)

The ink (described in the Experimental section) was inkjet printed onto PEDOT:PSS coated ITO substrates (inkjet printing parameters described in the Experimental section) using the Dimatix 2831 Materials Printer. Empirically, it was found that a single printed layer was not sufficient to fully cover the surface of the substrate; pinhole defects in the dried film were clearly visible to the naked eye. To offset this, a second layer was printed to decrease the number of pinhole defects – however, improper drying of the inks cause wave-like drying patterns in the final film [15] as seen in Figure 4.12. This is hypothesized to be the main cause of non functioning devices,

as discussed in the upcoming sections - when the aluminum cathode comes in contact with film defects and pinholes, it has a higher chance to come in contact with the underlying anode (ITO), and thereby shunt the device.

For future iterations of this experiment, more effort must be paid towards optimizing the film formation and controlling the drying process of the film. A much more in-depth study needs to be conducted with respect to platen temperature (see Chapter 5).

4.6.4 Film Thickness

From Chapter 3, the film thickness for the inkjet printed film is estimated to be ~150nm.The spincoated film thickness is also assumed to be around ~150nm, as the spincoating parameters used in this thesis chapter were the same as the parameters used by Ulum et al. [17,18].

4.6.5 Device Performance : Spin Coating Vs Inkjet Printing

8 OPV films were spincoated, and another 8 OPV films were inkjet printed. Each film has a total of 12 devices, formed by vacuum-deposition of aluminum cathodes through a shadow mask. Among the 12 devices, there are 6 "smallest area" devices having a surface area of $0.017cm^2$, 4 "small area" devices having a surface area of $0.034cm^2$, 1 "medium area" device having a surface area of $0.096cm^2$ and finally 1 "large area" device of surface area $0.196cm^2$. The cartoon represented in Figure 4.13, is representative of a typical OPV film studied in this thesis.
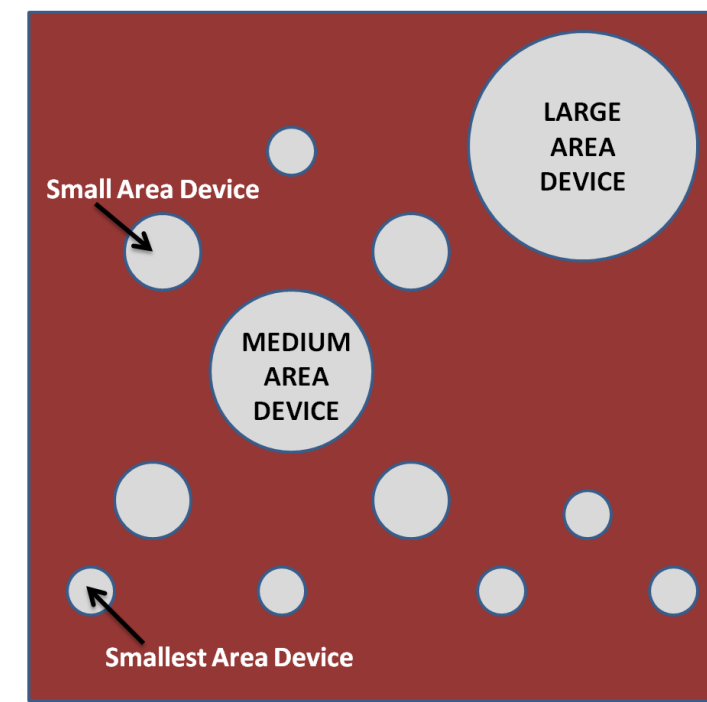
Figure 4.13 : Cartoon showing devices located on each printed film

The power conversion efficiencies for the devices were tabulated with respect to (i) process , (ii) film and (iii) device area, as follows: (all measurements marked with a "-" indicates that the device was not functional i.e. it behaved like a resistor and did not yield a power conversion efficiency)

	SPINCOATED DEVICE EFFICIENCIES (%)							
DEVICE AREA	Film 1	Film 2	Film 3	Film 4	Film 5	Film 6	Film 7	Film 8
Large Area	0.08	0.135	0.09	0.01	0.07	0.053	-	-
Medium Area	-	0.21	0.16	0.15	0.05	0.11	0.02	-
Small Area 1	-	0.53	-	0.39	-	-	0.33	0.0004
Small Area 2	0.04	-	-	0.32	0.21	-	0.16	0.01
Small Area 3	0.01	0.26	0.17	0.37	0.1	0.0027	0.23	-
Small Area 4	0.079	0.1	0.33	0.13	0.05	-	-	0.01
Smallest Area 1	0.03	0.71	0.63	0.92	0.53	0.67	0.12	0.04
Smallest Area 2	-	-	0.54	0.03	0.2	0.36	-	0.11
Smallest Area 3	0.14	0.14	-	0.61	0.17	-	0.12	0.01
Smallest Area 4	-	-	-	0.68	0.35	-	-	0.11
Smallest Area 5	-	-	-	0.74	-	0.14	0.7	0.14
Smallest Area 6	-	0.42	0.02	0.63	0.32	-	0.22	0.07

	INKJET PRINTED DEVICE EFFICIENCIES (%)							
DEVICE AREA	Film 1	Film 2	Film 3	Film 4	Film 5	Film 6	Film 7	Film 8
Large Area	0.11	0.006	0.003	0.0002	0.001	-	0.001	-
Medium Area	0.35	0.04	0.002	0.01	-	0.28	0.027	0.02
Small Area 1	0.3	-	0.122	0.03	0.21	-	0.21	0.21
Small Area 2	-	-	-	0.01	0.41	-	0.2	-
Small Area 3	0.02	-	0.05	0.31	-	0.02	0.03	-
Small Area 4	0.08	-	-	-	-	-	-	-
Smallest Area 1	-	-	-	-	-	-	-	-
Smallest Area 2	-	-	-	-	-	-	-	-
Smallest Area 3	-	-	-	-	-	-	-	-
Smallest Area 4	-	-	-	-	-	-	-	-
Smallest Area 5	-	-	-	-	-	-	-	-
Smallest Area 6	-	-	-	-	-	-	-	-

Table 4.3 : Device efficiencies tabulated with respect to device area as well as the process used.

From Table 4.3 and Figure 4.14, it is seen that the spin coated devices are less prone to failure as compared to the inkjet printed devices. The spin coated devices also have higher power conversion efficiencies than the inkjet printed devices, on average. Currently, the author does not have a concrete reason as to why the PCE% ranges between 0.0001% and 1% - a range spanning 4 orders of magnitude. Indeed, for the inkjet printed films, none of the "smallest area" devices were seen to work - this is indicative of extremely poor contact between the aluminum cathode and the underlying active layer(as can be seen from Figure 4.10(a)); this concern should be addressed in future iterations of inkjet printing experiments.

68.75% of the Spincoated devices were functional

- Functioning Spincoted devices
- Non-functioning spincoated devices

29.1% of the Inkjet Printed devices were functional

- Functioning Inkjet Printed devices
- Non-functioning Inkjet Printed devices
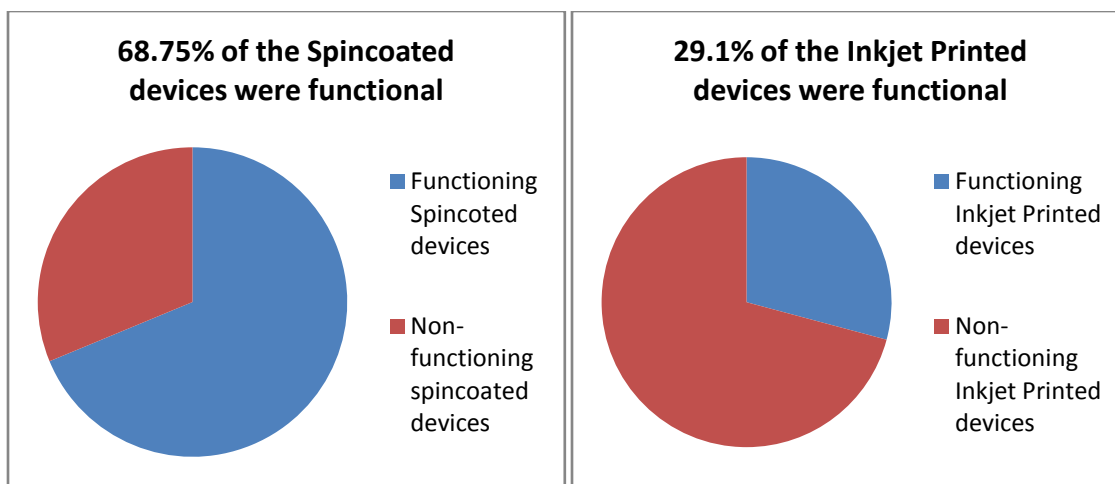
Figure 4.14: Pie charts showing the success/failure rate of the devices ; spincoated vs. inkjet printed

PCE% ranges of working devices

- % of Working Spincaoted devices
- % of Working Inkjet Printed devices

Percentage of Working devices

Power Conversion Efficiency ranges	Spincoated	Inkjet Printed
0-0.15	45.5	67.9
0.15-0.3	12.12	21.43
0.3-0.45	15.2	10.71
0.45-0.6	6.1	0
0.6-0.75	18.2	0
0.75-1	3.03	0
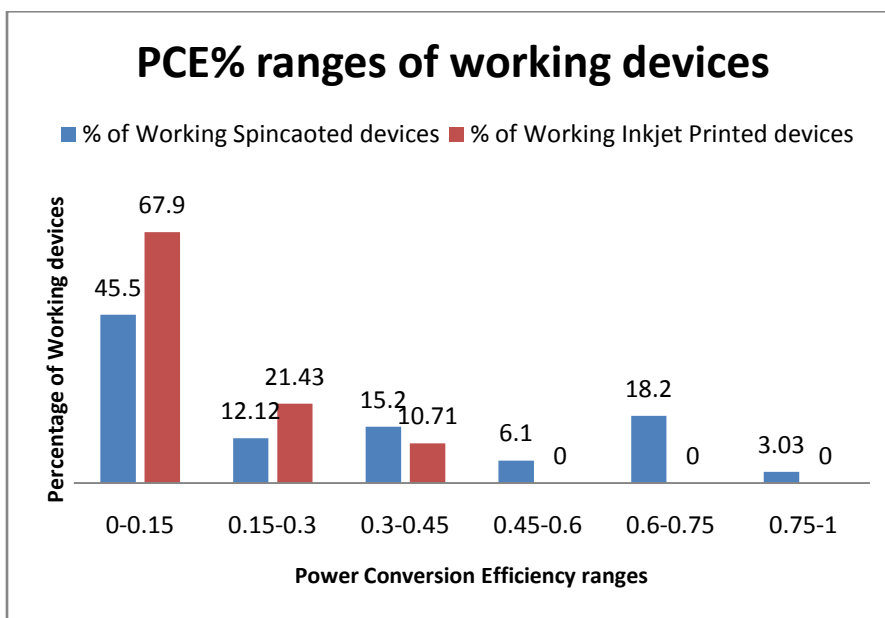
Figure 4.15 : Distribution of power conversion efficiencies obtained from the working P3HT:PCBM nanoparticle OPV devices. The distribution of PCE had a very high standard deviation; values for both spincoated and inkjet printed devices ranged between 0.0001 and 1%.
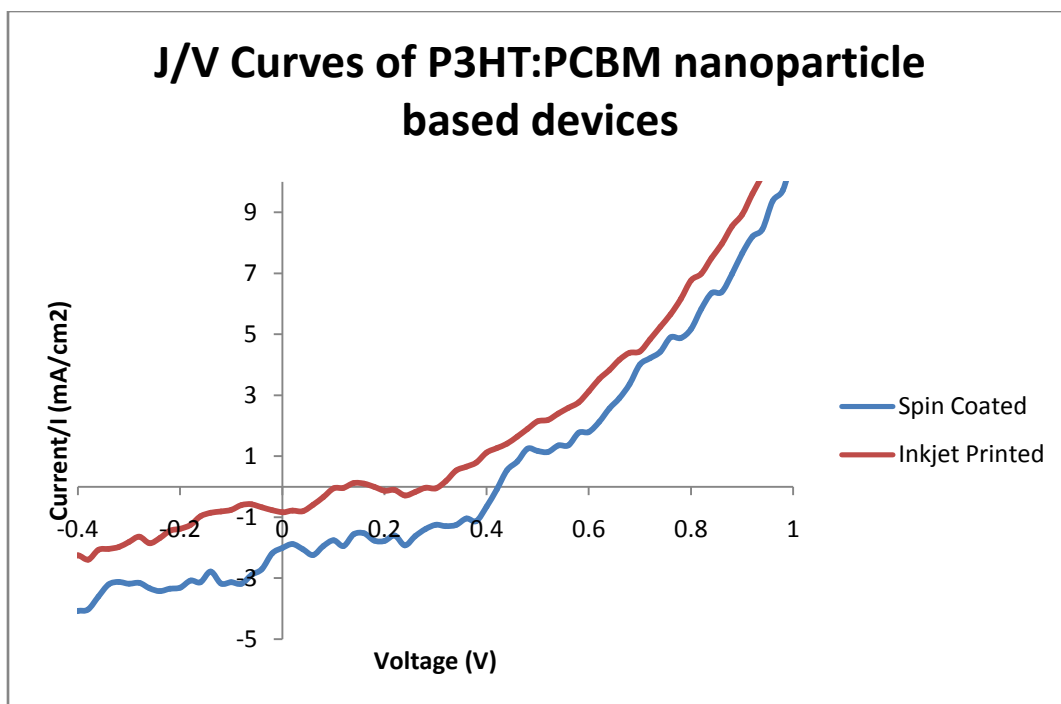
Figure 4.16 : J/V Characteristics of the best device obtained through inkjet printing

	Spincoated Devices	Inkjet Printed Devices
Best (Hero) PCE%	0.92%	0.41%
Average PCE%	0.236%	0.109%

Table 4.4 : Best and Average power conversion efficiencies obtained from spincoated and inkjet printed P3HT:PCBM nanoparticle devices.

From Figure 4.16 and Table 4.4 : Spin coated devices yielded an average power conversion efficiency of 0.24%, with the best device efficiency peaking at 0.92%. The inkjet printed devices yielded an average power conversion efficiency of 0.11% with the best device efficiency peaking at 0.41%.

4.7 Conclusion

In this chapter, blended P3HT:PCBM nanoparticles were dispersed in water, using the miniemulsion method. By using UV-vis absorbance and fluorescence measurements, the PCBM was confirmed to blend with the P3HT inside the nanoparticle. This result is consistent with results obtained by Ulum et al. [17,18] , where it was shown that the PCBM formed the core of the P3HT:PCBM nanoparticle, due to its higher surface energy relative to the P3HT. This blending is crucial for efficient organic photovoltaics; when donor:acceptor domains are blended, higher amounts of charges dissociate at the donor:acceptor interface [26]. Next, P3HT:PCBM nanoparticle inks were formulated and used to fabricate working OPV devices using spin coating and inkjet printing. Though the device performances are modest as compared to the spin-cast device results obtained by Dastoor et al. [17] and Venkataraman et al. [10], the objective of fabricating chlorinated solvent-free organic photovoltaics was acheived using inkjet printing as a roll-to-roll process analogue. Thus, inkjet printing is demonstrated to be a viable stepping stone between spin casting and roll-to-roll printing of OPVs, and using a water-based ink is proof-of-concept for scaling up into a process that is environmentally friendly.

The results obtained in this chapter are , as mentioned previously, quite modest; for future studies, the quality of data may be improved by breaking down the inkjet printing process and systematically testing each part of the process. This breakdown is given in Chapter 5, along with a set of experimental outlines that can be followed to iteratively improve the complete process.

4.8 REFERENCES

[1]Espinosa, Nieves, Rafael Garcia-Valverde, Antonio Urbina, and Frederik C. Krebs. "A life cycle analysis of polymer solar cell modules prepared using roll-to-roll methods under ambient conditions." *Solar Energy Materials and Solar Cells* 95, no. 5 (2011): 1293-1302.

[2] Espinosa, Nieves, Markus Hösel, DechanAngmo, and Frederik C. Krebs. "Solar cells with one-day energy payback for the factories of the future."*Energy & Environmental Science* 5, no. 1 (2012): 5117-5132.

[3] Søndergaard, Roar, Martin Helgesen, MikkelJørgensen, and Frederik C. Krebs. "Fabrication of polymer solar cells using aqueous processing for all layers including the metal back electrode." *Advanced Energy Materials* 1, no. 1 (2011): 68-71.

[4]Emmott, Christopher JM, Antonio Urbina, and Jenny Nelson. "Environmental and economic assessment of ITO-free electrodes for organic solar cells." *Solar Energy Materials and Solar Cells* 97 (2012): 14-21.

[5] Watts, Benjamin, Warwick J. Belcher, Lars Thomsen, Harald Ade, and Paul C. Dastoor. "A quantitative study of PCBM diffusion during annealing of P3HT: PCBM blend films." *Macromolecules* 42, no. 21 (2009): 8392-8397.

[6]Landfester, Katharina. "The generation of nanoparticles in miniemulsions." *Advanced Materials*13, no. 10 (2001): 765-768.

[7]Larsen-Olsen, Thue T., Thomas R. Andersen, BirgittaAndreasen, Arvid PL Böttiger, Eva Bundgaard, KionNorrman, Jens W. Andreasen, MikkelJørgensen, and Frederik C. Krebs. "Roll-to-roll processed polymer tandem solar cells partially processed from water." *Solar Energy Materials and Solar Cells* 97 (2012): 43-49.

[8] Landfester, Katharina, Nina Bechthold, Franca Tiarks, and Markus Antonietti. "Formulation and stability mechanisms of polymerizableminiemulsions." *Macromolecules* 32, no. 16 (1999): 5222-5228.

[9]Bag, Monojit, Timothy S. Gehan, Dana D. Algaier, Feng Liu, GavvalapalliNagarjuna, Paul M. Lahti, Thomas P. Russell, and DhandapaniVenkataraman. "Efficient Charge Transport in Assemblies of Surfactant-Stabilized Semiconducting Nanoparticles." *Advanced Materials* 25, no. 44 (2013): 6411-6415.

[10]Bag, Monojit, Timothy S. Gehan, Lawrence A. Renna, Dana D. Algaier, Paul M. Lahti, and DhandapaniVenkataraman. "Fabrication conditions for efficient organic photovoltaic cells from aqueous dispersions of nanoparticles." *RSC Advances* 4, no. 85 (2014): 45325-45331.

[11] Feron, K., X. Zhou, W. J. Belcher, C. J. Fell, and P. C. Dastoor. "A dynamic Monte Carlo study of anomalous current voltage behaviour in organic solar cells." *Journal of Applied Physics* 116, no. 21 (2014): 214509.

[12] Kietzke, Thomas, Dieter Neher, Rivelino Montenegro, Katharina Landfester, Ullrich Scherf, and H-H. Hoerhold. "Nanostructured solar cells based on semiconducting polymer nanospheres

(SPNs) of M3EH-PPV and CN-Ether-PPV." In *Optical Science and Technology, SPIE's 48th Annual Meeting*, pp. 206-210. International Society for Optics and Photonics, 2004.

[13] Kietzke, Thomas, Burkhard Stiller, Katharina Landfester, Rivelino Montenegro, and Dieter Neher. "Probing the local optical properties of layers prepared from polymer nanoparticles." *Synthetic metals* 152, no. 1 (2005): 101-104.

[14] Kietzke, Thomas, Dieter Neher, Michael Kumke, Rivelino Montenegro, Katharina Landfester, and Ullrich Scherf. "A nanoparticle approach to control the phase separation in polyfluorene photovoltaic devices." *Macromolecules* 37, no. 13 (2004): 4882-4890.

[15] Kietzke, Thomas, Dieter Neher, Katharina Landfester, Rivelino Montenegro, Roland Güntner, and Ullrich Scherf. "Novel approaches to polymer blends based on polymer nanoparticles." *Nature materials* 2, no. 6 (2003): 408-412.

[16]Zhou, Xiaojing, Warwick Belcher, and Paul Dastoor. "Solar Paint: From Synthesis to Printing." *Polymers*6, no. 11 (2014): 2832-2844.

[17] Ulum, Syahrul, Natalie Holmes, Matthew Barr, AL David Kilcoyne, Bill Bin Gong, Xiaojing Zhou, Warwick Belcher, and Paul Dastoor. "The role of miscibility in polymer: fullerene nanoparticulate organic photovoltaic devices." *Nano Energy* 2, no. 5 (2013): 897-905.

[18] Ulum, Syahrul, Natalie Holmes, DarmawatiDarwis, Kerry Burke, AL David Kilcoyne, Xiaojing Zhou, Warwick Belcher, and Paul Dastoor. "Determining the structural motif of P3HT: PCBM nanoparticulate organic photovoltaic devices." *Solar Energy Materials and Solar Cells* 110 (2013): 43-48.

[19] Nagarjuna, Gavvalapalli, Mina Baghgar, Joelle A. Labastide, Dana D. Algaier, Michael D. Barnes, and DhandapaniVenkataraman. "Tuning aggregation of poly (3-hexylthiophene) within nanoparticles." *ACS nano* 6, no. 12 (2012): 10750-10758.

[20] Vyavahare, Omkar. "Fabrication and characterization of organic light emitting diodes for display applications." (2009).

[21] Yang, Xiaoniu, and Joachim Loos. "Toward high-performance polymer solar cells: the importance of morphology control." *Macromolecules* 40, no. 5 (2007): 1353-1362.

[22]Schwartz, Benjamin J. "Conjugated polymers as molecular materials: How chain conformation and film morphology influence energy transfer and interchain interactions." *Annual review of physical chemistry* 54, no. 1 (2003): 141-172.

[23]Halls, J. J. M., K. Pichler, R. H. Friend, S. C. Moratti, and A. B. Holmes. "Exciton diffusion and dissociation in a poly (p-phenylenevinylene)/C60 heterojunction photovoltaic cell." *Applied Physics Letters* 68, no. 22 (1996): 3120-3122.

[24]Peumans, Peter, AharonYakimov, and Stephen R. Forrest. "Small molecular weight organic thin-film photodetectors and solar cells." *Journal of Applied Physics* 93, no. 7 (2003): 3693-3723.

[25] Li, Gang, Yan Yao, Hoichang Yang, Vishal Shrotriya, Guanwen Yang, and Yang Yang. "" Solvent annealing" effect in polymer solar cells based on poly (3-hexylthiophene) and methanofullerenes."*Advanced Functional Materials* 17, no. 10 (2007): 1636.

[26]Brabec, Christoph J., Martin Heeney, Iain McCulloch, and Jenny Nelson. "Influence of blend microstructure on bulk heterojunction organic photovoltaic performance." *Chemical Society Reviews* 40, no. 3 (2011): 1185-1199.

[27] Müller, Christian, Toby AM Ferenczi, Mariano Campoy-Quiles, Jarvist M. Frost, Donal DC Bradley, Paul Smith, Natalie Stingelin-Stutzmann, and Jenny Nelson. "Binary organic photovoltaic blends: a simple rationale for optimum compositions." *Advanced Materials* 20, no. 18 (2008): 3510-3515.

CHAPTER 5 - Future Work

5.1 Introduction

In Chapter 4, it was reported that P3HT:PCBM nanoparticles suspended in a water-based ink were inkjetted to fabricate working devices. Objectively, if this result is to be improved in future iterations of experiments, the concept of "Inkjet Printing of OPV" must be reviewed once again.
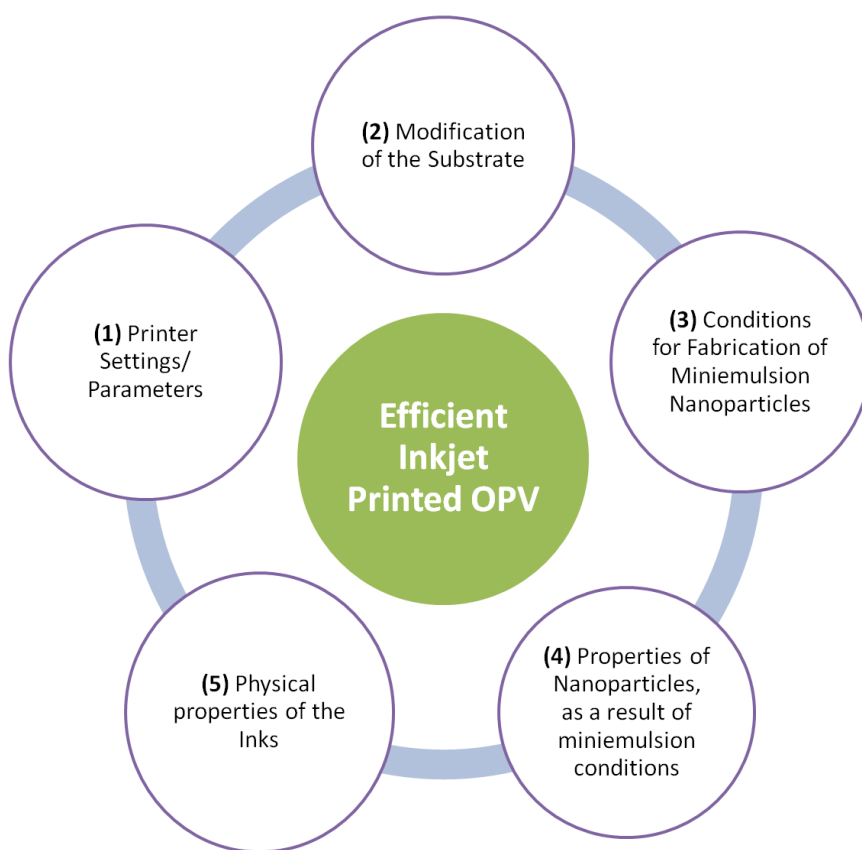
Figure 5.1 : Five facets of the inkjet printing process encountered in this thesis that need to be addressed rigorously in future works, to improve the OPV devices

There are in fact at least five inter-dependent steps of the OPV inkjet process that need to be addressed [1,2,3,4,5], as shown in Figure 5.1.

In this chapter, each step is further broken down into smaller facets - These parameters are explained in some detail. Future experimental work is outlined based on optimizing each relevant facet. By optimizing the facets, the overall step may be optimized. By systematically optimizing all five steps, the dream of a high-efficiency, water-based, inkjet printed OPV device may be achieved.

5.2 Step (1) - Printing Settings/ Parameters

Uniform deposition and film formation via inkjet printing is highly dependent on the printing parameters. Each of the parameters are outlined in Figure 2, and in the text following.
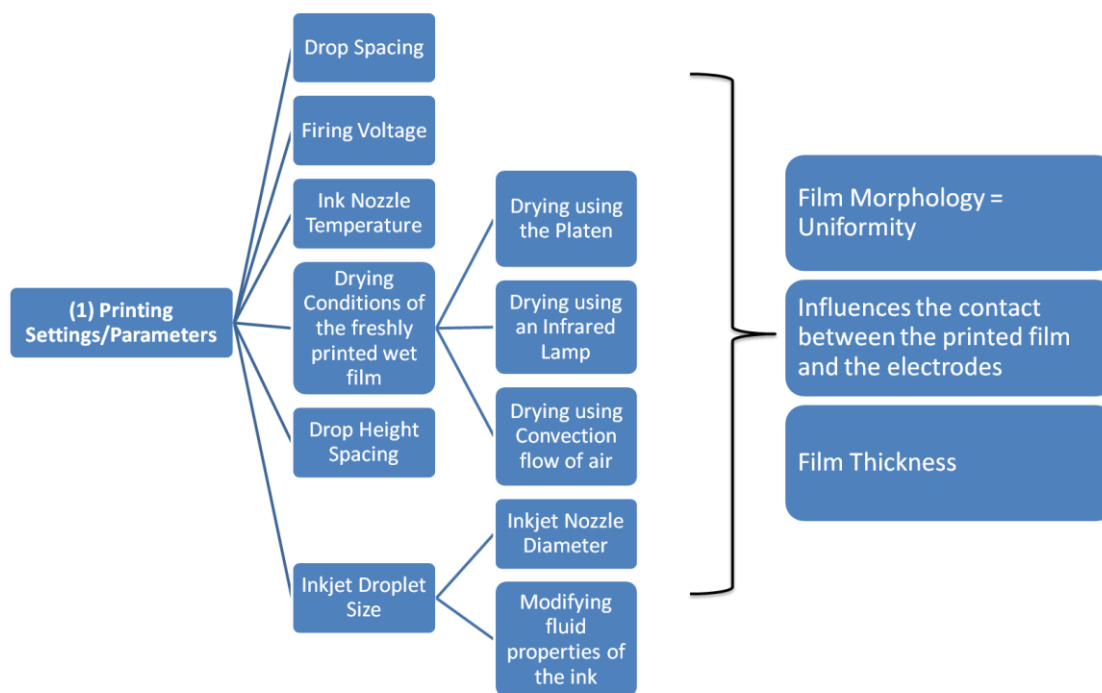
Figure 5.2 : The breakdown of the various Printing parameters, and their effect on the final printed film

Drop Spacing - the drop spacing determines the distance between successive inkjet drops as they fall from the inkjet nozzle, towards the substrate. For instance, if the desired printed film needs to be a uniform thin line , the drop spacing needs to be adjusted such that the individual deposited ink droplets join and coalesce with each other. If the drop spacing is too large, then the printed line would not be connected as the ink droplets will not join with each other. If the drop spacing is too small, then the printed line can be seen to "bulge" as the individual ink droplets are being deposited on top of one another due to overlap - this has been detailed in the work conducted by Soltman and Subramaniam[5]. This dependence of uniformity of the printed line on the drop spacing was also reported by Stringer and Derby[6].Teichler et al. outlined the importance of optimizing the drop spacing when printing polymer thin films, using inkjet printing [7].

Drop Height Spacing - A parameter that was not investigated in this thesis is the drop height spacing. In the Inkjet Printing setup used in this thesis, the height difference between the inkjet nozzle and the substrate is set at 1mm, by default. Thus the ink droplet has to travel a distance of 1 mm before it impacts the surface of the substrate. Perelaer et al. reported that by increasing the height spacing, the in-flight evaporation of the solvent can be increased[8]. They showed that, depending on the solid loading fraction of the inks, the droplet diameter could be reduced by almost half through this method. By reducing the amount of solvent on the substrate, the "coffee-ring" (as described in Chapter 3) may be reduced significantly, leading to more uniform printed films.

Firing Voltage- From Chapter 2 and Chapter 3, the cause of inkjetting is described.In brief, a piezoelectric diaphragm is connected to the ink reservoir, with both being located inside the ink cartridge and a voltage pulse is sent through this piezoelectric element, causing it to change

shape. This change in shape creates an artificial pressure inside the reservoir, pushing out the ink. Thus, by changing the intensity and frequency of this "firing" voltage pulse, the frequency of the jetting action as well as the velocity of the jetted droplets can be modified. High viscosity inks require a high firing voltage for efficient jetting, and vice versa for low viscosity inks[9]. Thus the frequency and velocity with which the droplet is jetted [10], need to be matched with the drop spacing for printing uniform films.

Drying Conditions of the freshly printed wet film - Efficient drying/evaporation of solvent from the printed film is desired for rapid processing. As has been described in Chapter 3, the platen temperature ,or general method by which the film is dried, impacts the final morphology of the film. Having a high temperature may not be conducive to good film formation - each solvent system has its own optimal range of platen heating temperatures [7,12]. For instance, a P3HT:PCBM ink, dissolved in a 68% o-Dichlorobenzene and 32% Mesitylene mixture, requires a platen temperature of 40°C, as determined by Hoth et al.[11] through trial and error. The optimum platen temperature setting was not systematically determined for the devices reported in Chapter 4 - a platen temperature of 35°C was arbitrarily chosen; this resulted in highly non-uniform dried films.

Thus, for the future, a large emphasis needs to be placed on determining the *optimum platen temperature ranges for aqueous P3HT:PCBM nanoparticle inks. The possibility of drying the films using *infrared dryers and through *convection, should also be addressed [13].

Inkjet Droplet Size - Another inkjetting parameter that impacts the final printed film, but one which has not been explored in the results of this thesis, is the inkjet droplet size. The size of the droplet is primarily influenced by the inkjet nozzle diameter [14]. Finer, higher resolution printed features require smaller nozzle diameters. The droplet size produced by the Dimatix

printer used in this thesis has a diameter for a 10 picolitre drop; the drop size can be further

brought down to 1 picolitre diameter droplets, by using the 1 picolitre ink cartridges sold by

Dimatix. Since the printer was essentially used for "coating" squares and not for printing fine

features[15], this printing parameter may be investigated fully at a later time.

5.2.1 Future experiments and testable Hypotheses for Step (1) - Printing Settings / Parameters

HYPOTHESIS 1 : By improving the uniformity of the printed film, the Power Conversion Efficiency

can be improved.
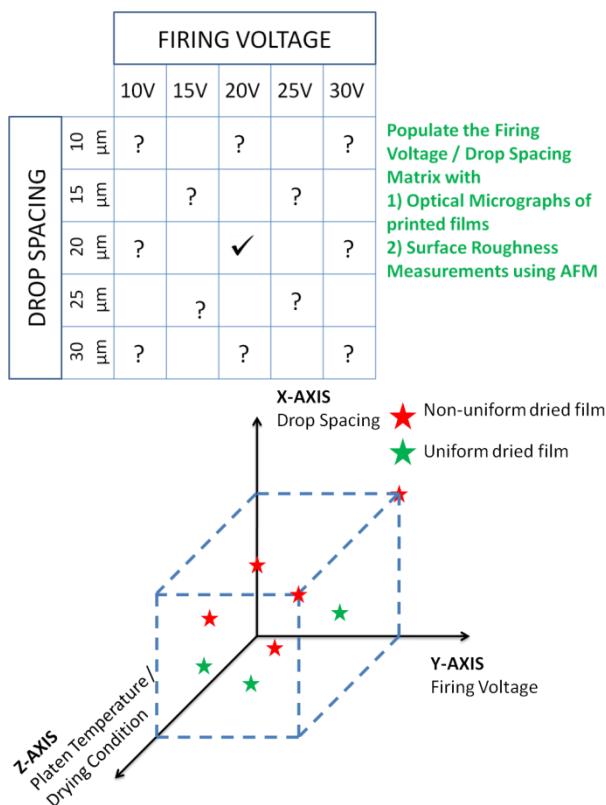
Figure 5.3 : Mockup of Firing Voltage + Drop Spacing matrix Vs Drying conditions

EXPERIMENT 1 :As shown in Determine the relation between Firing Voltage + Drop Spacing with

film formation for water-based P3HT:PCBM nanoparticle inks, as described in Chapter 4.After

determining the optimum drop spacing and firing voltage ranges, systematically determine the

PLATEN TEMPERATURE required for forming uniform films.

1) Record the film morphology and features using an optical microscope.

2) Gather Surface Roughness data of the printed film using optical profilometry and/or Atomic

Force Microscopy.

3) Determine which printing + drying settings yield "uniform" (low surface roughness) and "non-

uniform" (high surface roughness) films..

4) Fabricate devices on said "uniform" and "non-uniform" films. Characterize the Power

Conversion Efficiency of the films and plot the distribution of efficiencies for the uniform and

non-uniform films.
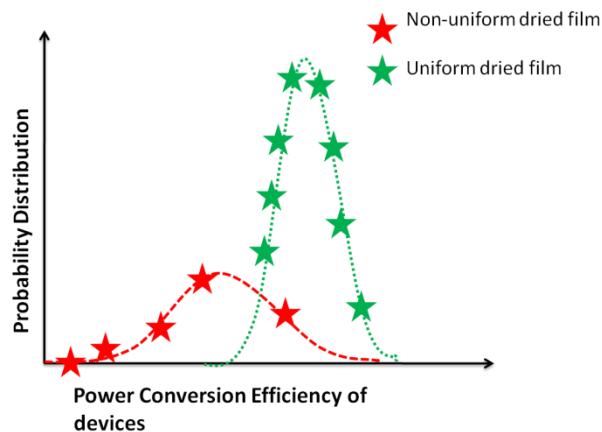
Figure 5.4 : Frequency/ Normal distribution of device efficiencies w.r.t the drying conditions of the film. (Keeping in mind that the drying is itself a product of firing voltage, drop spacing and heating of the wet film.)

5) Confirm that the Non-uniform films yield devices which perform poorly as compared to the

uniform films, as shown in Figure 5.4.

5.3 Step (2) - Modification of the substrate

The next printing step that needs to be addressed is the Substrate onto which the ink is being printed. More specifically, the appropriate substrate modification must be determined such that the final printed film is optimized for device use. Some of the substrate modification routes are shown in Figure 5.By matching the surface energies and the morphology of the substrate with that of the ink, wetting of the ink can be effectively controlled leading to uniformly printed films.
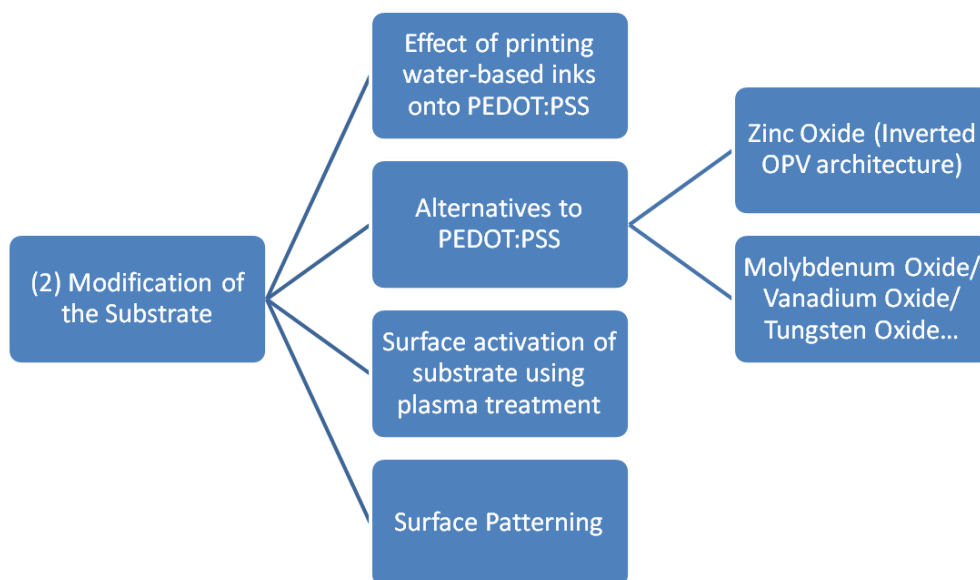
Figure 5.5 : The breakdown of some of the common substrate modification techniques used in literature, for their effect on making substrates more amenable for printing water-based inks.

Effect of printing water-based inks onto PEDOT:PSS - A concern that needs to be addressed is the stability of the PEDOT:PSS buffer layer towards a water-based ink. PEDOT:PSS is a very hygroscopic material; the absorption of ambient water-vapor by the PEDOT:PSS, has been often cited as one of the main reasons for deteriorating OPV device performance [16]. By allowing water molecules to infiltrate the PEDOT:PSS chains, the PEDOT:PSS film experiences decohesion

failure where the PEDOT:PSS film succumbs to mechanical fracture - the "glue" that holds the PEDOT:PSS film together is coulombic attraction between the PEDOT and the PSS; it was shown by Dupont et al[16]. that water forms powerful hydrogen-bonding with the strained SO_3^- groups present on the PEDOT and overcomes the coulombic interaction. This degradation of the PEDOT:PSS layer results in deteriorated charge mobility and hole collection, and eventually turns the PEDOT:PSS/ Active Layer interface into a region of high electrical resistance, as shown by Kawano et al.[17]

In this thesis work, a water-based ink was directly printed on top of the PEDOT:PSS layer, and the resulting films were converted to OVP devices with modest performances, as reported in Chapter 4. For future work, the following question needs to be answered: what is the impact of the water-based ink on the underlying PEDOT:PSS layer, and thereby what is the effect of the change in the PEDOT:PSS (if any) on the resulting power conversion efficiency? This understanding will help narrow down on factors that limit water-based nanoparticle OPV performance. As it currently stands, this question has not been explicitly addressed in literature, in the case of water-based nanoparticle OPV devices. Dastoor and colleagues [19,20] have fabricated nanoparticle OPV devices using spin coating, and have stated that they did not observe any deterioration of the PEDOT:PSS layer, due to the fact that the time of interaction between the water-based ink and the PEDOT:PSS was very low - the same may not be said for inkjet printing because water-based ink spends a lot more on the surface of the PEDOT:PSS as it has to dry by solvent evaporation.

Alternatives to PEDOT:PSS - Owing to the shortcomings of PEDOT:PSS, a lot of research focus has been placed on finding alternatives to PEDOT:PSS as buffer layer materials for OPVs.

* Zinc Oxide (Inverted OPV architecture)

Zinc Oxide(ZnO) has been used as an electron collection material (PEDOT:PSS is a hole collection material), in an OPV device architecture that follows the following OPV structure:

Cathode (ITO) /Electron Collection Layer(ZnO)/Active Layer/Anode

This is known as the Inverted OPV architecture [16,21,22] and has been shown to exhibit higher functioning lifetimes[22]due to the fact that the PEDOT:PSS has been replaced.

* Other hole collection layers such as Molybdenum Oxide, Vanadium Oxide and Tungsten Oxide

Metal oxides such as Molybdenum Oxide (MoO_x) [23], Vanadium Oxide (VO_x)[24] , Tungsten Oxide (WO_x)[25,26], Titanium Oxide (TiO_x)[27] are currently being investigated for their usage as hole collection layers in OPVs. The main promise of using these materials lies in the fact that they do not degrade in the presence of water vapor, unlike PEDOT:PSS. (Some preliminary work can be seen in Appendix A, where PEDOT:PSS and MoO_x buffer layer devices were compared for their power conversion efficiencies) Thus, another study is the inkjet printing of water-based inks on these metal oxide layers, and the subsequent device performances.

*Surface Activati*on - By exposing the surface of the substrate to an oxygen/atmospheric plasma treatment, the surface energies of the substrate can be modified to improve wetting and spreading of inks [28]. This method was used in Chapter 4, where PEDOT:PSS coated ITO substrates were exposed to the oxygen plasma treatment for 2 minutes. This may give rise to a few new questions: apart from improving the wettability of the substrate, does the oxygen plasma have a positive/negative effect on the substrate's electronic properties? PEDOT:PSS is a polymer based buffer layer, and MoO_x etc. are metallic - will the oxygen plasma completely deteriorate the PEDOT:PSS after excessive exposure? Is oxygen plasma treatment better suited

for metallic oxide layers? A study conducted by Sun et al.[29] reports that plasma treatment of a MoO$_3$hole collection layer causes it to get reduced to MoO$_x$, where x<3, leading to superior OPV device performance. If so, this may be doubly beneficial for water-based OPV devices; (i) the plasma treated metal oxide layer will facilitate good wetting of the ink and (ii) the plasma treatment itself will improve conductivity of the metal oxide layer through surface activation.

Surface Patterning - Morphology of the substrate may also be used to influence printed film formation. The substrate can be patterned with materials of low and high surface energies. Sirringhaus et al. [30] were able to pattern polyimide coated glass substrate using photolithography, introducing 50nm tall features on the substrate. By inkjet printing the water-based inks in between the hydrophobic polyimide features, they were able to fabricate thin film transistors. A similar approach was reported by Hendriks et al., where the substrate was patterned using a hot-embossing method [31]. In this case, grooves with fixed widths and depths were introduced into the glass substrates. When the ink is printed on top of these grooves, it flows down into the groove to form patterned films. Surface patterning is especially useful for the formation of high resolution printed features; it still remains to be seen if this approach can be adapted for forming uniform films from the water based OPV inks (as opposed to single lines).

5.3.1 Future experiments and testable Hypotheses for Step (2) - Modification of the substrate

HYPOTHESIS 2 : Oxygen plasma treatment of different buffer layers (PEDOT:PSS, MoO$_x$) will improve the wetting of the printed ink. Improved wetting will give rise to better dried film formation, leading to higher power conversion efficiencies of devices made from those films. However, the plasma treatment will impact the electrical properties of the buffer layer itself leading to improved/deteriorated device performance as a function of plasma treatment

duration. For instance, the PEDOT:PSS buffer layer would be expected to get heavily oxidized by extensive plasma treatment step, resulting in a deteriorated PEDOT:PSS film. This could lead to a reduced PCE% of the overall device.

Figure 5.6 : Experimental matrix studying the effect of Substrate Vs. Surface treatment conditions on the power conversion efficiency

EXPERIMENT 2 : As shown in Figure 5.6, calculate the power conversion efficiencies of devices fabricated using the conditions specified in the experimental matrix.

(i) Record the contact-angle of the ink on each different substrate/treatment configuration - this yields quantitative information as to how well the printed film will wet the surface as well as the film formation of the dried film.
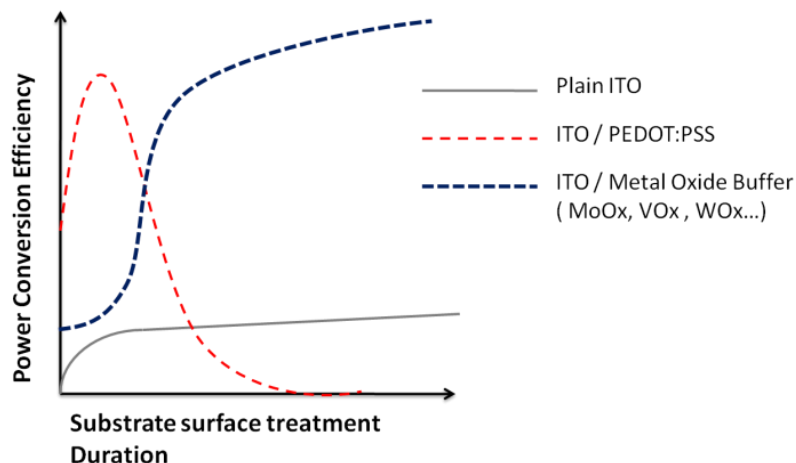
Figure 5.7 : Plotting the change in power conversion efficiency w.r.t (i) the different buffer layer used as well as (ii) the duration and /or intensity of surface treatment on each buffer layer.

(ii) Record the power conversion efficiencies and plot the data as shown in Figure 5.7.

5.4 Step (3) - Conditions for Fabrication of Miniemulsion Nanoparticles

The way the miniemulsion is prepared influences the average size distribution of the nanoparticles. Size is of utmost importance; if the nanoparticles are too large, it gives rise to a larger probability for the inkjet printer nozzles to clog. The Dimatix printer specifications state that the maximum particle size may be <200nm in diameter. The following step, as shown in Figure 5.8, outlines the major factors within the miniemulsion process that influence nanoparticle size.
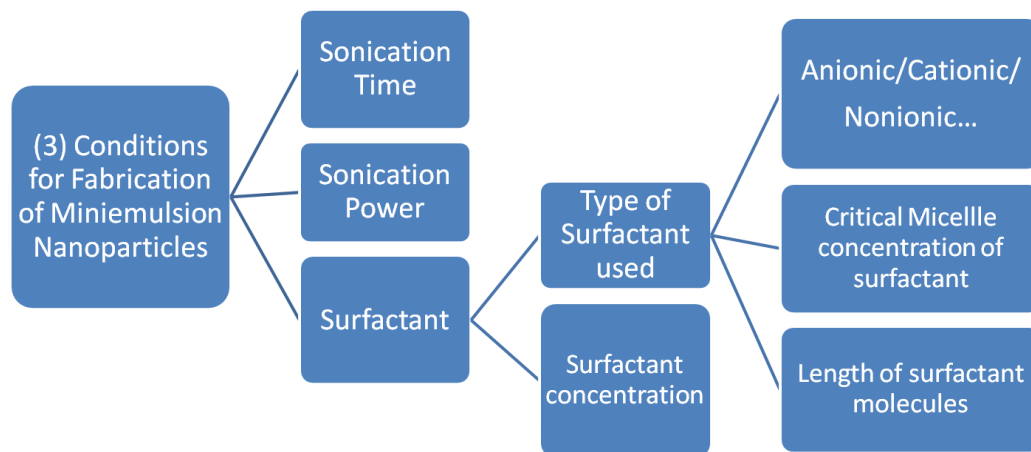
Figure 5.8 : The breakdown of parameters that influence the nanoparticles fabricated in the miniemulsion

Sonication Time/Duration - In the miniemulsion, the nanoparticle droplets are created through the application of sonication i.e. high shear force. This shear causes the constant fusion and fission of the droplets - this continues until the droplet size becomes highly homogeneous. Thus the sonication duration directly impacts the final particle size [32]

Sonication Power/Intensity - Similar to the sonication duration, the sonication intensity also impacts the final particle size distribution. The higher the sonication power, the smaller the nanoparticle size. [33,34]

Surfactant - The crucial ingredient for a miniemulsion is the emulsifying agent i.e. the surfactant. The final size of the nanoparticle depends on the miniemulsion droplet size. This droplet size is directly influenced by the *concentration of the surfactant[35] where high concentration of surfactants lead to smaller droplet sizes after sonication, and thus smaller nanoparticle size distributions. Hand in hand with the surfactant concentration, the *type of surfactant[36]also influences droplet size. For instance, *anionic surfactants may adsorb differently to the surface of the suspended nanoparticle than cationic or nonionic surfactants[37]; different surfactants

have *different critical micelle concentrations, *different molecule sizes/chain lengths[38]

which end up playing a large role in droplet formation.

5.4.1 Testable hypotheses for Step (3) - Conditions for Fabrication of Miniemulsion

Nanoparticles

HYPOTHESIS 3: Sonication Time , Sonication Power and the Surfactant concentration can be manipulated to yield highly monodisperse nanoparticles for water-based OPV inks
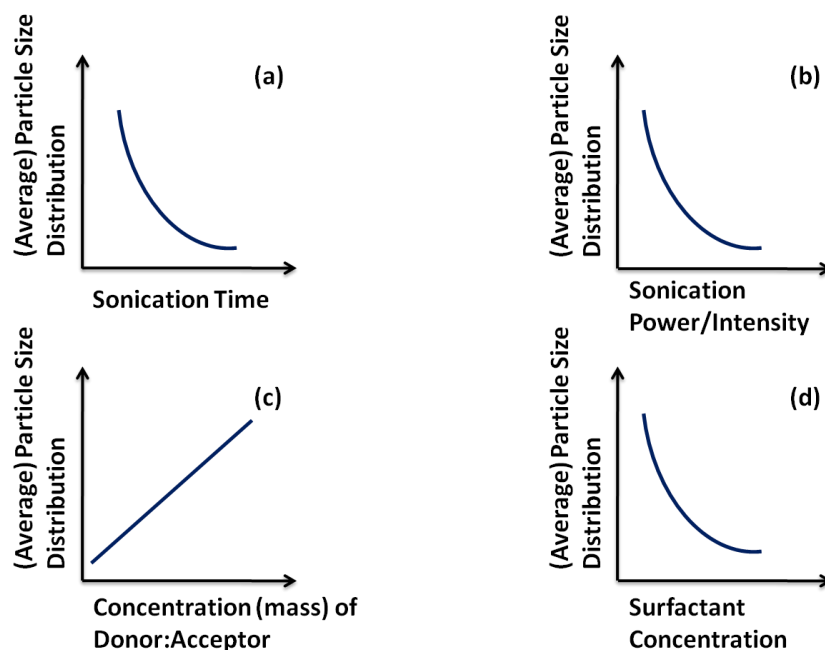
Figure 5.9 : Hypothetical calibration curves that yield particle size distributions as a function of (a)Sonication Time, (b)Sonication Power/Intensity, (c)Concentration of donor:acceptor suspended and (d)surfactant concentration.

EXPERIMENT 3 : Plot the calibration curves (as shown in Figure 9) to confirm the control of

particle size distributions using the miniemulsion approach.

Record the particle size distributions using the Quasi-Elastic Light scattering method outlined in

Chapter 2 and Chapter 4.

Plot:

(i) Particle Size Distribution Vs. Sonication Time

(ii) Particle Size Distribution Vs. Sonication Power

(iii) Particle Size Distribution Vs. Concentration of donor:acceptor dissolved in the "oil-phase" of the miniemulsion

(iv) Particle Size Distribution Vs. Surfactant concentration (and different surfactants)

5.5 Step (4) - Properties of Nanoparticles as a result of miniemulsion conditions
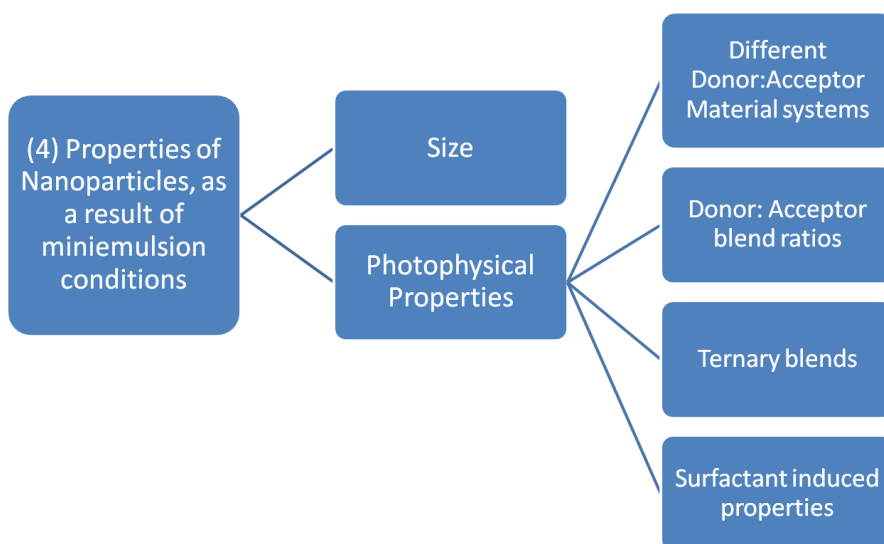
Figure 5.10 : The breakdown of the properties of the nanoparticles that can be synthesized based on the miniemulsion conditions.

From Figure 5.10, the nanoparticle parameters are broken down into the following

Size - As discussed in STEP 3, the miniemulsion conditions determine the particle size distributions.

*Photophysical propertie*s - the act of generating charge originates in the absorption of light and therefore the photophysical properties of the donor:acceptor materials used within the

~ 98 ~

nanoparticle. By *improving the Donor: Acceptor material systems (and blend ratios)

[39,40,41,42,43] light may be absorbed more effectively resulting in increased power conversion

efficiencies.*Another concept that might be worth investigating is the ternary blends of

donor:acceptor materials within the nanoparticle [44]. In Ternary blends, 2 donors materials

with differing (often complimentary) ranges of light absorbance and 1 acceptor (or 1 donor and

2 acceptor) have been shown to greatly increase device efficiency, as a much larger spectrum of

light is seen to be absorbed. *Finally, Tan et al. showed that changing the conjugation length

between the donor:acceptor materials using different surfactant molecules [38] can lead to

better device performance. Thus, by investigating the above methods , nanoparticle based OPV

device performance may be further improved.

5.5.1 Testable hypotheses for Step (4) - Properties of Nanoparticles as a result of miniemulsion

conditions

HYPOTHESIS 4: Particle Size and size distributions impact the final printed film thickness and

uniformity of the film. Particle Size distribution also determines the power conversion efficiency

obtained from the films as different particle sizes would lead to different length scales that the

excitons generated within the nanoparticle will have to traverse based on the internal makeup

of the particle (again, this comes back to the donor:acceptor materials and their blend ratio; for

a well mixed nanoparticle, exciton diffusion may be highly efficient regardless of particle size as

there is a large chance for the generated exciton pair to diffuse towards the Donor:Acceptor

interface. However, the larger the particle, the probability for the generated exciton pair to get

trapped in impurities/structural defects of the nanoparticle). Finally, Power conversion

Efficiency is related to the uniformity of the film; the rougher the printed film, the higher the

chances of device failure due to short circuiting of the electrodes (see HYPOTHESIS 1)
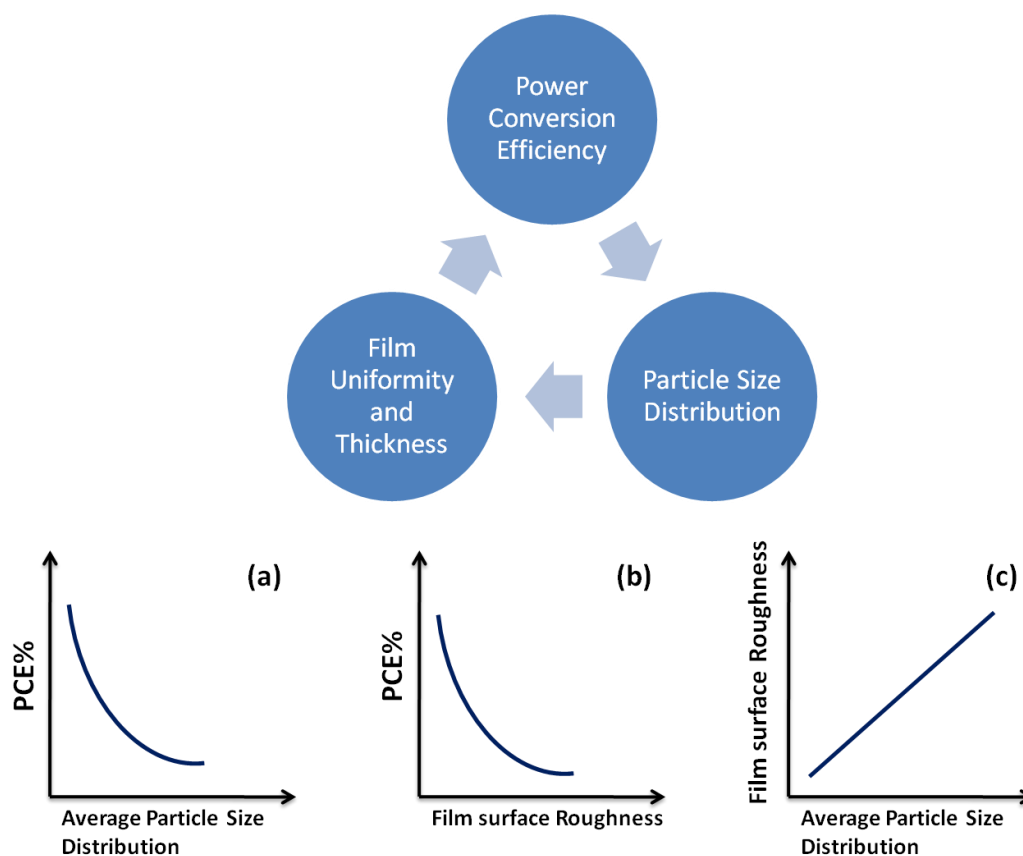
Figure 5.11 : Interdependency between Power Conversion Efficiency, Particle Size Distribution and Printed/ Spin Coated Film uniformity

EXPERIMENT 4: Confirm the relation between particle size distribution, film uniformity (surface roughness) and resulting power conversion efficiencies.

By plotting the calibration curves for the relations outlined in Figure 5.11, a firm understanding for the structure-property relation of the nanoparticle OPV can be developed - where a much more uniform film structure may give rise to a higher PCE%

HYPOTHESIS 5: Different Donor:Acceptor material systems will yield efficient power conversion efficiencies when the blend ratio between each donor:acceptor system has been optimized.

(See blend ratio study in Chapter 4)
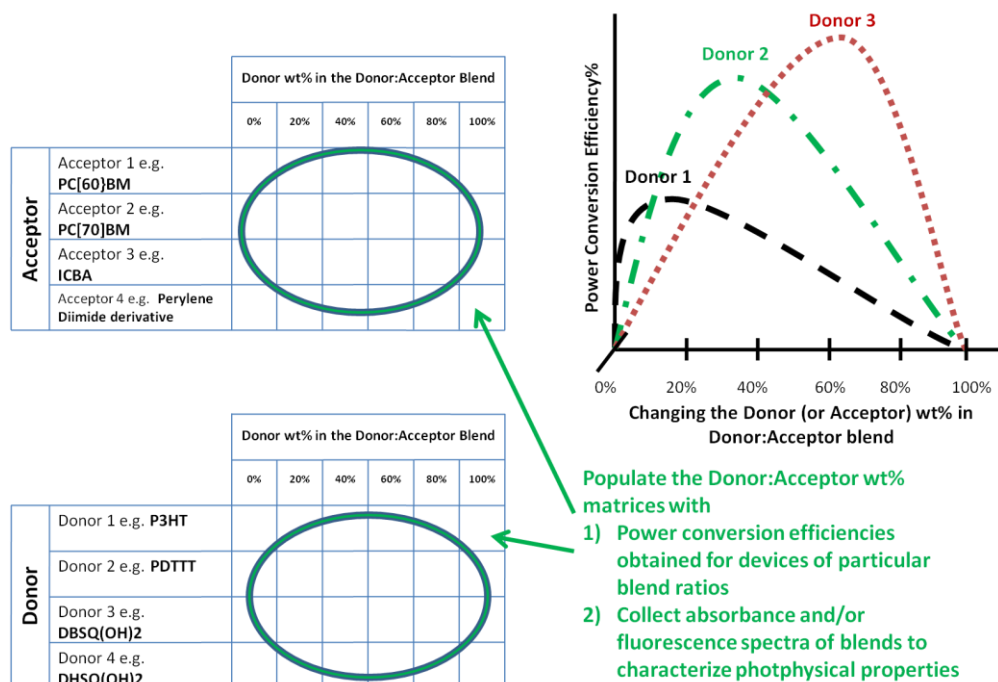
Figure 5.12 : Power conversion efficiencies obtained from nanoparticle OPV devices made from different Donor:Acceptor Materials and different blend ratios

EXPERIMENT 5 : Find out the power conversion efficiencies of nanoparticle OPVs made by the following conditions:

(i) Donor is kept constant - Acceptor is changed in different wt% ratios

(ii) Acceptor is kept constant - Donor is changed in different wt% ratios

(iii) Changing the conjugation length of the Surfactant used - thereby improving charge mobility through the nanoparticle film

By populating the experimental matrices and plotting the calibration curves for each as outlined in Figure 5.12, further structure-property relations between the donor:acceptor blends and device efficiency can be understood - ultimately guiding the researchers to develop better materials in order to achieve higher device performance.

5.6 Step (5) - Physical Properties of the Ink

The "final" step that needs to be addressed is the ink itself; the physical, fluid properties of the ink vehicle influences inkjetting behaviour (thereby influencing the change in inkjet printing parameters as seen in Step 1 - this completes the cycle). The fluid properties of the ink also influence how the ink wets the substrate (influencing Step 2 - substrate modification). The main properties of the ink are tabulated in Figure 5.13, and detailed in the following sections.
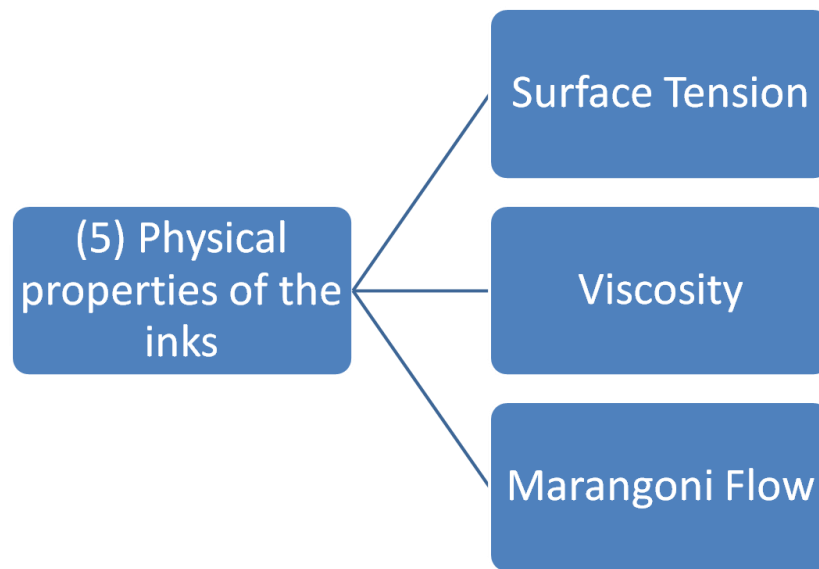
Figure 5.13 : Breakdown of the physical/fluid properties of the ink vehicle

Surface Tension–It is the surface tension of the ink vehicle that (i) holds the ink liquid at the inkjet nozzle[1],preventing leaking/dripping in the absence of negative pressure within the ink cartridge and (ii)influences the spreading/wetting of the ink droplet on the substrate[45].

Viscosity - The viscosity of the ink influences (i) the final printed shape[1] and also (ii) the printing parameters used in Step 1 , such as the pulse Firing Voltage. High Viscosity inks require high firing voltages as it requires a higher amount of energy to be ejected from the ink nozzle[45,46]

Marangoni Flow–Marangoni flow was discussed in Chapter 3. In the case of "pure" solvent systems such as 100% water or 100% o-Dichlorobenzene, the final dried film will have a coffee-ring formation due to the capillary flow of the liquid towards the periphery of the ink droplet, when the solvent is being evaporated. By introducing a surface tension gradient within the solvent (usually by adding a secondary co-solvent with a different surface tension) an inward-flow of liquid can be induced; thus, the coffee-ring effect can be significantly reduced, leading to more uniform film formation. This inward, uniform flow is called Marangoni Flow[47,48].

5.7 Conclusion

Inkjet printing parameters, selection of printing machine specifications, modification of the susbtrates, ink fabrication and nanoparticle sizes are only a few of the many parameters that need to be optimized for the fabrication of efficient nanoparticle OPV devices; what adds to the complexity of the problem is that all these parameters are directly dependent on one another.

In this chapter, the various parameters were discussed in brief. Experimental outlines for testing these parameters were also suggested. By changing these parameters systematically and measuring the effects on specific measurables, it is hoped that the process of inkjet printing of OPV can be streamlined iteratively, in future studies.

5.8 REFERENCES

[1]Singh, Madhusudan, Hanna M. Haverinen, ParulDhagat, and Ghassan E. Jabbour. "Inkjet printing-process and its applications." *Advanced materials* 22, no. 6 (2010): 673.

[2] Derby, Brian. "Inkjet printing of functional and structural materials: fluid property requirements, feature stability, and resolution." *Annual Review of Materials Research* 40 (2010): 395-414.

[3] Tekin, Emine, Patrick J. Smith, and Ulrich S. Schubert. "Inkjet printing as a deposition and patterning tool for polymers and inorganic particles." *Soft Matter*4, no. 4 (2008): 703-713.

[4] De Gans, Berend-Jan, Paul C. Duineveld, and Ulrich S. Schubert. "Inkjet printing of polymers: state of the art and future developments." *Advanced materials* 16, no. 3 (2004): 203-213.

[5] Soltman, Dan, and Vivek Subramanian. "Inkjet-printed line morphologies and temperature control of the coffee ring effect." *Langmuir* 24, no. 5 (2008): 2224-2231.

[6] Stringer, Jonathan, and Brian Derby. "Formation and stability of lines produced by inkjet printing." *Langmuir* 26, no. 12 (2010): 10365-10372.

[7]Teichler, Anke, Rebecca Eckardt, Christian Friebe, JolkePerelaer, and Ulrich S. Schubert. "Film formation properties of inkjet printed poly (phenylene-ethynylene)-poly (phenylene-vinylene) s." *Thin Solid Films* 519, no. 11 (2011): 3695-3702.

[8]Perelaer, Jolke, Patrick J. Smith, Mike MP Wijnen, Erwin van den Bosch, Rebecca Eckardt, Peter HJM Ketelaars, and Ulrich S. Schubert. "Droplet tailoring using evaporative inkjet printing." *Macromolecular Chemistry and Physics* 210, no. 5 (2009): 387-393.

[9] Tsai, M. H., Weng-Sing Hwang, H. H. Chou, and P. H. Hsieh. "Effects of pulse voltage on inkjet printing of a silver nanopowder suspension." *Nanotechnology*19, no. 33 (2008): 335304.

[10] Reis, Nuno, Chris Ainsley, and Brian Derby. "Ink-jet delivery of particle suspensions by piezoelectric droplet ejectors." *Journal of Applied Physics* 97, no. 9 (2005): 094903.

[11]Hoth, Claudia N., Stelios A. Choulis, Pavel Schilinsky, and Christoph J. Brabec. "High photovoltaic performance of inkjet printed polymer: fullerene blends." *Advanced Materials* 19, no. 22 (2007): 3973-3978.

[12] Lim, Guan-Hui, Jing-Mei Zhuo, Loke-Yuen Wong, Soo-Jin Chua, Lay-Lay Chua, and Peter KH Ho. "A transition solvent strategy to print polymer: fullerene films using halogen-free solvents for solar cell applications." *Organic electronics* 15, no. 2 (2014): 449-460.

[13]Yu, Jong-Su, Inyoung Kim, Jung-Su Kim, Jeongdai Jo, Thue T. Larsen-Olsen, Roar R. Søndergaard, Markus Hösel, DechanAngmo, MikkelJørgensen, and Frederik C. Krebs. "Silver front electrode grids for ITO-free all printed polymer solar cells with embedded and raised topographies, prepared by thermal imprint, flexographic and inkjet roll-to-roll processes." *Nanoscale* 4, no. 19 (2012): 6032-6040.

[14] Kung, Chung-yi, Michael D. Barnes, Noah Lermer, William B. Whitten, and J. Michael Ramsey. "Single-molecule analysis of ultradilute solutions with guided streams of 1-μm water droplets." *Applied optics* 38, no. 9 (1999): 1481-1487.

[15] Goghari, A. Amirzadeh, and S. Chandra. "Producing droplets smaller than the nozzle diameter by using a pneumatic drop-on-demand droplet generator."*Experiments in Fluids* 44, no. 1 (2008): 105-114.

[16] Krebs, Frederik C., Suren A. Gevorgyan, and Jan Alstrup. "A roll-to-roll process to flexible polymer solar cells: model studies, manufacture and operational stability studies." Journal of Materials Chemistry 19, no. 30 (2009): 5442-5451

[17]Dupont, Stephanie R., Fernando Novoa, EszterVoroshazi, and Reinhold H. Dauskardt. "Decohesion kinetics of PEDOT: PSS conducting polymer films."*Advanced Functional Materials* 24, no. 9 (2014): 1325-1332.

[18] Kawano, Kenji, Roberto Pacios, Dmitry Poplavskyy, Jenny Nelson, Donal DC Bradley, and James R. Durrant. "Degradation of organic solar cells due to air exposure." Solar energy materials and solar cells 90, no. 20 (2006): 3520-3530.

[19] Ulum, Syahrul, Natalie Holmes, Matthew Barr, AL David Kilcoyne, Bill Bin Gong, Xiaojing Zhou, Warwick Belcher, and Paul Dastoor. "The role of miscibility in polymer: fullerene nanoparticulate organic photovoltaic devices." *Nano Energy* 2, no. 5 (2013): 897-905.

[20] Ulum, Syahrul, Natalie Holmes, DarmawatiDarwis, Kerry Burke, AL David Kilcoyne, Xiaojing Zhou, Warwick Belcher, and Paul Dastoor. "Determining the structural motif of P3HT: PCBM nanoparticulate organic photovoltaic devices." *Solar Energy Materials and Solar Cells* 110 (2013): 43-48.

[21]Guo, Xugang, Nanjia Zhou, Sylvia J. Lou, Jeremy Smith, Daniel B. Tice, Jonathan W. Hennek, Rocío Ponce Ortiz et al. "Polymer solar cells with enhanced fill factors." *Nature Photonics* 7, no. 10 (2013): 825-833.

[22]Kyaw, A. K. K., X. W. Sun, C. Y. Jiang, G. Q. Lo, D. W. Zhao, and D. L. Kwong. "An inverted organic solar cell employing a sol-gel derived ZnO electron selective layer and thermal evaporated MoO3 hole selective layer." Appl. Phys. Lett 93, no. 22 (2008): 221107.

[23]Li, Ning, Brian E. Lassiter, Richard R. Lunt, Guodan Wei, and Stephen R. Forrest. "Open circuit voltage enhancement due to reduced dark current in small molecule photovoltaic cells." *Applied Physics Letters* 94, no. 2 (2009): 023307.

[24]Shrotriya, Vishal, Gang Li, Yan Yao, Chih-Wei Chu, and Yang Yang. "Transition metal oxides as the buffer layer for polymer photovoltaic cells." *Applied Physics Letters* 88, no. 7 (2006): 073508.

[25]Han, Seungchan, Won Suk Shin, MyungsooSeo, Dipti Gupta, Sang-Jin Moon, and SeunghyupYoo. "Improving performance of organic solar cells using amorphous tungsten oxides as an interfacial buffer layer on transparent anodes." *Organic Electronics* 10, no. 5 (2009): 791-797.

[26] Choi, Hana, BongSoo Kim, Min Jae Ko, Doh-Kwon Lee, Honggon Kim, Sung Hyun Kim, and Kyungkon Kim. "Solution processed WO 3 layer for the replacement of PEDOT: PSS layer in organic photovoltaic cells." *Organic Electronics* 13, no. 6 (2012): 959-968.

[27]Waldauf, C., M. Morana, P. Denk, P. Schilinsky, K. Coakley, S. A. Choulis, and C. J. Brabec. "Highly efficient inverted organic photovoltaics using solution based titanium oxide as electron selective contact." *Applied Physics Letters*89, no. 23 (2006): 233517.

[28]Tendero, Claire, ChristelleTixier, Pascal Tristant, Jean Desmaison, and Philippe Leprince. "Atmospheric pressure plasmas: A review." *SpectrochimicaActa Part B: Atomic Spectroscopy* 61, no. 1 (2006): 2-30.

[29] Sun, Jen-Yu, Wei-Hsuan Tseng, ShiangLan, Shang-Hong Lin, Po-Ching Yang, Chih-I. Wu, and Ching-Fuh Lin. "Performance enhancement in inverted polymer photovoltaics with solution-

processed MoO X and air-plasma treatment for anode modification." *Solar Energy Materials and Solar Cells* 109 (2013): 178-184.

[30]Sirringhaus, H., T. Kawase, R. H. Friend, T. Shimoda, M. Inbasekaran, W. Wu, and E. P. Woo. "High-resolution inkjet printing of all-polymer transistor circuits."*Science* 290, no. 5499 (2000): 2123-2126.

[31]Hendriks, Chris E., Patrick J. Smith, JolkePerelaer, Antje MJ Van den Berg, and Ulrich S. Schubert. ""Invisible" Silver Tracks Produced by Combining Hot-Embossing and Inkjet Printing." *Advanced Functional Materials* 18, no. 7 (2008): 1031-1038.

[32]Mateovic, T., B. Kriznar, M. Bogataj, and A. Mrhar."The influence of stirring rate on biopharmaceutical properties of Eudragit RS microspheres." *Journal of microencapsulation* 19, no. 1 (2002): 29-36

[33] Amsden, Brian. "The production of uniformly sized polymer microspheres."*Pharmaceutical research* 16, no. 7 (1999): 1140-1143.

[34] Sansdrap, Pascale, and André-Jules Moës. "Influence of manufacturing parameters on the size characteristics and the release profiles of nifedipine from poly (DL-lactide-co-glycolide) microspheres." *International journal of pharmaceutics* 98, no. 1 (1993): 157-164.

[35]Staff, Roland H., Katharina Landfester, and Daniel Crespy. "Recent advances in the emulsion solvent evaporation technique for the preparation of nanoparticles and nanocapsules." In *Hierarchical Macromolecular Structures: 60 Years after the Staudinger Nobel Prize II*, pp. 329-344. Springer International Publishing, 2013.

[36]Nizri, Gilat, Serge Lagerge, Alexander Kamyshny, Dan T. Major, and ShlomoMagdassi. "Polymer–surfactant interactions: binding mechanism of sodium dodecyl sulfate to poly (diallyldimethylammonium chloride)." *Journal of colloid and interface science* 320, no. 1 (2008): 74-81.

[37]Cho, Jangwhan, Seongwon Yoon, Jaeun Ha, and Dae Sung Chung. "Utilization of a Non-Ionic Surfactant in the Fabrication of Water-Borne Polymeric Semiconductor Nanoparticles for High-Performance, Green Organic Electronics." *ECS Transactions* 69, no. 5 (2015): 89-94.

[38]Tan, Bin, Yancen Li, Maria Francisca Palacios, Joel Therrien, and Margaret J. Sobkowicz. "Effect of surfactant conjugation on structure and properties of poly (3-hexylthiophene) colloids and field effect transistors." *Colloids and Surfaces A: Physicochemical and Engineering Aspects* (2015).

[39]Cates, Nichole C., Roman Gysel, Zach Beiley, Chad E. Miller, Michael F. Toney, Martin Heeney, Iain McCulloch, and Michael D. McGehee. "Tuning the properties of polymer bulk heterojunction solar cells by adjusting fullerene size to control intercalation." *Nano letters* 9, no. 12 (2009): 4153-4157.

[40]Chen, Guo, Hisahiro Sasabe, Zhongqiang Wang, Xiaofeng Wang, Ziruo Hong, Junji Kido, and Yang Yang. "Solution-processed organic photovoltaic cells based on a squaraine dye." *Physical Chemistry Chemical Physics* 14, no. 42 (2012): 14661-14666.

[41]Müller, Christian, Toby AM Ferenczi, Mariano Campoy-Quiles, Jarvist M. Frost, Donal DC Bradley, Paul Smith, Natalie Stingelin-Stutzmann, and Jenny Nelson. "Binary organic photovoltaic blends: a simple rationale for optimum compositions." *Advanced Materials* 20, no. 18 (2008): 3510-3515.

[42]Hestand, Nicholas J., Chenyu Zheng, Anirudh Raju Penmetcha, Brandon Cona, Jeremy A. Cody, Frank C. Spano, and Christopher J. Collison. "Confirmation of the Origins of Panchromatic Spectra in Squaraine Thin Films Targeted for Organic Photovoltaic Devices." *The Journal of Physical Chemistry C* 119, no. 33 (2015): 18964-18974.

[43] Zheng, Chenyu, Anirudh Raju Penmetcha, Brandon Cona, Susan D. Spencer, Bi Zhu, Patrick Heaphy, Jeremy A. Cody, and Christopher J. Collison. "Contribution of Aggregate States and Energetic Disorder to a Squaraine System Targeted for Organic Photovoltaic Devices." *Langmuir* 31, no. 28 (2015): 7717-7726.

[44] Huang, Jing-Shun, Tenghooi Goh, Xiaokai Li, Matthew Y. Sfeir, Elizabeth A. Bielinski, Stephanie Tomasulo, Minjoo L. Lee, NilayHazari, and André D. Taylor. "Polymer bulk heterojunction solar cells employing Forster resonance energy transfer." *Nature Photonics* 7, no. 6 (2013): 479-485.

[45] Calvert, Paul. "Inkjet printing for materials and devices." *Chemistry of materials*13, no. 10 (2001): 3299-3305.

[46]Perelaer, Jolke, Patrick J. Smith, Erwin van den Bosch, Stephen SC van Grootel, Peter HJM Ketelaars, and Ulrich S. Schubert. "The Spreading of Inkjet-Printed Droplets with Varying Polymer Molar Mass on a Dry Solid Substrate." *Macromolecular chemistry and physics* 210, no. 6 (2009): 495-502.

[47]Hu, Hua, and Ronald G. Larson. "Marangoni effect reverses coffee-ring depositions." *The Journal of Physical Chemistry B* 110, no. 14 (2006): 7090-7094.

[48] Pesach, Dora, and Abraham Marmur. "Marangoni effects in the spreading of liquid mixtures on a solid." *Langmuir* 3, no. 4 (1987): 519-524.

APPENDIX A–Using Molybdenum Oxide as a replacement for PEDOT:PSS

***ABSTRACT/OBJECTIVE* –** Solution processed Molybdenum Oxide is used as a substitute for PEDOT:PSS Hole Transport Layer in P3HT:PCBM devices . Performance and Efficiencies were compared between devices containing PEDOT:PSS and those containing MoO_x. Device Performance was found to be very comparable. Thus, MoO_x may be used in water-based Nanoparticulate OPV due to its higher stability.

A.1 Introduction

Hole Transport Layers (HTL)/ Electron Blocking Layers (EBL) are commonly used to induce direction of flow of photogenerated charges within the active layer of the OPV. For instance, the Hole transport layer which would lie between the Anode and the Active Layer will have a HOMO level which will facilitate hole movement , but since the LUMO is too high, the electron will be blocked and must travel in the OTHER direction. Thus, charge is transported in one direction and efficiency is improved.

One of the most (if not most) commonly used Hole Transport layers is PEDOT:PSS.[1] It is used in all varieties of organic electronic devices from OPVs to OLEDs. It is even being studied to be used as an alternative to ITO, as an electrode[2,3].

However, PEDOT:PSS has a major weakness - it degrades very quickly in the presence of water. Since it is amphiphilic, the Hydrophilic (and Hygroscopic) PSS retains moisture from the

atmosphere and this severely impacts device performance. Indeed, it has been seen that the major reason for declining device performance can be linked to the degradation of the PEDOT:PSS[4]. Thus there is a need to develop a water-stable alternative to PEDOT:PSS if devices are to be made using water-based active layer inks.

An alternative to PEDOT:PSS can be developed in two ways –

1) Changing the device architecture [5] such as an Inverted OPV structure– Instead of using PEDOT:PSS as a HTL between the Anode and Active layer, an Electron Transport Layer may be implemented between the Cathode and Active Layer. Zinc Oxide (ZnO) is commonly used as the ECL, in this case. This method was shown to decrease degradation. However, the author's expertise does not lie in fabricating inverted solar cells, thus this method was not considered.

2) Replacing the PEDOT:PSS itself - Metal Oxides have been and are still being studied for their usage in OPVs and other organic devices. Oxides like Vanadium Oxide, Molybdenum Oxide and Tungsten Oxide [6] are some promising candidates that work as charge transport layers.

Molybdenum Oxide (MoO_x) was chosen as the replacement to PEDOT:PSS due to its ease of processability [7,8,9].

Spun-cast P3HT:PCBM devices with PEDOT:PSS and devices with MoO_x were fabricated; device performance were characterized and compared – it was found that the device performances were very comparable indicating that MoO_x may be used as a Hole Transport Layer in water-based nanoparticulate OPV.

A.2 Experiment

Molybdenum Oxide Preparation : The method was derived from [9]. Ammonium MolybdateTetrahydrate was purchased from Sigma Aldrich and used without further modification. Ammonium MolybdateTetrahydrate $(NH_4)_6Mo_7O_{24}.4H_2O$ is a precursor material that dissociates into MoO_3 , NH_3 (gas) and H_2O upon dissolving in Water and subsequent heating.

400mg of $(NH_4)_6Mo_7O_{24}.4H_2O$ was dissolved in 10ml of DI Water to yield a 4% w/v solution. This solution was stirred for 70 minutes at 200rpm while heating at 80^oC – this is sufficient for adequate dissolution of the precursor – the solution was then further diluted to a 0.2% w/v solution. This solution was subsequently spincoated onto pre-cleaned ITO slides at 4000rpm for 30 seconds. MoOx films were finally annealed at 300^oC for 12 minutes prior to application of P3HT:PCBM active layer.

PEDOT:PSS Preparation: 2.5ml of PEDOT:PSS and 2.5ml of DI water was mixed and filtered through a 0.45 micron PTFE syringe filter. This solution was subsequently spincoated onto pre-cleaned ITO slides at 5000rpm for 45 seconds. PEDOT:PSS films were annealed/heated at 100^oC for 30 minutes prior to application of P3HT:PCBM active layer.

*Active layer Preparation and device fabrication:*15.1 (+/- 0.1) mg of P3HT and 12.0 (+/- 0.1) mg of PCBM were dissolved in 1ml of Chloroform to yield a P3HT:PCBM solution in the ratio 1:0.8. This solution was sonicated and gently heated so as to completely dissolve the materials inside the chloroform. P3HT:PCBM active layers were spincoated onto MoOx/PEDOT:PSS pre-coated films at 800rpm for 18 seconds, inside the glove box. All active layer films were then annealed at 120^oC for 10 minutes before putting them inside the evaporator. Finally, the aluminum cathodes was evaporated onto the P3HT:PCBM films at a pressure of $<10^{-6}$Torr.

A.3 Results, Discussion and Conclusion

Power Conversion efficiencies of the devices were measured using a Newport 91159 Full Spectrum solar simulator with a power density of 100 mW cm-2 (1-sun illumination). The xenon lamp in the solar simulator is calibrated with a Round-Robin InGaAs photovoltaic cell fabricated at NASA. The OPV devices were tested immediately after fabrication.

Tabulated as follows are the measured device performance results.
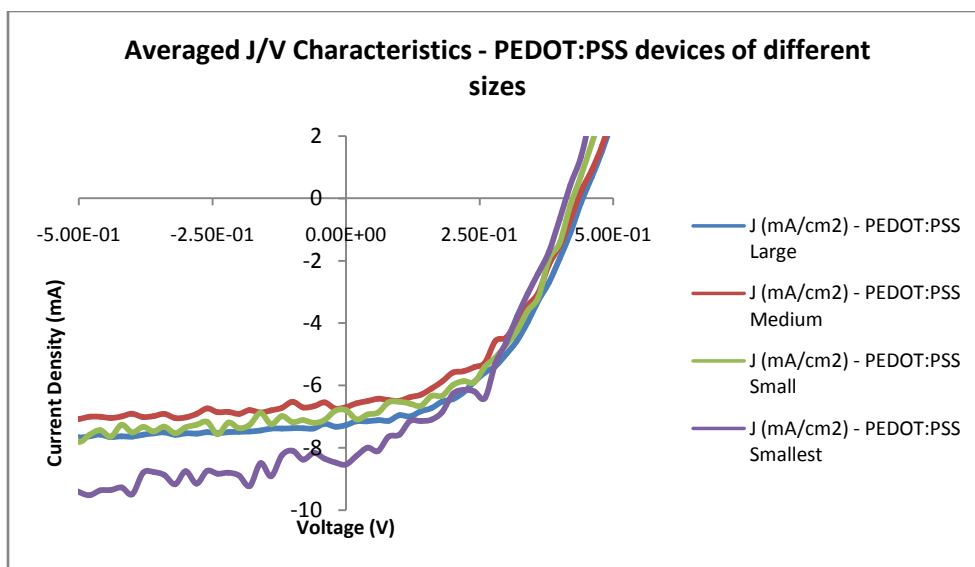
Figure A.1 : J/V Curves of PEDOT:PSS devices

PEDOT:PSS				
Device Area (cm^2)	No. of devices	Largest PCE %	Avg PCE%	St. Dev.
Largest - 0.1963495cm^2	2	1.53	1.515	0.02121320
Medium - 0.096211275cm^2	2	1.42	1.385	0.04949747
Small - 0.034636059cm^2	8	1.64	1.5025	0.10819955
Smallest - 0.0176714587cm^2	7	1.96	1.691428571	0.20979581

Table A.1 : PEDOT:PSS Hole Transport layer device results
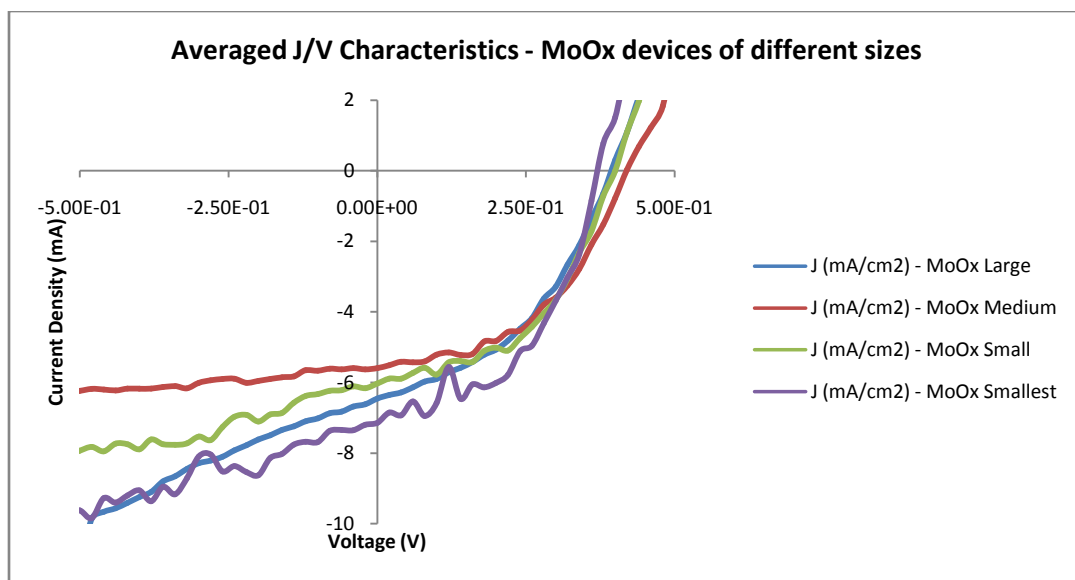
Figure A.2 : J/V Curves of MoOx devices

MoO$_x$				
Device Area(cm^2)	No. of devices tested	Largest Power Conversion Efficiency%	Average Power Conversion Efficiency%	Standard Deviation
Largest - 0.1963495cm^2	4	1.55	1.48	0.112694277
Medium - 0.096211275cm^2	4	1.31	1.25	0.09539392
Small - 0.034636059cm^2	15	1.62	1.228	0.199291603
Smallest - 0.0176714587cm^2	10	2.6	1.398	0.447953371

Table A.2 : MoO$_x$ Hole Transport Layer device results
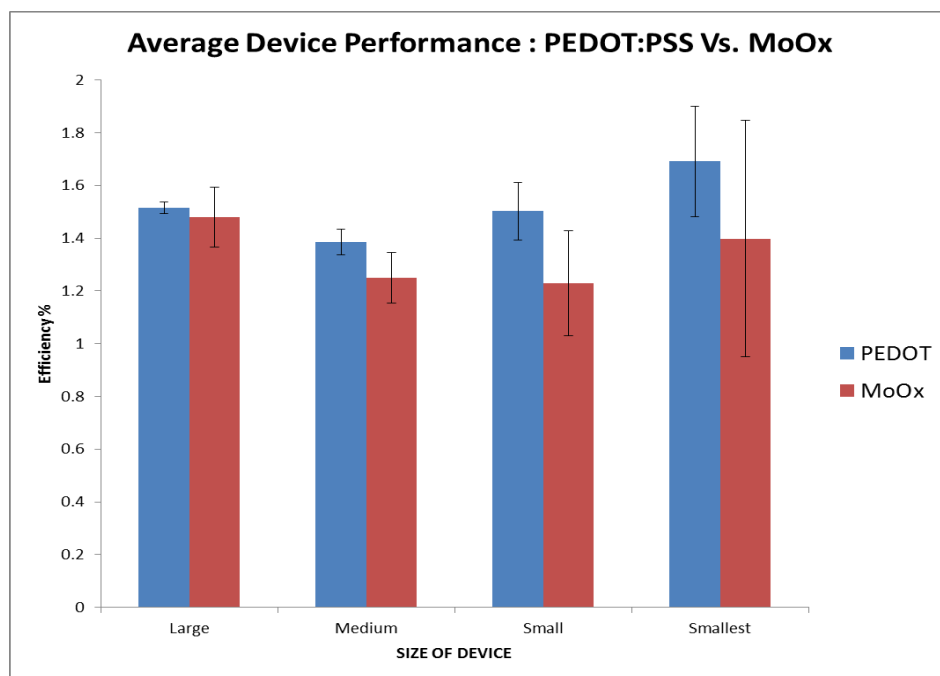
Figure A.3 : Comparing Average Device Performance between PEDOT:PSS and MoO$_x$ based devices
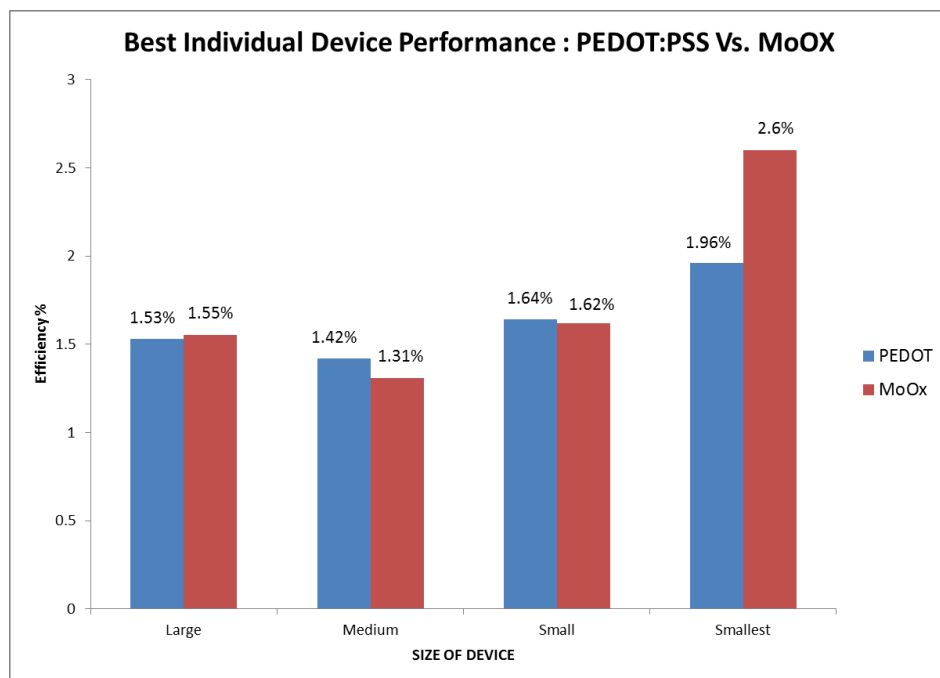
Figure A.4 : Comparing the Best Individual Device Performance (per device area) between PEDOT:PSS and MoO$_x$ based devices

From Figure A.3 and A.4, The PEDOT:PSS and MoO$_x$ based devices were found to have very comparable power conversion efficiencies, across all device areas. As PEDOT:PSS devices are a benchmark OPV material, this result indicates that the MoO$_x$ can be used as an effective Hole Transport layer instead of PEDOT:PSS.

However, further study is still required in understanding and determining if MoO$_x$ is indeed a better alternative to PEDOT:PSS when it comes to water-based nanoparticle OPV devices. Some of the points of interest that need to be addressed in future studies are –

1) Impact of water-based ink on the morphology of the PEDOT:PSS/MoO$_x$.

2) Rearrangement of underlying PEDOT:PSS /MoO$_x$ layer by the water.

3) Wetting of water-based ink on the surface of PEDOT:PSS/MoO$_x$.

4) Modification of surface energies of PEDOT:PSS/MoO$_x$ by ozone plasma treatment.

5) MoOx surface activation/ modification of HOMO/LUMO levels by ozone plasma treatment – can the charge transfer at the MoO$_x$ be further improved?

6) Characterize thickness of MoO$_x$ films and its impact on device performance.

A.4 REFERENCES

[1] Groenendaal, L., Friedrich Jonas, Dieter Freitag, Harald Pielartzik, and John R. Reynolds. "Poly (3, 4-ethylenedioxythiophene) and its derivatives: past, present, and future." *Advanced Materials* 12, no. 7 (2000): 481-494.

[2] Zhang, Wenfeng, Baofeng Zhao, Zhicai He, Xuemei Zhao, Haitao Wang, Shangfeng Yang, Hongbin Wu, and Yong Cao. "High-efficiency ITO-free polymer solar cells using highly conductive PEDOT: PSS/surfactant bilayer transparent anodes." *Energy & Environmental Science* 6, no. 6 (2013): 1956-1964.

[3] Alemu, Desalegn, Hung-Yu Wei, Kuo-Chuan Ho, and Chih-Wei Chu. "Highly conductive PEDOT: PSS electrode by simple film treatment with methanol for ITO-free polymer solar cells." *Energy & environmental science* 5, no. 11 (2012): 9662-9671.

[4] Dupont, Stephanie R., Fernando Novoa, Eszter Voroshazi, and Reinhold H. Dauskardt. "Decohesion kinetics of PEDOT: PSS conducting polymer films."*Advanced Functional Materials* 24, no. 9 (2014): 1325-1332.

[5] Tong, Xiaoran, Brian E. Lassiter, and Stephen R. Forrest. "Inverted organic photovoltaic cells with high open-circuit voltage." *Organic electronics* 11, no. 4 (2010): 705-709.

[6] Vidmar, Tjaša, Marko Topič, Petr Dzik, and Urša Opara Krašovec. "Inkjet printing of sol–gel derived tungsten oxide inks." *Solar Energy Materials and Solar Cells* 125 (2014): 87-95.

[7] Hammond, Scott R., Jens Meyer, N. Edwin Widjonarko, Paul F. Ndione, Ajaya K. Sigdel, Andrés Garcia, Alexander Miedaner et al. "Low-temperature, solution-processed molybdenum oxide hole-collection layer for organic photovoltaics." *Journal of Materials Chemistry* 22, no. 7 (2012): 3249-3254.

[8] Griffin, Jonathan, Andrew J. Pearson, Nicholas W. Scarratt, Tao Wang, David G. Lidzey, and Alastair R. Buckley. "Organic photovoltaic devices incorporating a molybdenum oxide hole-extraction layer deposited by spray-coating from an ammonium molybdate tetrahydrate precursor." *Organic Electronics* 15, no. 3 (2014): 692-700.

[9] Murase, Seiichiro, and Yang Yang. "Solution processed MoO3 interfacial layer for organic photovoltaics prepared by a facile synthesis method." *Advanced Materials* 24, no. 18 (2012): 2459-2462.

APPENDIX B - Fabrication of P3HT-PCBM nanoparticles using the reprecipitation method

ABSTRACT/OBJECTIVE - P3HT:PCBM nanoparticle dispersions were fabricated using the flash-precipitation/nano-precipitation/reprecipitation technique. Nanoparticles were characterized for their size and blending using UV-Vis absorbance and fluorescence spectroscopy. A correlation between spectral features and particle size was found.

B.1 Introduction

Reprecipitation is commonly used in drug manufacturing where the drug molecule is crystallized into nanoparticles by solvent shifting [3]. Recently, these reprecipitation methods were utilized by Jason McNeill et al and Andre Gesquiere et al to make nanoparticles of their analytes. These analytes were then subjected to their Single Particle/Molecule Spectroscopy/Studies. Reprecipitation is conventionally used for understanding BULK characteristics on NANO SCALE; a single molecule of the analyte by itself may not give enough information about its properties in devices. In bulk films of the analyte we may not really study individual domains – the idea being that different sized domains may have different electronic properties. In nanoparticles however, the bulk characteristics of multiple molecules coming together combined with smaller more reproducible domain sizes means that researchers may effectively study the electronic properties of the materials more effectively [4-10].

In this appendix section, the reprecipitation method is described in some detail. This method is used to fabricate P3HT:PCBM nanoparticle dispersions. These nanoparticles are then characterized for their size, blending of P3HT:PCBM and photophysical properties.

B.2 Experimental Section

B.2.1 Nanoparticle Synthesis using the reprecipitation method

P3HT and P3HT:PCBM blends were dissolved in THF to make precursor solutions. By modifying the concentration of the P3HT/PCBM within the precursor, the size of the resulting nanoparticle can be modified. A [1:0] precursor solution is one where 1mg of P3HT and 1mg of PCBM are dissolved in 10ml of THF ; Similarly, a [2:2] precursor solution is one where 2mg of P3HT and 2mg of PCBM are dissolved in 10ml of THF

THF is a weak solvent for P3HT and PCBM. The precursor solution needs to be sonicated/heated for a while before the P3HT gets dissolved. One would know that the P3HT has dissolved when it is seen that the dark-pink turbid polymer solution has turned into a clear orange solution. If these precursors are left alone and not used immediately, the P3HT starts to gel [15,16]. This behooves the experimenter to "re-dissolve" the polymer.

A scintillation vial containing 10ml of water was placed in a bath sonicator. 1ml of desired blend precursor solution was injected into this vial , while the vial was being sonicated. A VWR pipette with 1000 microliter pipette tips was used to inject this precursor solution manually. The pipette tip was placed close to the middle of the vial (underneath the surface of the water) and the solution was manually injected over a period of 10 seconds; the sonication continued for another 10 seconds before it was stopped.

The change from solution to dispersion for P3HT and P3HT:PCBM blends can be visibly seen as the color would change from yellow/orange to pink.

B.2.2 Filtration of Dispersions

Syringe filters were used to determine the size of the nanoparticles. The larger the average size distribution of the nanoparticles, the more material lost in the filters. This loss in material should be reflected in UV-Vis absorbance spectra of the nanoparticle dispersions before and after filtration. Once the dispersions are made, the THF is evaporated off from each dispersion by heating it for ~3 hours at 65 C, while stirring at 1200rpm or by gently evaporating the THF at room temperature for ~24 hours.

Once the THF was removed, 4ml of the chosen dispersion was decanted into a fresh sterile syringe. A 200nm PES filter from VWR was fitted onto the syringe and the dispersion was gently filtered.

B.2.3 Spectroscopy

Absorbance was measured using a Shimadzu UV-2100PC spectrophotometer. Measurements were taken at 0.5nm intervals using a Fast scan speed. (See Chapter 2)

Photoluminescence was measured using a HORIBA Jobin -Yvan Fluoro Max fluorimeter. Measurements were taken at 1nm intervals using a 1 second integration time. Slit Widths of 5nm

B.3 Results and Discussion

B.3.1 Confirming blending of P3HT:PCBM in nanoparticles using absorbance and fluorescence spectroscopy
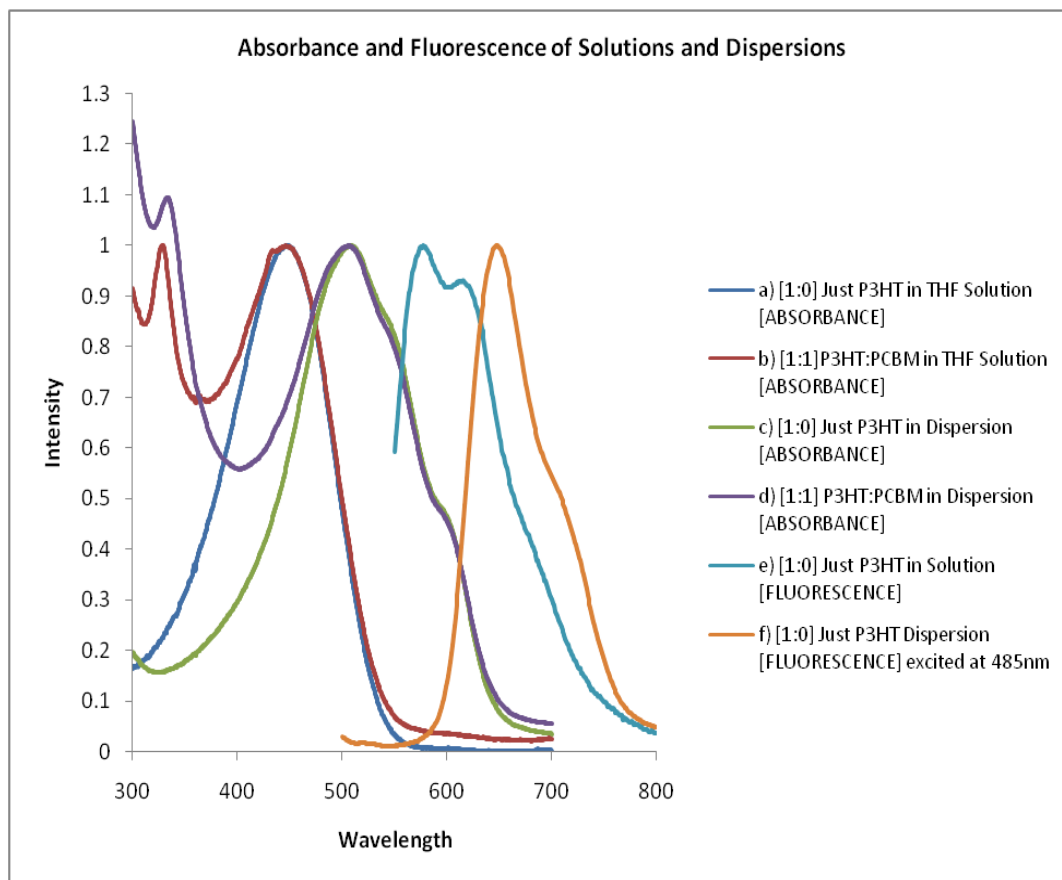
Figure B.1: Normalized Absorbance and Fluorescence spectra of P3HT and P3HT:PCBM in solution and dispersion.

Figure B.1 shows the absorbance and fluorescence profiles of the P3HT and P3HT:PCBM in solution and in dispersions.

For the P3HT in solution the absorption max occurs at 446nm. When PCBM is added to the solution, the absorption max for P3HT is still the same, a characteristic peak at 325nm appears

for the PCBM indicating that it is in solution. Moreover there is also a small feature at around 430nm which is attributed to the characteristic absorbance of PCBM.

Now, the absorbance of the dispersions is red shifted from 446nm to 505nm. This is because the molecules of the P3HT are now interacting with each other; the spectra of nano-solid state domains of P3HT .Packing restricts the torsional motion of the backbone and therefore increases the conjugation. There will also be J- and H-aggregates that will form. Aggregation may be computed by looking at the structure of the absorbance; This is a qualitative assessment that is backed by work done by Spano and colleagues [12,13]. An interesting side track here is that , for future projects, models developed by the Spano group can be used to model the occurrence of aggregates based on domain size of the crystal (which is the particle size of the nanoparticles).[18,20,21]

Their spectra is also more resolved i.e. 3 distinct features for the P3HT are seen to form– a major peak at 505nm, a shoulder at 550nm and a second shoulder at 605nm. The PCBM absorbance max is also red-shifted from 325nm to around 332nm. This indicates that the PCBM is also in solid state [11].

By observing the fluorescence of the solutions it is seen that there is negligible quenching of fluorescence with an increase in PCBM. This is due to the P3HT and PCBM molecules having negligible interaction with each other in solution. PCBM will typically not quench that well (if at all) through Forster energy transfer because the band gap for PCBM is bigger than that for P3HT. DEXTER Energy Transfer quenching is required and this needs close interaction.

In the precipitated nanoparticles increasing the PCBM concentration lead to fluorescence getting rapidly quenched.
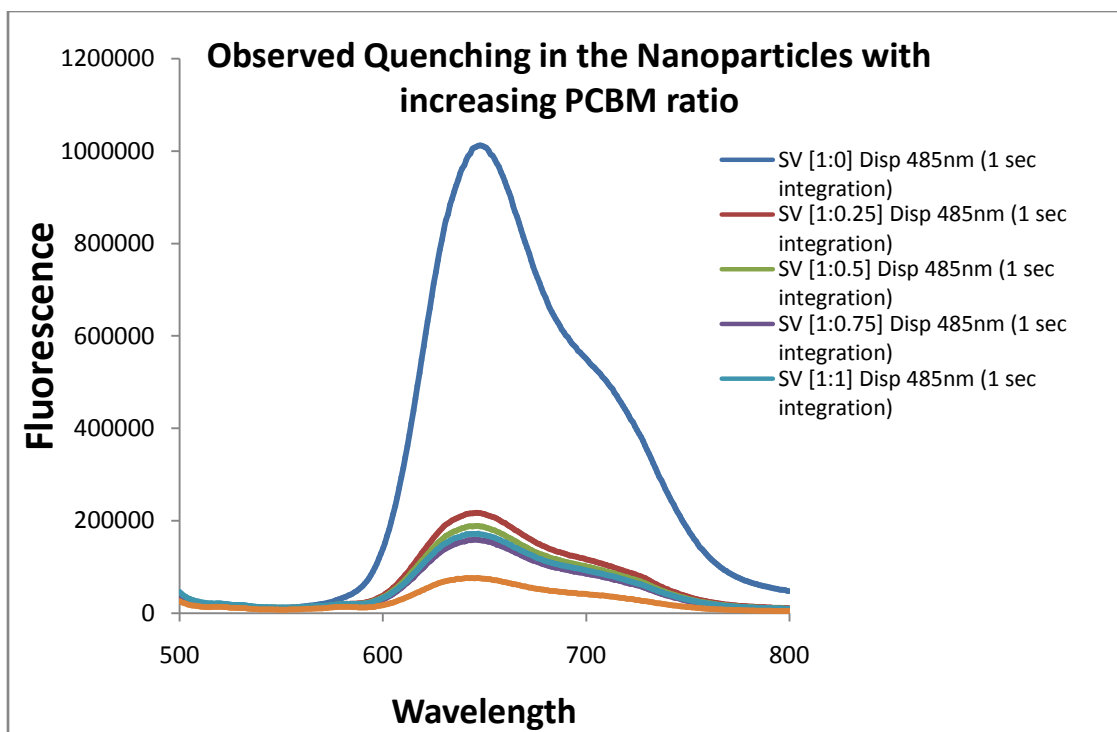
**Figure B.2 :** Raw Fluorescence spectra of P3HT:PCBM nanoparticles where the PCBM ratio is changed.
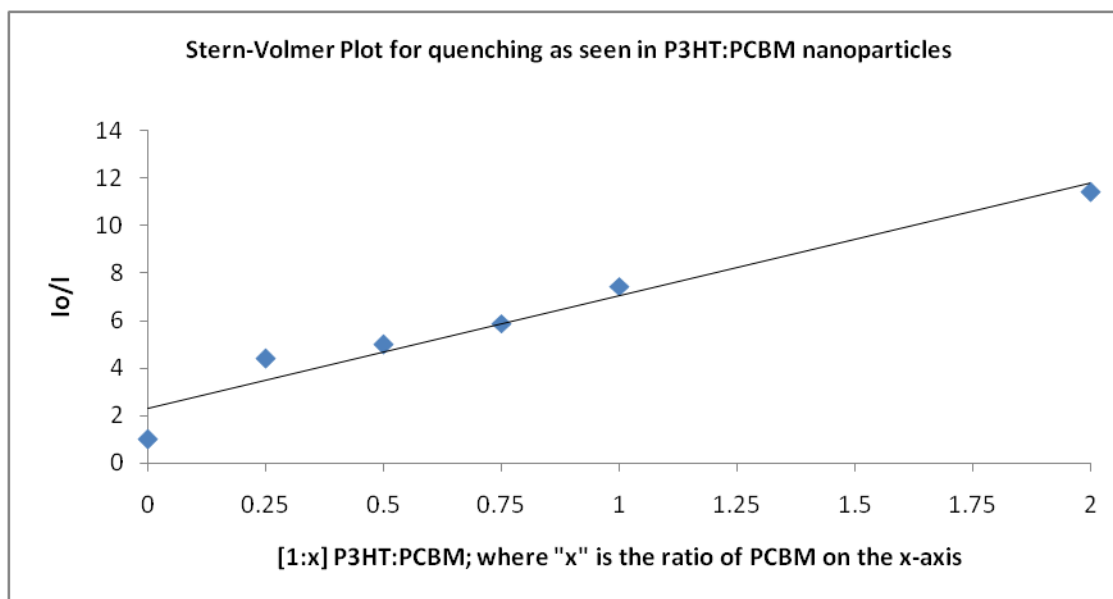
Figure B.3 : Stern Volmer Plot of P3HT:PCBM nanoparticles. The chromophore here is the P3HT and the PCBM acts as the quencher.

Figure B.3 is a Stern Volmer plot of the P3HT:PCBM nanoparticles where the ratio of the PCBM (quencher) is increased, keeping the P3HT constant. The assumption here is that since the nanoparticles are being made the same way, the majority of quenching must be coming from the PCBM. The ratio of the PCBM is plotted on the x-axis and (Io/I) is plotted on the y-axis. Here , (Io/I)=(Unquenched Fluorescence/Fluoescence with quencher)

It has been shown in literature on multiple occasions that the PCBM has a higher surface energy than the P3HT [17] . It makes sense that the P3HT likes to form a shell around the PCBM, to form a core-shell nanoparticle. So when the P3HT is kept constant and the PCBM concentration is increased, it behooves the P3HT to become more "spread-out" (because there is more PCBM domains to latch on to) i.e the PCBM is severely disrupting the P3HT domains. This is reflected in the SV plot.

B.3.2 Confirming particle size of nanoparticles using uv-vis absorbance and filtration experiments
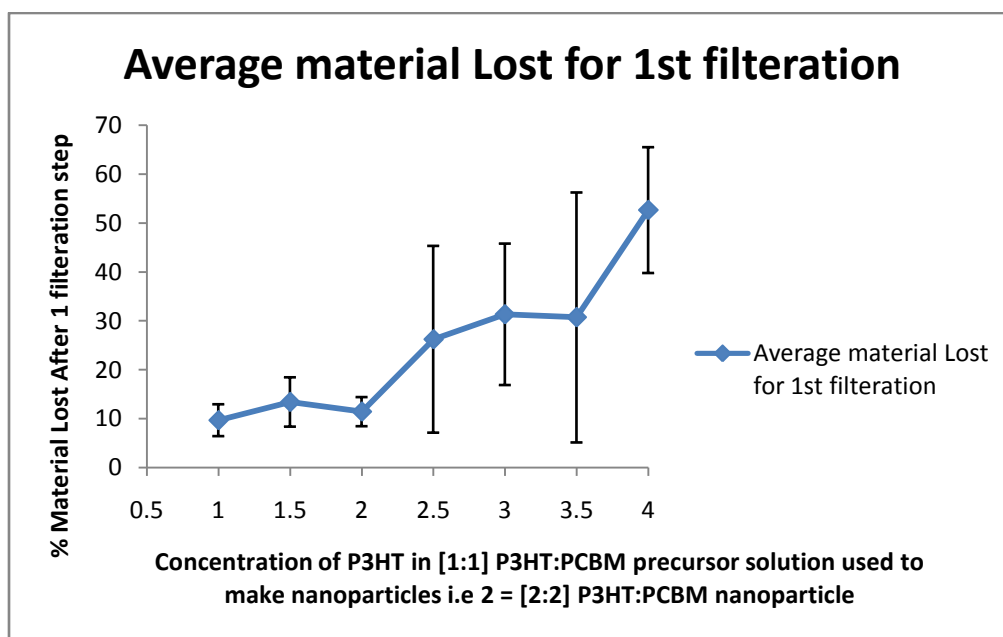
Figure B.4 : Average material lost after filtering through a 200nm pore syringe filter.

(Dispersions are measured for UV-vis absorbance before and after filtering. The decrease in absorbance intensity is directly proportional to material loss.)
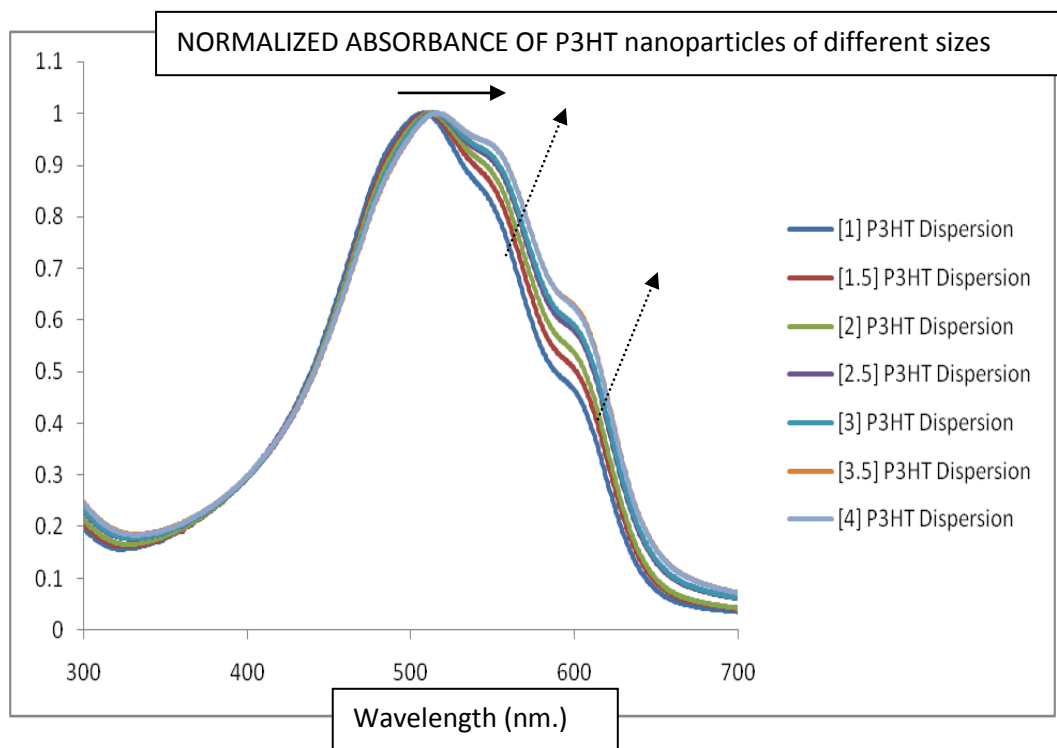
Here, the concentration of the precursor solution is plotted on the x-axis. The solution is of [1:1] ratio P3HT:PCBM in THF. So for example "2" on the x-axis means that 2mg of P3HT and 2mg of PCBM was dissolved in 10ml of THF. This solution was then used to make nanoparticles with [2:2] P3HT:PCBM ratio. This is different from a [1:1] in terms of CONCENTRATION. The y-axis shows the % material lost after filtering 4ml of the dispersion through a 200nm pore syringe filter.

The hypothesis here is that by increasing the concentration of the precursor, the average size of the precipitated nanoparticle dispersion will also increase.

From Figure B.4 - For "low" concentration precursor solutions, material loss is quite low – around 10% for 1 filtration step. As we increase the concentration of the precursor (2.5mg P3HT + 2.5mg PCBM dissolved in 10ml THF) material loss is significantly higher. This means that more material is getting lost in the filters as the average particle size is becoming larger in size, thus lending credence to the hypothesis made before. The concentration of the polymer: fullerene inside the THF-water domain is increased due to more material dissolved inside it, thereby resulting in larger droplet sizes. This finally leads to larger particles that get precipitated out.

Concentration (mg/10mlTHF)	Average material Lost for 1st filtration (%)	Standard Deviation 1st Filtration
1	10.07844797	3.628356445
1.5	13.41943285	5.0406365
2	11.44169166	2.977219023
2.5	32.53926859	26.98631388
3	31.94499831	15.48568765
3.5	39.92587946	31.66347412
4	57.91762148	10.56052252

Table B.1 : Raw data of material loss for each concentration of precursor after filtering through a 200nm syringe filter.

Figure B.5 : Increase in Vibronic Peaks at 550nm and 605nm w.r.t particle size.

As seen before , it was determined that as the precursor solution concentration was increased, the particle size also increased.

Here, it turns out that there is spectroscopic evidence that also tells us that the nanoparticle dispersions are of different size distributions; there are multiple features in the absorbance spectra that change with the change in concentration of the dispersion i.e different particle sizes / domain sizes distributions have different absorbance profiles in the case of P3HT. For instance, the red-shifting of the peak at 500nm, and the steady increase in shoulder intensities at 550nm and 605nm as seen in Figure B.5.

B.3.3 Disruption of aggregation by PCBM in P3HT:PCBM nanoparticles

Gesquiere et al [10] used a variety of techniques such as SEM, AFM, TEM to determine particle sizes of their P3HT:PCBM particles. In that process they also used a Confocal microscope setup to determine fluorescence-quenching characteristics of their nanoparticles , where they were looking at nanoparticles with increasing PCBM ratio.

They determined that PCBM got stuck inside the P3HT chains. They also determined that increasing PCBM ratio caused more disruption of P3HT interchain interactions, disruption of P3HT crystallinity also. This concept of PCBM disrupting P3HT crystallinity is not new and has been shown before with experiments on P3HT:PCBM thin films [19].
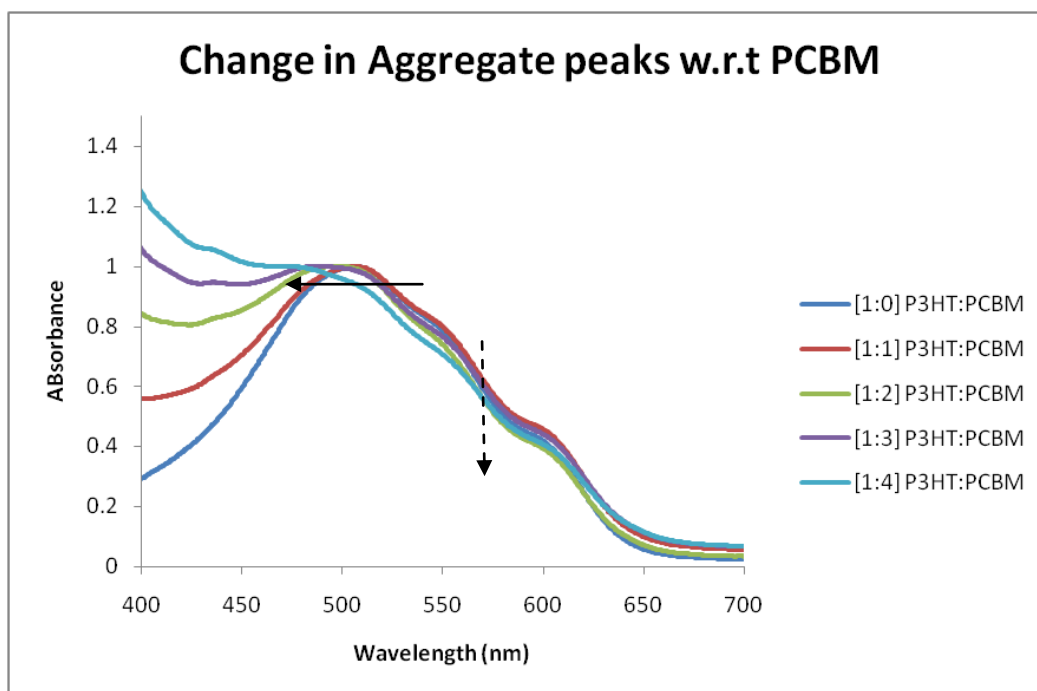
Figure B.6 : Blue-shifting of main P3HT peak at 500nm, with respect to increasing PCBM concentration within the P3HT:PCBM nanoparticles

P3HT:PCBM Blend ratio	Absorbance Wavelength Max. for P3HT
[1:1]	505.5nm
[1:2]	497.5nm
[1:3]	487.5nm
[1:4]	465.5nm

Table B.2 : Absorbance max. of P3HT with increasing PCBM inside the nanoparticle

From Figure B.6 and Table B.2, it is seen that this trend persists in the nanoparticles as well - the P3HT crystalline peaks at 505nm, 550nm and 605nm are affected with increasing the presence of PCBM.

B.4 REFERENCES

[1] Søndergaard, Roar, Martin Helgesen, Mikkel Jørgensen, and Frederik C. Krebs. "Fabrication of polymer solar cells using aqueous processing for all layers including the metal back electrode." *Advanced Energy Materials* 1, no. 1 (2011): 68-71.

[2] Pecher, Johannes, and Stefan Mecking. "Nanoparticles of conjugated polymers." *Chemical reviews* 110, no. 10 (2010): 6260-6279.

[3] Zhang, Chuan, Vikram J. Pansare, Robert K. Prud'Homme, and Rodney D. Priestley. "Flash nanoprecipitation of polystyrene nanoparticles." *Soft Matter* 8, no. 1 (2012): 86-93.

[4] Grey, John K., Doo Young Kim, Brent C. Norris, William L. Miller, and Paul F. Barbara. "Size-dependent spectroscopic properties of conjugated polymer nanoparticles." *The Journal of Physical Chemistry B* 110, no. 51 (2006): 25568-25572.

[5] Barbara, Paul F., Andre J. Gesquiere, So-Jung Park, and Young Jong Lee. "Single-molecule spectroscopy of conjugated polymers." *Accounts of chemical research* 38, no. 7 (2005): 602-610.

[6] Gesquiere, Andre J., Takayuki Uwada, Tsuyoshi Asahi, Hiroshi Masuhara, and Paul F. Barbara. "Single molecule spectroscopy of organic dye nanoparticles." *Nano letters* 5, no. 7 (2005): 1321-1325.

[7] Szymanski, Craig, Changfeng Wu, Joseph Hooper, Mary Alice Salazar, Alejandro Perdomo, Albert Dukes, and Jason McNeill. "Single molecule nanoparticles of the conjugated polymer MEH-PPV, preparation and characterization by near-field scanning optical microscopy." *The Journal of Physical Chemistry B* 109, no. 18 (2005): 8543-8546.

[8] Yu, Jiangbo, Changfeng Wu, Zhiyuan Tian, and Jason McNeill. "Tracking of single charge carriers in a conjugated polymer nanoparticle." *Nano letters* 12, no. 3 (2012): 1300-1306.

[9] Tenery, Daeri, and Andre J. Gesquiere. "Interplay between fluorescence and morphology in composite MEH-PPV/PCBM nanoparticles studied at the single particle level." *Chemical Physics* 365, no. 3 (2009): 138-143.

[10] Hu, Zhongjian, Daeri Tenery, Maxwell S. Bonner, and Andre J. Gesquiere. "Correlation between spectroscopic and morphological properties of composite P3HT/PCBM nanoparticles studied by single particle spectroscopy." *Journal of Luminescence* 130, no. 5 (2010): 771-780.

[11] SCHNEIDER-POLLACK, S. A. M. A. N. T. H. A., MONA DOSHI, JEFF GELDMEIER, and ANDRE J. GESQUIERE. "P3HT chain morphology in composite P3HT/PCBM nanoparticles studied by single particle fluorescence excitation polarization spectroscopy."*Biophysical Reviews and Letters* 8, no. 03n04 (2013): 243-253.

[12] Spano, Frank C. "Modeling disorder in polymer aggregates: The optical spectroscopy of regioregular poly (3-hexylthiophene) thin films." *The Journal of chemical physics* 122, no. 23 (2005): 234701.

[13] Clark, Jenny, Carlos Silva, Richard H. Friend, and Frank C. Spano. "Role of intermolecular coupling in the photophysics of disordered organic semiconductors: aggregate emission in regioregular polythiophene." *Physical review letters* 98, no. 20 (2007): 206406.

[14] Chambon, Sylvain, Christophe Schatz, Vivien Sébire, Bertrand Pavageau, Guillaume Wantz, and Lionel Hirsch. "Organic semiconductor core–shell nanoparticles designed through successive solvent displacements." *Materials Horizons* 1, no. 4 (2014): 431-438.

[15] Koppe, Markus, Christoph J. Brabec, Sabrina Heiml, Alois Schausberger, Warren Duffy, Martin Heeney, and Iain McCulloch. "Influence of molecular weight distribution on the gelation of P3HT and its impact on the photovoltaic performance." *Macromolecules* 42, no. 13 (2009): 4661-4666.

[16] Hoth, Claudia N., Stelios A. Choulis, Pavel Schilinsky, and Christoph J. Brabec. "On the effect of poly (3-hexylthiophene) regioregularity on inkjet printed organic solar cells." *Journal of Materials Chemistry* 19, no. 30 (2009): 5398-5404.

[17] Clafton, Scott N., David M. Huang, William R. Massey, and Tak W. Kee. "Femtosecond dynamics of excitons and hole-polarons in composite P3HT/PCBM nanoparticles." *The Journal of Physical Chemistry B* 117, no. 16 (2013): 4626-4633.

[18] Spencer, Susan, Jeremy Cody, Scott Misture, Brandon Cona, Patrick Heaphy, Garry Rumbles, John Andersen, and Christopher Collison. "Critical Electron Transfer Rates for Exciton Dissociation Governed by Extent of Crystallinity in Small Molecule Organic Photovoltaics." *The Journal of Physical Chemistry C* 118, no. 27 (2014): 14840-14847.

[19] Li, Gang, Yan Yao, Hoichang Yang, Vishal Shrotriya, Guanwen Yang, and Yang Yang. ""Solvent annealing" effect in polymer solar cells based on poly (3-hexylthiophene) and methanofullerenes."*Advanced Functional Materials* 17, no. 10 (2007): 1636.

[20] Zheng, Chenyu, Anirudh Raju Penmetcha, Brandon Cona, Susan D. Spencer, Bi Zhu, Patrick Heaphy, Jeremy A. Cody, and Christopher J. Collison. "Contribution of Aggregate States and Energetic Disorder to a Squaraine System Targeted for Organic Photovoltaic Devices." *Langmuir* 31, no. 28 (2015): 7717-7726.

[21] Hestand, Nicholas J., Chenyu Zheng, Anirudh Raju Penmetcha, Brandon Cona, Jeremy A. Cody, Frank C. Spano, and Christopher J. Collison. "Confirmation of the Origins of Panchromatic Spectra in Squaraine Thin Films Targeted for Organic Photovoltaic Devices." *The Journal of Physical Chemistry C* 119, no. 33 (2015): 18964-18974.